POLITECNICO DI MILANO

Scuola di Ingegneria Industriale e dell'Informazione
Corso di Laurea Magistrale in Ingegneria Biomedica

THE INFLUENCE OF RESIDUAL LIMB AND LINER MATERIAL PROPERTIES ON STRESS DISTRIBUTION IN A TRANSTIBIAL AMPUTEE: A FINITE ELEMENT ANALYSIS

Advisor: Prof. Carlo Albino Frigo

Co-advisor: Ing. Hossein Ansaripour

Author: Marina Clementi

ID: 945039

Academic Year 2020/2021

Contents

Index of figures

Index of tables

Abstract

Introduction

This project seeks to determine whether a better liner-to-stump fit exists, in terms of stresses at the interface and within the soft tissues. The liner serves as the interface between the socket and the stump. It is an essential component of a transtibial prosthesis because it transfers loads and reduces pressures and shear strains on the residual limb. In reality, there is little information concerning this subject in the literature, therefore clinicians often choose the liner based on intuition, product literature, peer suggestions, or previous experiences. Gel liners based on elastomeric polymers such as silicone, urethane, and thermoplastic elastomer are commonly utilized.

Focus of the work is a comparison of different material properties and loading conditions. To obtain it, a finite element analysis (FEA) on a patient specific transtibial prosthesis was implemented. FEA is a potential tool that helps the prosthetist in the design process by providing a prediction of fit prior to manufacture, as well as clinicians in the evaluation of pressure on the stump. Considering the scenarios, the first analysis simulated the donning procedure, that had the aim to reach the best fit on the stump. Then the standing upright and two phases of the walking stride, Foot Flat and Mid Stance, were evaluated. Contact pressures and shear stresses were analyzed at the interface between liner and stump, whereas Von Mises stresses were evaluated in the internal volume of the residual limb. In each mentioned phase the material properties of both liner and soft tissue were changed. These variations were made to verify how the stress distribution was influenced by the liner, and if a different description of the residual limb could modify the results.

Material and methods

The starting point of this work was a collection of STL files referring to an MRI of an amputee transtibial patient's residual limb. They represented skin, femur, patella, and tibia. Instead, files with soft tissue, liner, and socket had to be created. They were obtained by working in *Meshmixer*, starting from the STL file with the skin. For what concerns soft tissue, the skin was filled with material to create a homogeneous bulk.

To build up the liner and socket, their shapes were depicted on the skin surface, and then, with an offset tool, the thickness was given to the parts. After that, the software *Geomagic Design X* was used to convert the STL files into STEP files and to improve the shapes and surfaces of each part. The subsequent step, the FEA, was performed by means of *Abaqus*/CAE to analyze the complete model that was given by three bones, namely femur, patella and tibia, soft tissue, liner, and socket, to get the results. The work done in *Geomagic Design X* was done because *Abaqus*/CAE does not support STL files. So, all parts were imported into *Abaqus*/CAE and then the work was divided into different phases, each one identifying a module of the software: part, property, assembly, step, mesh, interaction, load, and job. In the property module, for the soft tissue, two different materials that had been called flaccid soft tissue and contracted soft tissue were considered, where the latter one was stiffer than the first. Instead, for the liner, an example of silicone, urethane, and TPE was analyzed. Bone, liner, and socket were modeled as linear elastic materials and material parameters are shown in Table 1. Instead, the Neo-Hookean constitutive model, that is a hyperelastic material model, was used for the soft tissue and material parameters are depicted in Table 2.

Structure	K (MPa)	ν
Bones	15000	0.3
Silicone liner	0.384	0.4992
Urethane liner	0.318	0.4997
TPE liner	0.144	0.4998
Socket	1500	0.39

Table 1 Material parameters for bones, liner and socket

Structure	C (kPa)	D (MPa^{-1})
Soft tissue - flaccid	6.2	1.62
Soft tissue - contracted	8.075	1.234

Table 2 Material parameters for the soft tissue

Concerning the mesh, for bones and soft tissue, tetrahedral elements were used, and for the liner triangular prisms. Instead, the socket was meshed with triangular shells. The steps were of two kinds: static general for donning and standing simulation, and implicit dynamic quasi-static for the gait. Then, the interaction between the parts was defined. A tie constraint was assigned at the interface between bones and soft tissue,

so no relative motion was allowed. Instead, a surface-to-surface interaction was defined between liner-socket and soft tissue-liner contacts and a friction coefficient was given to each one: 0.5 for the liner-socket contact and 2, 0.5, 1.5 for the contact of soft tissue with silicone, urethane, and TPE liner respectively. To improve the model, two axial connectors were added. They simulated the presence of patellar and quadriceps tendons. All the simulations were anticipated by a first analysis of the donning, which brought some pre-stresses. The donning was simulated by means of displacement controls applied at the base of the socket. Instead, for standing and walking, concentrated loads and moments were applied at the center of the knee. During donning and standing patella and tibia were kept in position by means of a set of encastres of 4 nodes; whereas the top of the femur was coupled to a node fixed with an encastre. Instead, during gait phases bones were not allowed to move through encastres at the ends of the connectors. Moreover, the outer surface of the liner was rigidly fixed along the longitudinal direction, assuming the socket would offer rigid support.

After defining all the characteristics of the model, an input file was created and submitted for the analysis.

Results and discussion

At the conclusion of the analysis an *.odb* file containing the results was created. CPRESS, CSHEAR, and Von Mises stress were the factors studied. CPRESS was the pressure at the interface between two surfaces, in this case the liner and the soft tissue. CSHEAR was the frictional shear stress measured at the same interface as the preceding variable. Von Mises stress was used to analyze the stresses in the internal volume of the soft tissue. To compute this study, the entire mass of the stump was not considered, but the focus was two sections obtained by means of the *View cut* tool: one was at the level of femur and patella, the other at the level of the tibia. Von Mises stresses were analyzed on a *path*, that was a line defined by specifying a series of points in one of the sections where greater values were detected.

Regarding the contact pressure, higher results were obtained in the sub-patellar region and lateral and medial part of the tibia, so the analysis mainly focused in these areas. All of the obtained values proved to be lower than the threshold for pain and tolerance. As a result, in all combinations analyzed, the patient's discomfort and pain from excessive pressure were avoided. When the peak of normal and shear stresses across liner materials were compared, urethane and TPE exhibited lower values than silicone. Furthermore, TPE had a better stress distribution. These trends were valid in all the evaluated scenarios, even if silicone showed a greater decrease in contact pressure passing from Foot Flat to Mid Stance and standing. Moreover, if the different scenarios

were compared, contact pressures were higher in Foot Flat for all the liners. In this phase of the gait stresses variations between different liner materials were also greater with respect to standing and Mid Stance. Then, when the results obtained changing the material properties of the soft tissue were compared, there were no significant variations at the contact except in donning in which the stiffer soft tissue showed a higher resistance to the displacement of the socket.

Instead, the evaluation of the internal stresses of the soft tissue in Foot Flat and Mid Stance revealed that the stiffer the residual limb, the higher the results obtained. The distribution of these stresses, however, was unchanged. On the contrary, the analysis of the standing did not show any relevant changes in stress values. When alternative liner materials were evaluated, there were no differences, too. As a result, the liner had no effect on what happened inside the residual limb.

Conclusions

This work analyzed the influence of the material properties of liner and soft tissue in stress distribution by means of finite element analysis. For what concern the liner, changes were noticed predominantly at the interface liner-soft tissue when the peak of the normal and shear stresses were evaluated. In general, urethane and TPE seemed to be better than silicone, because they showed lower peak values, even if stress distribution was comparable in standing and Mid Stance. Instead, the most interesting results regarding changing the material properties of soft tissue were obtained studying the internal stress distribution inside the stump. Higher stress values were detected with stiffer residual limb, even if the stress distribution inside the soft tissue resulted unaffected by the change of the material properties.

A more accurate description of the material properties of the residual limb can be the subject of future research, in particular detecting features of the soft tissue as close as possible to the real ones and characterizing the stump with different layers, like skin, muscles and fat tissue. Moreover, there are several factors that might affect findings, like temperature and humidity. These elements have an influence on both liner and soft tissue, modifying their material properties in time. Examine how these changes have an impact on the results would be fascinating.

Sommario

Introduzione

Questo lavoro si pone come obiettivo quello di verificare l'esistenza di un miglior accoppiamento della cuffia con il moncone in termini di sforzi all'interfaccia e all'interno dei tessuti molli. La cuffia è l'interfaccia tra la protesi e il moncone. Essa ricopre un ruolo molto importante in una protesi per amputato transtibiale perché aiuta a trasferire i carichi e a ridurre le pressioni e gli sforzi di taglio sull'arto residuo. Ci sono pochi dati scientifici su questo argomento e per questo motivo i clinici spesso scelgono questo componente sulla base di intuizioni, letteratura, raccomandazioni da parte di colleghi o esperienza personale. I materiali generalmente utilizzati sono gel realizzati con un polimero elastomerico come il silicone, il poliuretano e un elastomero termoplastico.

Lo studio si focalizza sul confronto di diverse proprietà dei materiali e condizioni di carico. Per ottenerlo, è stata implementata un'analisi agli elementi finiti (FEA) su una protesi per amputato transtibiale paziente-specifico. FEA è uno strumento che aiuta il protesista nel processo di progettazione fornendogli una previsione di come la protesi si adatta al moncone prima della produzione, così come i clinici nella valutazione delle pressioni sull'arto residuo. Per quanto riguarda gli scenari realizzati, una prima analisi ha simulato la fase di calzata, che ha lo scopo di raggiungere la miglior posizione sul moncone. Poi sono state valutate la postura eretta in appoggio bipodalico e le due fasi del passo di Foot Flat e Mid Stance. Le pressioni di contatto e gli sforzi di taglio sono stati analizzati all'interfaccia tra cuffia e moncone, mentre gli sforzi di Von Mises sono stati valutati nella parte interna dell'arto residuo. In ogni fase citata le proprietà del materiale sia della cuffia che dei tessuti molli sono state cambiate. Queste modifiche sono state apportate per verificare come la distribuzione degli sforzi fosse influenzata dalla cuffia, e se una diversa descrizione dell'arto residuo potesse modificare i risultati.

Materiali e metodi

Il punto di partenza di questo lavoro è una raccolta di file STL che fanno riferimento alla risonanza magnetica dell'arto residuo di un paziente con amputazione a livello transtibiale. Queste rappresentavano la pelle, il femore, la patella e la tibia. Invece, i file contenenti i tessuti molli, la cuffia e l'invaso dovevano essere creati. Questo lavoro è stato svolto attraverso *Meshmixer*. Per quanto riguarda i tessuti molli, è stata preso il file con la rappresentazione della pelle ed è stato fatto in modo di riempirla con del materiale in modo da creare una massa omogenea all'interno. Per realizzare la cuffia e

l'invaso, le loro forme sono state raffigurate sulla superficie della pelle e poi con uno strumento di offset è stato assegnato loro uno spessore. Successivamente, il software *Geomagic Design X* è stato utilizzato per convertire i file STL in file STEP e per migliorare le forme e le superfici di ogni parte.

Il passaggio successivo, il FEA, è stato realizzato per mezzo del software *Abaqus*/CAE per analizzare il modello completo formato da tre ossa, ossia femore, patella e tibia, i tessuti molli, la cuffia e l'invaso, in modo da ottenere i risultati. Il lavoro svolto in *Geomagic Design X* è stato eseguito perché *Abaqus*/CAE non supporta i file STL. Quindi, tutte le parti sono state importate in *Abaqus*/CAE e poi il lavoro è stato suddiviso in diversi passaggi, ognuno identificato da un modulo del software: *part*, *property*, *assembly*, *step*, *mesh*, *interaction*, *load* and *job*. Nel modulo *Property*, per quanto riguarda i tessuti molli sono stati considerati due diversi materiali, che sono stati chiamati *flaccid soft tissue* e *contracted soft tissue*, dove quest'ultimo era più rigido rispetto al primo. Invece per la cuffia è stato analizzato un caso per ciascun tipo di materiale: silicone, uretano e TPE. Ossa, cuffia e invaso sono stati modellati con materiali elastici lineari e i parametri dei materiali sono mostrati in Tabella 1. Invece per i tessuti molli è stato utilizzato il modello costitutivo Neo-Hookean, che è un modello iperelastico, e i parametri dei materiali sono rappresentati in Tabella 2.

Materiale	K (MPa)	ν
Ossa	15000	0.3
Cuffia-silicone	0.384	0.4992
Cuffia-uretano	0.318	0.4997
Cuffia-TPE	0.144	0.4998
Invaso	1500	0.39

Table 1 Parametri dei materiali di ossa, cuffia e invaso

Materiale	C (kPa)	D (MPa^{-1})
Soft tissue - flaccid	6.2	1.62
Soft tissue - contracted	8.075	1.234

Table 2 Parametri del materiale per i tessuti molli

Per quanto riguarda la mesh, per le ossa e i tessuti molli sono stati utilizzati elementi tetraedrici e per la cuffia prismi triangolari. Invece, per l'invaso sono stati usati elementi di tipo shell triangolari. Gli step erano di due tipi: Static/General per la

simulazione della calzata e dell'appoggio bipodalico e implicito dinamico quasi statico per il cammino. In seguito, sono state definite le interazioni tra le parti. È stato assegnato un vincolo di tipo *Tie* all'interfaccia tra le ossa e i tessuti molli, in questo modo non è stato consentito alcun movimento relativo tra di essi. Invece è stata definita un'interazione *Surface-to-Surface* tra cuffia e invaso e tra tessuti molli e cuffia, e a ciascuno è stato assegnato un coefficiente di attrito: 0.5 per il contatto cuffia-invaso e 2, 0.5, 1.5 per il contatto dei tessuti molli rispettivamente con la cuffia in silicone, uretano e TPE. Per migliorare il modello sono stati aggiunti due connettori assiali. Questi hanno simulato la presenza del tendine rotuleo e del quadricipite. Tutte le simulazioni sono state anticipate da una prima analisi della calzata, che ha aggiunto dei pre-stress. La calzata è stata simulata mediante dei controlli di spostamento applicati alla base dell'invaso. Per il cammino invece sono stati applicati forze e momenti al centro del ginocchio. Durante la calzata e l'appoggio la patella e la tibia sono state mantenute in posizione da un set di incastri con 4 nodi ciascuno; mentre la parte superiore del femore è stata accoppiata con un nodo fissato con un incastro. Invece, nelle fasi del passo alle ossa non è stato permesso di muoversi attraverso degli incastri alle estremità dei connettori. Inoltre, la superficie esterna della cuffia è stata fissata lungo la direzione longitudinale, assumendo che l'invaso offra un supporto rigido.

Dopo aver definito tutte le caratteristiche del modello, è stato creato un file di input che è stato sottoposto all'analisi.

Risultati

Quando l'analisi è conclusa, viene creato un file *.odb* che contiene i risultati. Le variabili che sono state analizzate sono CPRESS, CSHEAR e gli sforzi di Von Mises. CPRESS era la pressione di contatto all'interfaccia tra due superfici, in questo caso la cuffia e tessuti molli. CSHEAR rappresentava gli sforzi di taglio ed è sato analizzato alla stessa interfaccia della variabile precedente. Infine, gli sforzi di Von Mises sono stati utilizzati per valutare gli sforzi nel volume interno dei tessuti molli. Per svolgere questo studio non è stata considerata l'intera massa del moncone, ma ci si è concentrati su due sezioni ottenute attraverso lo strumento *View cut*: una è stata presa a livello del femore e della patella, l'altra a livello della tibia. Gli sforzi di Von Mises sono stati analizzati su un *path*, che è una linea definita specificando dei punti in una delle sezioni dove i valori maggiori sono stati rilevati.

Per quanto riguarda le pressioni di contatto, i risultati più elevati sono stati ottenuti nella regione sotto-patellare e nelle parti laterale e mediale della tibia; quindi, l'analisi si è focalizzata prevalentemente in queste aree. Tutti i risultati ottenuti hanno dimostrato di essere inferiori rispetto ai valori di soglia del dolore e di tolleranza al

dolore. Quindi, il disagio del paziente e il dolore per pressioni eccessive sono stati evitati in tutte le combinazioni analizzate. Andando a confrontare gli sforzi di picco normali e di taglio per i diversi materiali della cuffia, il poliuretano e il TPE mostravano valori inferiori rispetto a quelli ottenuti con il silicone. Inoltre, il TPE presentava anche una distribuzione degli sforzi migliore. Questi andamenti erano validi in tutti gli scenari valutati, anche se il silicone mostrava una diminuzione maggiore nelle pressioni di contatto passando dalla fase di Foot Flat a quella di Mid Stance e all'appoggio bipodalico. Inoltre, se i diversi scenari sono confrontati, le pressioni di contatto erano più alte nella fase di Foot Flat per tutti i tipi di cuffia. In questo stadio del passo le variazioni degli sforzi tra i diversi materiali della cuffia erano più elevate rispetto all'appoggio bipodalico e alla fase di Mid Stance. Andando poi a confrontare i risultati ottenuti cambiando le proprietà dei materiali dei tessuti molli, non erano presenti grandi cambiamenti all'interfaccia ad eccezione della fase di calzata, dove tessuti molli più rigidi mostravano una resistenza maggiore allo spostamento dell'invaso.

Invece, la valutazione degli sforzi interni nel moncone ha rivelato che maggiore è la rigidezza dell'arto residuo e più elevati sono i valori ottenuti. Comunque, la distribuzione degli sforzi era la stessa. Al contrario, l'analisi della fase di appoggio monopodalico non ha mostrato nessun cambiamento rilevante nei valori degli sforzi. Nessuna differenza è stata rilevata anche quando i diversi materiali della cuffia sono stati analizzati. Questo significa che la cuffia non va a influenzare ciò che accade all'interno del moncone.

Conclusioni

Questo lavoro ha analizzato l'influenza delle proprietà dei materiali di cuffia e tessuti molli nella distribuzione degli sforzi per mezzo di un'analisi agli elementi finiti. Per quanto riguarda la cuffia, i cambiamenti sono stati notati prevalentemente all'interfaccia, quando sono stati valutati gli sforzi di picco normali e di taglio. In generale, il poliuretano e il TPE sembrano migliori rispetto al silicone dato che presentano valori di sforzo minori. Invece, i risultati più interessanti per quanto riguarda i cambiamenti nelle proprietà dei materiali dei tessuti molli sono ottenuti studiando gli sforzi interni nel moncone. Sforzi più elevati sono stati rilevati con un arto residuo più rigido, anche se la distribuzione degli sforzi nei tessuti molli risulta inalterata dal cambiamento di proprietà.

Una descrizione più accurata delle proprietà dell'arto residuo può essere il soggetto di ricerche future, in particolare andando a individuare caratteristiche dei tessuti molli più vicine possibili a quelle reali e caratterizzando il moncone con diversi strati, come la pelle, i muscoli e il tessuto adiposo. Inoltre, ci sono diversi fattori che possono

influenzare i risultati, come la temperatura e l'umidità. Questi elementi vanno a influenzare sia la cuffia che i tessuti molli modificando le proprietà dei materiali nel tempo. Valutare come questi cambiamenti hanno un impatto sui risultati sarebbe interessante.

Introduction

A good quality of life for a transtibial amputee could be facilitated by an appropriate selection of the prosthetic liner. Generally, a clinician's decision about a liner for a specific patient is based on intuition, product literature, colleague recommendations, or prior experience. If a choice appears to be successful with one patient, then the clinician will often made it to other similar patients. In fact, despite the existence of many types of liners and suspension systems, there is a lack of scientific information to help the prescription practices of prosthetic liners [1].

The success of the liner choice is based on several characteristics like limb shape, tissue quality, socket design, anticipated volume change, and activity level. So, the features that must be evaluated are related to the characteristics of liner, socket and residual limb of the patient. The focus of this study is an analysis of the relation between material properties of soft tissue of an amputee and materials of liners on the market today in order to verify if a better stress distribution on the residual limb can be found. To do so, a finite element analysis (FEA) was implemented in *Abaqus*/CAE. In fact, this method demonstrated to be a useful tool to evaluate stress distribution. Scenarios taken into consideration were the standing and two phases of the gait: Foot-Flat and Mid Stance. All these situations were also preceded by a simulation of the donning, that has been proven to be an important stage in this kind of evaluation. The variables compared were pressures and shear stresses at the interface between liner and soft tissue. Then, an additional analysis was performed to evaluate internal stresses inside the stump to verify if liner material or material properties of the soft tissue have an influence on the results.

Thus, this work wants to increase the knowledge about the influence of the liner and the residual limb on the stress distribution considering different scenarios and material properties. This will help clinicians making a better choice and so improve the satisfaction of the patient, that is the main goal of this kind of analysis.

1. Amputation

Amputation is the surgical removal of a limb or other body part due to injury or disease. The primary goal of surgery is to remove diseased or damaged tissue so that healing can occur. Limb loss can be a devastating event in a person's life, with serious physical consequences as well as psychological and vocational consequences. It is divided into two types based on the location of the amputation: major and minor limb loss. A trans-humeral, trans-radial, trans-femoral, or trans-tibial amputation is a major limb loss. Amputation of the hand, digits, toes, or mid-foot level is considered minor limb loss [2].

8.1 Epidemiology

The number of patients with limb loss continues to rise due to a variety of factors, including an aging population, an increase in the number of dysvascular cases requiring amputation, and an increase in the prevalence of osteomyelitis. According to studies, the elderly dysvascular amputation population will double by 2030, and the overall amputation population prevalence will double by 2050. The majority of lower limb amputations (82%) are caused by disease processes such as diabetes mellitus (DM) or peripheral vascular disease (PVD) (Fig. 1.1). Other causes include trauma (16%), cancer (1%), and congenital abnormality (1%). Diabetes increases the risk of amputation more than smoking or hypertension. It is also reported to be responsible for 67% of all amputations, and smoking is linked to a 25-fold increase in reamputation risk compared to nonsmokers [3].

A recent study, however, discovered that indications for amputation have changed over time. For example, it was discovered that amputations caused solely by chronic ischaemia decreased by nearly a third, whereas the proportion of amputations that included infection in the presence of ischaemia nearly doubled. These findings highlight the importance of infections, especially in the context of an ischaemic limb. Instead, the prevalence of diabetes in amputations was found to be unchanged [4].

The incidence of amputation rose steeply with age; most amputations occurred in patients over 60 years. Moreover, in most centers the incidence was higher in men than women and the incidence of major amputations were more common than that of minor amputations [5].

The most prevalent level of lower extremity amputation varies depending on the etiology. Toe amputation is the most common level when both minor and major types

are considered. However, transtibial amputation is the most common amputation level in the lower extremity, with transfemoral amputation coming in second [3].

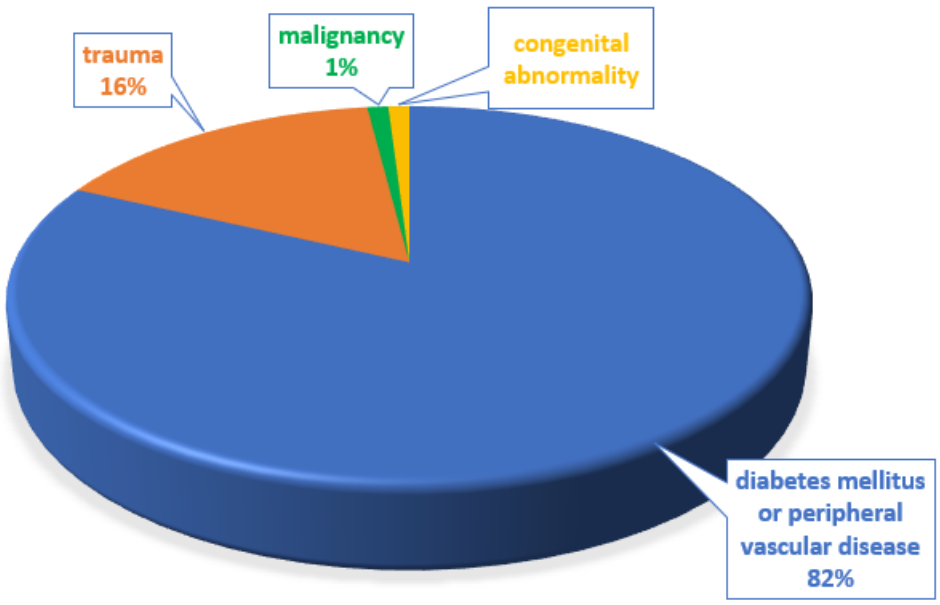

Figure 1.1 Causes of amputation

8.1 Etiology

The most common causes leading to amputation are diabetes mellitus, peripheral vascular disease, neuropathy, and trauma.

Diabetes mellitus is a group of chronic metabolic conditions, all of which are characterized by elevated blood glucose levels resulting from the body's inability to produce insulin or resistance to insulin action, or both. This group of conditions can be subdivided into four clinically different types: Type 1 diabetes is caused by autoimmune beta-cell destruction in the pancreas and is characterized by a complete lack of insulin production; type 2 diabetes is caused by an abnormally increased resistance to insulin action and the body is unable to produce enough insulin to overcome the resistance. , Gestational diabetes, a type of glucose intolerance that affects some pregnant women, and a group of other types of diabetes caused by specific genetic defects in beta-cell function or insulin action, pancreas diseases, or drugs or chemicals [6]. Patients with diabetes mellitus have a 30 times higher lifetime risk of amputation than patients without diabetes mellitus. These patients can have a wide range of symptoms, ranging from a non-healing foot wound with underlying osteomyelitis to a grossly infected wound that leads to septic shock [7].

Diabetes may cause peripheral artery disease (PAD) in some cases, which is caused by the narrowing of blood vessels that carry blood away from the heart to other parts of the body. As a result, blood vessels constrict, and PAD reduces blood flow to the legs

and feet. In its final stages, it can be a significant factor in patients requiring lower extremity amputations. Diabetes may also be a cause of neuropathy due to high glucose levels, which can damage nerves. Nerve damage reduces sensation in the limbs, which can result in unnoticed injuries that develop into skin ulcers or infections. Then, as another effect of diabetes, decreased blood flow to the feet prevents the wound from healing properly. The wounds cause tissue in the foot or leg to deteriorate, necessitating amputation [8].

Traumatic amputation, the second most common cause of amputation, can occur as a result of a motor vehicle accident, a farming accident, the use of power tools or firearms, or as a result of severe burns and electrocution. Because the mechanism of injury in traumatic amputation varies, this type of amputation is usually classified based on the severity of tissue damage. The movement of the object that caused the injury, the direction, magnitude, and speed of the energy vector, and the body tissue involved all interact to determine the extent of injury [9]. When combined with severe wound contamination and significant soft tissue loss, trauma can result in amputation in more than 20% of patients [7].

Cancer and congenital limb deficiency are two other reasons for amputation. In the United States, limb loss due to cancer is uncommon when compared to dysvascular causes, which account for less than one-hundredth of all amputations. The two most common bone cancers are osteosarcoma and Ewings sarcoma, which affect the long bones and central axis and can result in amputation. Congenital limb deficiency can be caused by genetic variation, environmental teratogen exposure, or gene-environment interactions. In this pathology, upper limb defects were more common than lower limb defects [2]. Focusing on tibial deficiency, it is a rare condition with an incidence of 1 in every million births. The type and degree of tibial deficiency can vary from a complete absence of the tibia to a partial deficiency with intact extensor mechanism. Congenital tibial deficiency is classified as follows (Fig. 1.2) [10]:

- type I: absence of the tibia (further divided in Ia: hypoplastic lower femoral epiphysis and Ib: normal lower femoral epiphysis)
- type II: absence of the distal tibia
- type III: proximal tibia not seen
- type IV: diastasis of the distal tibiofibular joint.

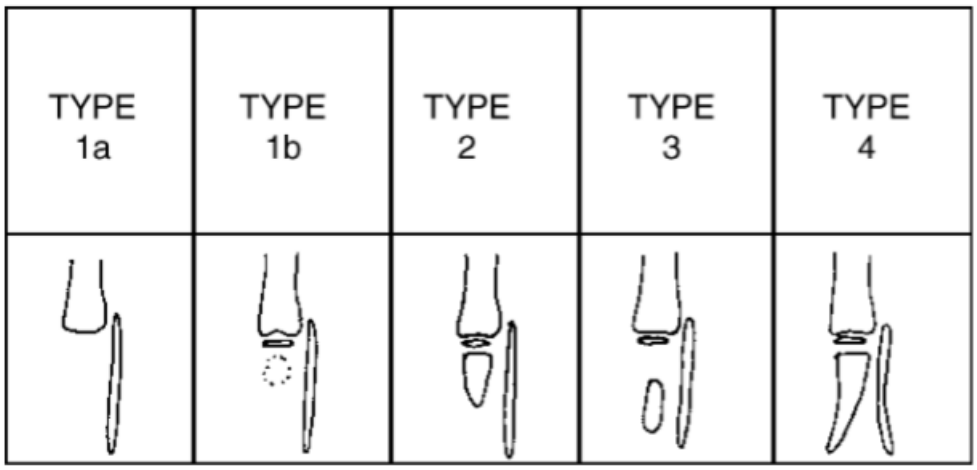

Figure 1.2 Classification of congenital deficiency [10]

Finally, amputations are caused by the cumulative illness burden rather than a single disease process. Then, in addition to etiology, age, gender, and race continue to play a role in limb loss [2].

8.1 Levels of amputation

According to the ISO 8549-2:1989 standard, amputation is classified as (Fig. 1.3) [11]:

- Partial foot amputation: amputation of lower limb distal to the ankle joint
- Ankle disarticulation: removal of lower limb at the ankle joint
- Trans-tibial amputation: lower limb is taken away between the knee joint and the ankle joint
- Knee disarticulation: lower limb eradication at the knee joint
- Trans-femoral amputation: lower limb is eliminated between the hip joint and the knee joint
- Hip disarticulation: amputation at the hip joint section
- Trans-pelvic disarticulation (or hemipelvectomy): entire lower limb amputation as well as a portion of the pelvis.

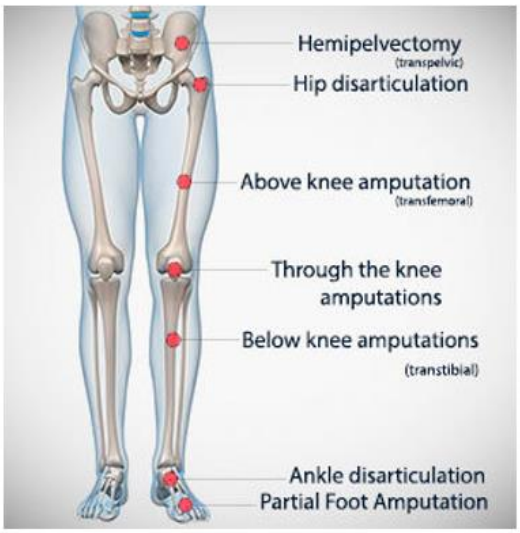

Figure 1.3 Levels of amputation [11]

Regardless of the level, there are some principles that are common to all levels of amputation in the surgical act: removal of diseased tissue, provision of a residual limb that allows for prosthetic fit, tapering the ends of bone to avoid sharp edges, provision of a conical shaped limb to allow for better prosthetic fit, control of postsurgical edema, avoidance of hematoma formation, allowing for nerve retraction, length preservation, and optimized postoperative pain control [7].

8.1 Surgical treatment

The primary goal of the amputation is to excise diseased or damaged tissue to allow healing. It is performed basing on the degree of tissue necrosis or viability. The performance can be either a single operation or a staged manner, that is the amputation followed by reconstruction. The choice of the approach depends largely on the clinical status of the patient and the quality of the soft tissue at the desired level of amputation. In general, soft tissue quality and the ability to obtain bone coverage will guide the adequacy of the level of amputation [7].

The patient is in the supine position and under general anesthesia or regional blockade. Then, it is used a pen to highlight the skin incision and the soft tissue flap and a torniquet to reduce blood loss. In general, in all levels of amputation, the arterial and venous supply are ligated to prevent hemorrhage, the muscles are transected and the bone is sawed through with an oscillating saw. After that, sharp and rough edges of the bone are filed down, skin and muscle flaps are then transposed over the stump [12].

Following the specific steps for formal below knee amputation are described [7]:

1. The level selected depends largely on soft tissue viability with the ideal length being approximately 12 to 18 cm from the tibial tubercle.

2. Skin flaps must be determined. A possible technique is to measure the diameter at the transection site and make the anterior flap one-half the circumference and the posterior long flap's full circumference. This prevents unnecessary tension at the time of closure.
3. The incisions are carried through the skin, subcutaneous tissue, and anterior muscle with suture ligation of vasculature identified.
4. The tibial bone gets transected with a power saw and tibial edges blunted by means of a rasper. The power saw or rasper can be used to bevel the anterior aspect of the tibia and this allows for less trauma to the posterior flap because it sits along a smooth surface.
5. The same process is repeated to transect the fibula at approximately 1 cm proximal to the tibial transection. Removing the sharp edges with rasper, a cornified aspect of the residual limb is obtained.
6. The posterior tissue is divided with amputation knife leaving only a thinned portion of the soleus but preserving the gastrocnemius.
7. Ligation of anterior tibial, posterior tibial, and peroneal arteries are performed before the tourniquet is released. The tibial, deep and superficial peroneal, and soleus nerves divide on tension.
8. The myodesis, a technique to secure the muscles in the residual limb, is performed by bringing the Achilles tendon to the tibia. Three osteotomies are created with a 2 mm drill bit in the anterior portion of the tibia. Fiber-wire or heavy braided nylon is used to secure the Achilles to the tibia using the three osteotomies.
9. Skin and subcutaneous tissues are closed in layers.

8.1 Complications

Lower extremity amputations involve significant perioperative morbidity and mortality. Thirty-day postoperative mortality rates can range from 4% to 22%. Long term mortality rates at 1, 3, and 5 years can reach 15%, 38%, and 68%, respectively. Mortality rates in diabetic lower extremity amputation patients can be as high as 77% at 5 years. Moreover, a review of 2879 amputees demonstrated the most common post-surgical complications included pneumonia (22%), acute kidney injury (15%), deep venous thrombosis (15%), acute lung injury/acute respiratory distress syndrome (13%), osteomyelitis (3%) and flap failure (6%) [7].

Another issue related to limb loss is the phantom limb pain (PLP), that is the pain present after complete tissue healing and is characterized by dysesthesia at the level of the absent limb. Patients describe this pain as burning, throbbing, stabbing, sharp as well as the sensation that the amputated limb is in an abnormal position. This pain can be present in 67% of patients at six months and 50% of patients at five to seven years. There are several risk factors for developing PLP, as the presence of pre-

amputation pain, female gender, upper extremity amputations and bilateral amputations of the upper and/or lower extremities. To decrease the risk of PLP a multidisciplinary approach which includes surgical technique, regional analgesia, pharmacological agents, physical therapy, and psychotherapy can be followed [7].

Psychological trauma can be also considered a complication of limb loss. In a recent review performed by Mckechnie et al. [13] it was discovered that depression can occur in 20.6 to 63% of patients (3 times higher than the general population) and anxiety in 25% to 57% (approximately the same as the general population) with 83% of patients attending a psychiatric clinic at one point after their surgery.

8.1 Changes in tissue composition

Following lower limb amputation, the residual skin and soft tissues become a critical interface. In fact, the vulnerability to damage of these tissue increases, particularly during the early rehabilitation phase. Experimental and numerical models indicate that large deformations over short periods of time are the most important factor in the causal pathway for Deep Tissue Injury (DTI), which initiates in muscle tissues. By contrast, external pressures and shear forces generally cause superficial pressure ulcers (PUs). Furthermore, residual limbs are subjected to difficult biomechanical conditions, impaired load tolerance due to comorbidities, significant variability in anatomy and surgical reconstruction, and the presence of scar tissue over vulnerable sites [14].

Soft tissue morphology and load tolerance change following amputation due to oedema, muscle atrophy, and tissue remodeling in biomechanical adaptation to prosthetic load bearing. In the months following surgery, the oedematous response to the trauma of amputation decreases gradually, and physiotherapy exercises help to reduce muscle atrophy and oedema. Despite these interventions, residual muscle atrophy occurs as a result of denervation and disuse, with adipose or fibrous tissue infiltration. Furthermore, in response to increased repetitive loading, the superficial tissues adapt. To adapt their vascular function, the skin and subdermal tissues may thicken and callus form [14].

2. Lower limb anatomy

Lower limb is specialized for body weight transmission and locomotion. The lower extremity can be divided into several parts: hip, thigh, knee, leg, ankle, foot. One of the most interesting parts is the knee that is the intermediate joint of the lower limb and allows the movement between femur, tibia, and patella. There is a normal distribution of the load forces on these three articular components in both the static load and during ambulation under normal condition. The understanding of anatomy and knee biomechanics is important for the gait analysis, the diagnosis of joint diseases and the design and development of prosthetic implants [15].

Following a brief description of the parts of interest of the lower limb anatomy will be presented.

2.1. Bones

The bones that are part of the knee joint are four in total: femur, tibia, fibula, and patella.

2.1.1. Femur

The femur (Fig. 2.1) is the longest and strongest bone of the body, present in the thigh. At the upper end it articulates with the hip bone to form the hip joint, and at the lower end it articulates with the patella and tibia [16]. It acts as the site of origin and attachment of many muscles and ligaments, and can be divided into three parts: proximal, shaft and distal. The proximal aspect of the femur articulates with the acetabulum of the pelvis to form the hip joint. It consists of a head and neck, and two bony processes, the greater and lesser trochanters. There are also two bony ridges connecting the two trochanters, the intertrochanteric line anteriorly and the trochanteric crest posteriorly. The shaft of the femur descends in a slight medial direction. This brings the knees closer to the body's centre of gravity, increasing stability. The distal end of the femur is characterized by the presence of the medial and lateral condyles, which articulate with the tibia and patella to form the knee joint [17]. The complex structure of knee joint is stabilized by ligaments: the proximal part of posterior cruciate ligament attaches to the lateral surface of medial condyle, while the anterior cruciate ligament is attached to the medial surface of lateral condyle. This is the most weightbearing articulation [11].

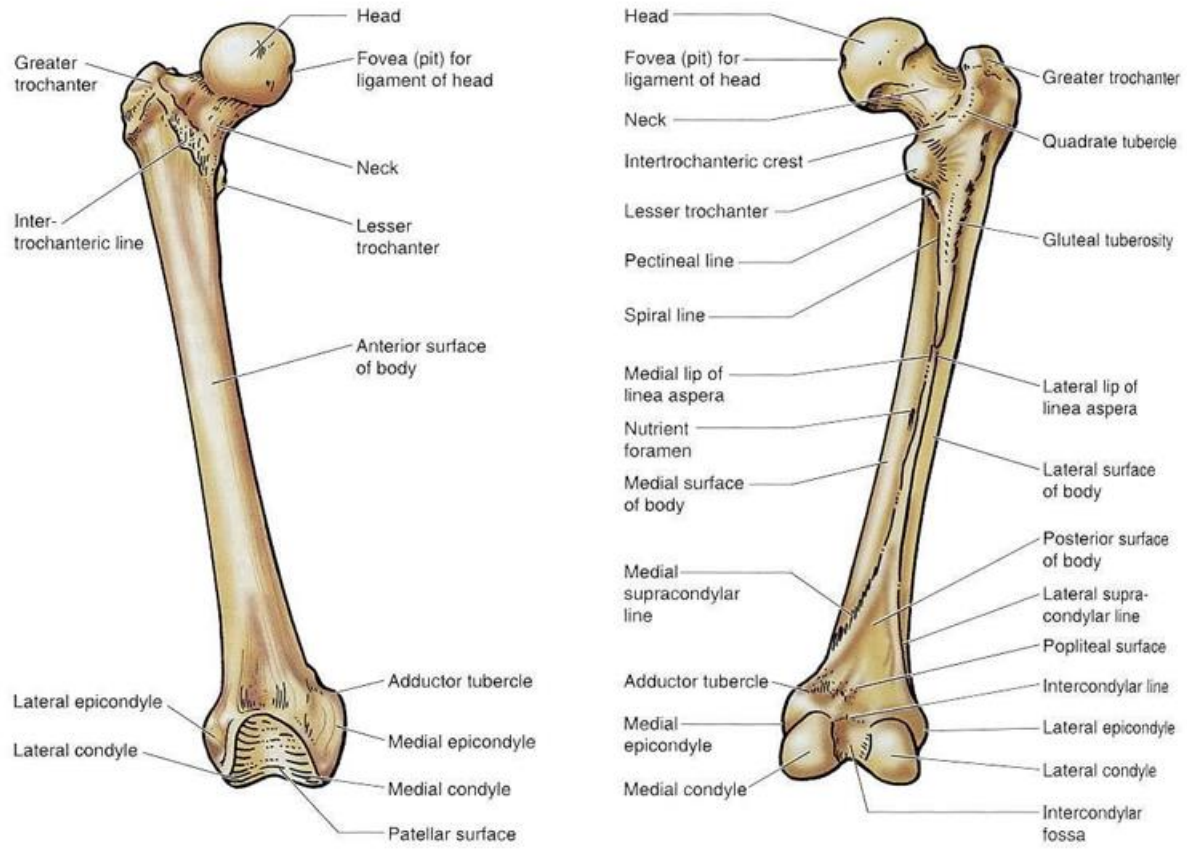

Figure 2.1 Femur: anterior and posterior view

2.1.2. Patella

The patella (Fig. 2.2) is the largest sesamoid bone situated in front of the knee joint. It has a triangular shape, with anterior and posterior surfaces. The apex of the patella is situated inferiorly and is connected to the tibial tuberosity by the patellar ligament. The base forms the superior aspect of the bone and provides the attachment area for the quadriceps tendon. The posterior surface articulates with the femur, and is marked by two facets: medial facet, that articulates with the medial condyle of the femur, and lateral facet, that articulates with the lateral condyle of the femur. The patella has two main functions [16,17]:

- leg extension: it enhances the leverage that the quadriceps tendon can exert on the femur, increasing the efficiency of the muscle,
- protection: it protects the anterior aspect of the knee joint from physical trauma.

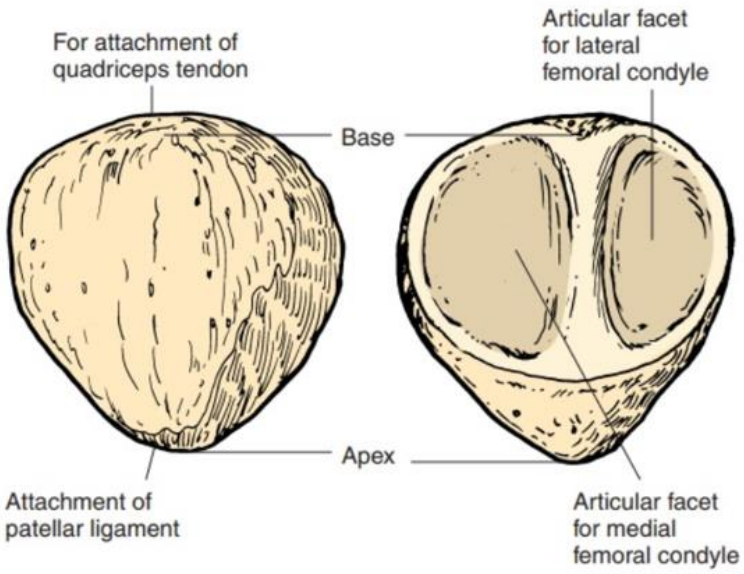

Figure 2.2 Patella

2.1.3. Tibia

The tibia (Fig. 2.3) is the second largest bone in the body and provides support for a significant portion of the weight-bearing forces transmitted from the rest of the body. It expands at its proximal and distal ends articulating at the knee and ankle joints respectively. Proximally in cross-section, the tibia assumes a pyramidal shape that articulates with the femur at the knee joint. The proximal tibia is widened by the medial and lateral condyles, which aid in weight-bearing. The condyles form a flat surface, known as the tibial plateau. The distal end of the tibia widens to assist with weight-bearing. The medial malleolus is a bony projection continuing inferiorly on the medial aspect of the tibia. It articulates with the tarsal bones to form part of the ankle joint. On the posterior surface of the tibia, there is a groove through which the tendon of tibialis posterior passes. Laterally there is the fibular notch, where the fibula is bound to the tibia, forming the distal tibiofibular joint [17,19].

2.1.4. Fibula

The fibula (Fig. 2.3) is a bone located within the lateral aspect of the leg. Its main function is to act as an attachment for muscles, and not as a weight-bearer. Upper part is at below knee level, so it doesn't interact with this joint. The upper extremity, that is the head of fibula, is irregular and quadrate, with a pointed apex on the lateral side. A superomedial facet articulates with the inferior aspect of lateral condyle of tibia [17,18].

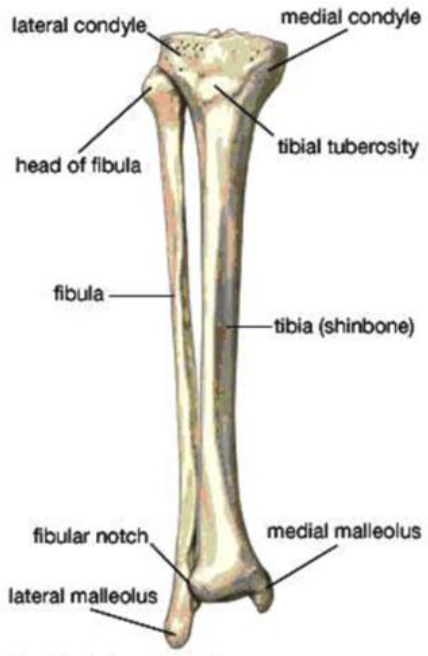

Figure 2.3 Tibia and fibula

2.2. Muscles

The muscles of the lower limb can be divided according to their locations. In Tables 2.1 and 2.2 the main muscles of leg and thigh are described (Fig.2.4) [17].

Muscle	Compartment	Origin	End	Action
Tibialis Anterior	Anterior	Lateral surface of the tibia	Medial cuneiform and base of metatarsal I	Dorsiflexion and inversion of the foot
Extensor Digitorum Longus	Anterior	Lateral condyle of the tibia and the medial surface of the fibula	Fibres converge into a tendon, which travels to the dorsal surface of the foot. The tendon splits into four, each inserting onto a toe	Extension of the lateral four toes and dorsiflexion of the foot
Gastrocnemius	Posterior (superficial)	Lateral head: lateral femoral condyle Medial head: medial femoral condyle	The fibres converge and form a single muscle belly. In the lower part of the leg, this muscle combines with the soleus to from the calcaneal tendon, with inserts onto the calcaneus	Minor flexion of knee and plantarflexion
Plantaris	Posterior (superficial)	Lateral supracondylar line of the femur	The muscle descends medially, condensing into a tendon that runs down the leg, between the gastrocnemius and soleus.	Flexes knee and plantar flexes foot

			The tendon blends with the calcaneal tendon	
Soleus	Posterior (superficial)	Soleal line of the tibia and proximal fibular area	Calcaneal tendon	Plantarflexes the foot at the ankle joint
Popliteus	Posterior (deep)	Lateral condyle of the femur and the posterior horn of the lateral meniscus	Above the origin of the soleus muscle	Medial rotation and flexion of knee
Tibialis Posterior	Posterior (deep)	Interosseous membrane between the tibia and fibula and posterior surfaces of the two bones.	Plantar surfaces of the medial tarsal bones	Inverts and plantarflexes the foot, maintains the medial arch of the foot

Table 2.1 Leg muscles

Muscle	**Compartment**	**Attachment**	**End**	**Action**
Vastus Lateralis	Anterior	Greater trochanter and the lateral lip of linea aspera	Patella via the quadriceps femoris tendon	Extends and stabilizes knee
Vastus Intermedius	Anterior	Anterior and lateral surfaces of the femoral shaft	Patella via the quadriceps femoris tendon	Extension of the knee
Vastus Medialis	Anterior	Intertrochan-teric line and medial lip of the linea aspera	Patella via the quadriceps femoris tendon	Extension of the knee
Rectus Femoris	Anterior	Anterior inferior iliac spine and the area of the ilium immediately superior to the acetabulum	Patella via the quadriceps femoris tendon	Extension of the knee and flexion of the hip
Sartorius	Anterior	Anterior superior iliac spine	Superior medial surface of the tibia	Hip joint: flexion, lateral rotation and abduction Knee joint: flexion and medial rotation
Biceps Femoris	Posterior	Long head: ischial tuberosity of the pelvis	The heads form a tendon, which inserts into the head of the fibula	Flexion of knee, laterally rotates leg at knee (when knee is flexed), extends hip joint

		Short head: linea aspera on posterior surface of the femur		
Semitendinosus	Posterior	Ischial tuberosity	Medial tibial condyle	Flexes knee, extends hip joint, medially rotates leg at knee
Semimembranosus	Posterior	Ischial tuberosity	Medial tibial condyle	Flexes knee, extends hip joint, medially rotates leg at knee
Gracilis	Medial	Inferior rami of the pubis and the body of the pubis.	Medial surface of the tibia, between the tendons of the sartorius (anteriorly) and the semitendinosus (posteriorly)	Adduction of the thigh at the hip, and flexion of the leg at the knee

Table 2.2 Thigh muscles

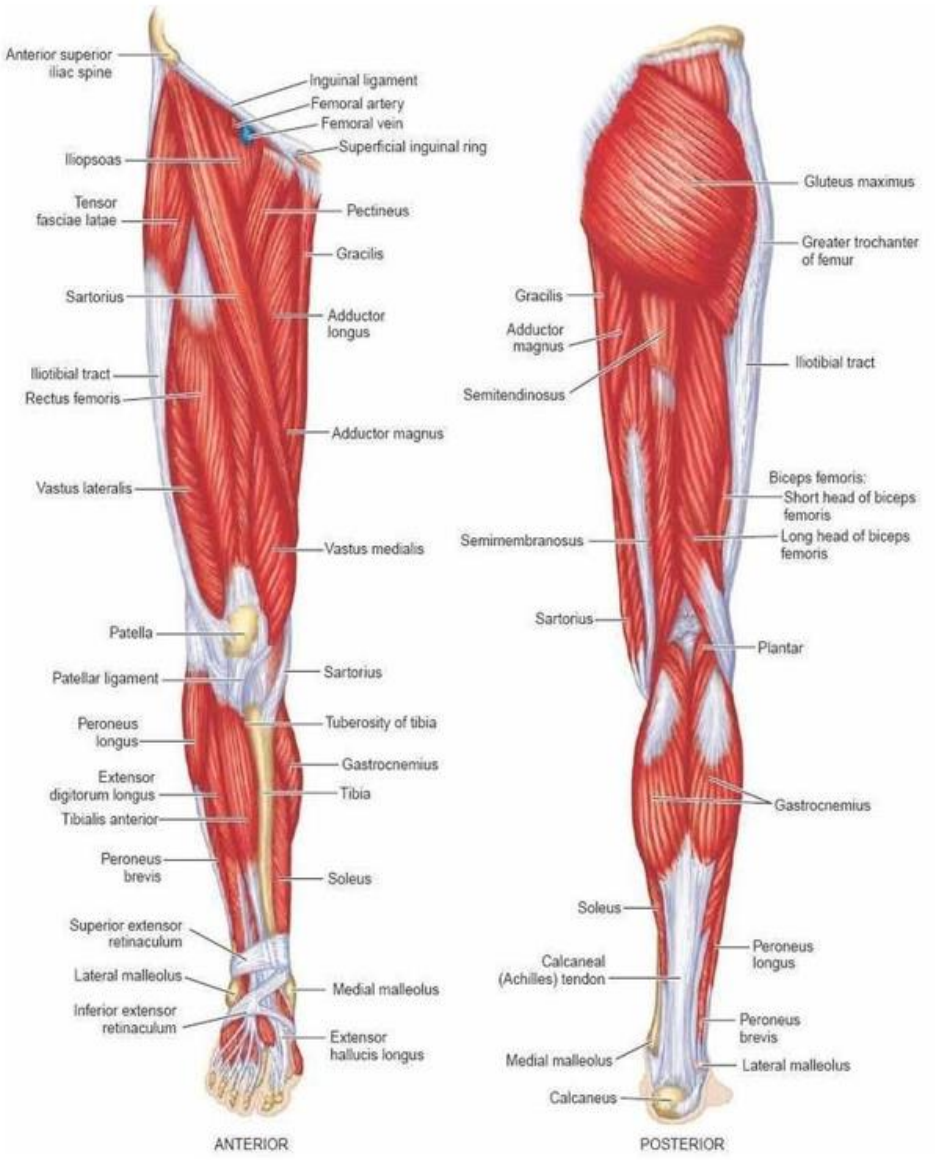

Figure 2.4 Lower limb muscles

2.3. Knee joint

The knee joint (Fig. 2.5) is a hinge type synovial joint, which mainly allows for flexion, extension and a small degree of medial and lateral rotation. It is formed by two articulations between patella, femur and tibia. They are tibiofemoral and patellofemoral articulations.

- Tibiofemoral: medial and lateral condyles of the femur articulate with the tibial condyles; it is the weight-bearing component of the knee joint.
- Patellofemoral: anterior aspect of the distal femur articulates with the patella; it allows the tendon of the quadriceps femoris to be inserted directly over the knee, increasing the efficiency of the muscle.

The menisci are fibro-cartilaginous structures that are interposed between the femoral condyles and the tibial plateaus. The lateral meniscus is more circular, while the medial is semicircular. Both are thicker at the periphery, becoming progressively thinner towards the centre of the tibial plateau. The medial is closely connected to the medial collateral ligament, while the lateral meniscus has greater freedom of movement during flexion and extension. The menisci act as joint shock absorbers by distributing evenly the load between the medial and lateral compartment. In the absence of the menisci the stress per unit area unavoidably increases. Furthermore, these two structures increase joint congruity and diffusion of synovial fluid along the articular surfaces. Then, there are the ligaments, that are fibrous connective tissue that connects bones to other bones. The major ligaments in the knee joint are:

- Patellar ligament: a continuation of the quadriceps femoris tendon distal to the patella. It attaches to the tibial tuberosity.
- Collateral ligaments: two strap-like ligaments. They act to stabilize the hinge motion of the knee, preventing excessive medial or lateral movement.
- Tibial (medial) collateral ligament: wide and flat ligament, found on the medial side of the joint. Proximally, it attaches to the medial epicondyle of the femur, distally it attaches to the medial condyle of the tibia.
- Fibular (lateral) collateral ligament: thinner and rounder than the tibial collateral. It attaches proximally to the lateral epicondyle of the femur, distally it attaches to a depression on the lateral surface of the fibular head.
- Cruciate ligaments: two ligaments that connect the femur and the tibia and in doing so, they cross each other.
- Anterior cruciate ligament: it attaches at the anterior intercondylar region of the tibia where it blends with the medial meniscus; it ascends posteriorly to attach to the femur in the intercondylar fossa. It prevents anterior dislocation of the tibia onto the femur.
- Posterior cruciate ligament: it attaches at the posterior intercondylar region of the tibia and ascends anteriorly to attach to the anteromedial femoral condyle. It prevents posterior dislocation of the tibia onto the femur.

The overall stability of the knee depends on the interaction of the capsule, menisci, ligaments and muscles, the geometry of the articular surfaces and the femoro-tibial modifications during loading. These are all interdependent, thus allowing a normal motility and, at the same time, an effective stability [15,17].

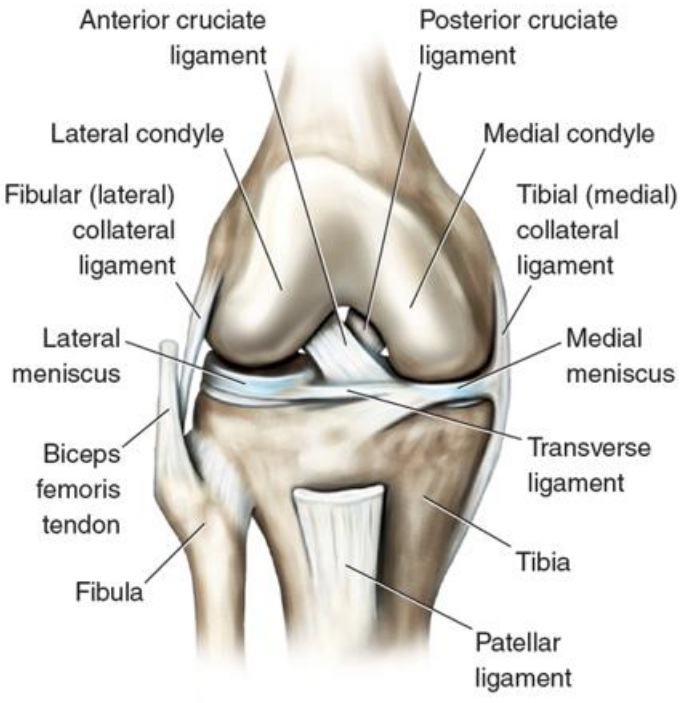

Figure 2.5 Knee joint

3. Prosthetic device

3.1. Historical background

Prosthetics have a long and illustrious history that dates back to around 1500 B.C. The first prosthesis was created by the Egyptians (Fig. 3.1), who used fiber to make prosthetic limbs. These early attempts were worn for a sense of "wholeness" rather than function, even though the world's first prosthetic toe, discovered in an Egyptian mummy, appears to have been functional as well [20]. Instead, the first lower limb prosthesis was discovered in a 300 B.C. Samnite tomb in the city of Capua. It was a wooden artificial knee reinforced with bronze, leather, and iron [21]. Other witnesses include Herodotus (424 B.C.) and the Roman scholar Pliny the Elder (23-79 A.D.). The first described a Persian seer who was sentenced to death but escaped by amputating his own foot and walking 30 miles to the next town with a wooden filler. The latter wrote about a Roman general in the Second Punic War who had the right arm amputated and an iron hand fashioned to hold his shield. Prosthetics were created during the Dark Ages to conceal deformities or injuries sustained in battle. During the Renaissance, the most common materials were iron, steel, copper, and wood [20].

Figure 3.1 Egyptian toe, the world's oldest prosthesis [22]

Ambroise Paré, a French Army barber/surgeon, is widely regarded as the founder of modern amputation surgery and prosthetic design. He introduced modern amputation procedures to the medical community (1529) and created prostheses (1536) for amputees of the upper and lower extremities. He also created an above-knee device, which was a kneeling peg leg and foot prosthesis with a fixed position, adjustable harness, knee lock control, and other engineering features found in modern devices. Another significant contribution came from Paré's colleague Lorrain, a French locksmith who created a prosthesis out of leather, paper, and glue instead of heavy iron [20].

From the 17th to the 19th centuries, prosthetics saw significant advancements. Pieter Verduyn invented the first non-locking below-knee prosthesis in 1696, which became the blueprint for modern joint and corset devices. In 1800, James Potts, a Londoner, created a prosthesis with a wooden shank and socket, a steel knee joint, and an articulated foot controlled by catgut tendons from the knee to the ankle. Dubois Parmlee invented a sophisticated prosthesis with a suction socket, polycentric knee, and multi-articulated foot in 1863. Later that year, in 1868, Gustav Hermann proposed using aluminum instead of steel, which made artificial limbs lighter and more functional. However, because of its lightness and workability, wood was the most commonly used material [20,21].

When the United States Civil War dragged on, the number of amputations skyrocketed, prompting Americans to enter the prosthetic field. With their refinements in the mechanisms and materials of the devices of the time, people like Hanger, Selpho, Palmer, and A.A. Marks helped transform and advance the prosthetics field. In contrast to the Civil War, World War I did not result in advancements in the field. However, the significance of discussing technology and the development of prostheses was recognized, which resulted in the formation of the American Orthotic & Prosthetic Association (AOPA), which is now a national trade association dedicated to providing high quality, unprecedented business services and products to O&P professionals. Veterans demanded improvements after WWII because they were dissatisfied with the lack of technology in their devices. The US government struck a deal with military contractors to improve prosthetic function rather than weapon function. This agreement paved the way for modern prostheses to be developed and manufactured [20].

Today's devices are much lighter, made of plastic, aluminum, and composite materials, and are intended to return amputees to their previous lifestyle rather than simply provide basic functionality or a more pleasing appearance. Furthermore, silicone covers make prostheses more realistic, and the function of a natural limb is more closely replicated now than ever before (Fig. 3.2) [20].

Figure 3.2 Evolution of lower limb prosthesis [22]

3.2. Classification

A lower limb prosthesis is a functional and/or cosmetic artificial replacement for any or all parts of the lower extremity. It has seen significant improvements in recent years as a result of the evolution of technologies and constituent materials. Today, two types of prostheses are distinguished based on their construction and composition: exoskeletal (traditional) and endoskeletal (modular) prostheses. Traditional ones (Fig. 3.3) are typically made of wood or plastic. The shape of this prosthesis is determined by its walls, which also serve a load-bearing function. Any changes can be made during trial fitting, but only minor static changes can be made after the final fitting. Exoskeletal prostheses have some drawbacks:

- They are heavy and cumbersome
- The alignment cannot be changed after final fitting
- They do not provide efficient stance and swing phase control
- They are not suitable for through knee amputation
- The fabrication time is much longer

They are still used in amputations where the length of the stump prevents the insertion of endoskeletal structure modules or in workplaces that are dusty and/or humid because they would quickly damage the metal components [21,23].

Figure 3.3 Exoskeletal prosthesis

For these reasons, endoskeletal prostheses (Fig. 3.4) are now the most commonly used. The load-bearing function of this type of prosthesis is ensured by a tubular structure, which can be made of aluminum, steel, carbon, or titanium and must be chosen based on the patient's weight [21]. Some of its advantages include increased wearing comfort, improved stance phase stability and swing phase control, a near-normal appearance, modular joints and adaptors that can be exchanged, allowing for adjustment at any time, suitability for all levels of amputation, and a much shorter time required for

fitment when compared to exoskeletal prosthesis. Endoskeletal prostheses are therefore not only better cosmetically and functionally, but they can also be provided to amputees as needed. They can, for example, provide stance phase stability to a feeble geriatric amputee or allow a young amputee to participate in games and sports [23].

Figure 3.4 Endoskeletal prosthesis

A second classification categorizes the prosthesis as [24]:

- Immediate/early prosthesis: used during surgery or before sutures are removed.
- Temporary/interim prosthesis: used after sutures are removed. Because it does not last very long (approximately two months), the material is not expensive. The stump is not yet ready for a permanent fit, but this prosthesis allows the amputee to walk out of the hospital. It is only worn for a short period of time each day, and its goal is to gradually improve the stump's resilience.
- Permanent prosthesis: designed for long-term use.
- Bathroom prosthesis: designed for use in water.

3.3. Transtibial prosthesis

Replacing human body movements with prosthetic components is a difficult and time-consuming task. Prosthetic components can imitate these movements to varying degrees of complexity, but the higher the level of imitation, the greater the complexity. A transtibial prosthesis typically consists of the following components (Fig. 3.5):

- socket
- suspension
- pylon
- foot

Figure 3.5 Below knee prosthetic components

3.3.1. Foot

A prosthetic foot can be made of wood, rubber, urethane, titanium, composite material based on fiber glass, or carbon fiber. They can be lightweight, energy-storing, or dynamic, and some even allow for heel height adjustment. A prosthetic foot should provide passive plantar flexion in early stance, neutral foot position in mid stance, and foot dorsiflexion in late stance. The most common types of prosthetic feet are non-articulated and articulated feet. SACH (Solid Ankle Cushion Heel) is one of the most common in the first group (Fig. 3.6). It is made up of a rigid foot with no ankle articulation, with the heel absorbing shock and the forefoot simulating dorsal flexion of the foot. There are feet on the market with varying degrees of heel cushoning. Despite its simple design, it is adequate in all phases of the gait. It is now typically used by less active people or in the initial fitting before moving on to more sophisticated foot design. When a flexibly keel is inserted inside the foot, a dynamic SACH foot is obtained. When a load is applied, the forefoot flexes, and when the load is released, the keel returns to its original shape. The SACH-rigid keel has a limitation in that it cannot bend [12].

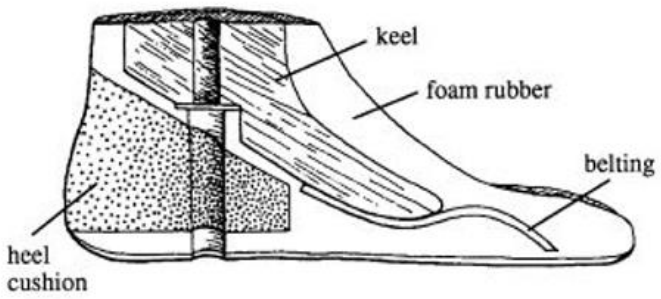

Figure 3.6 SACH foot

Conversely, articulated feet have varying degrees of cushoning in only the sagittal plane with plantar- and dorsiflexion movements, or in the sagittal and frontal planes with plantar- and dorsiflexion movements, as well as inversion and eversion (Fig. 3.7). Ankle movements are imitated for cosmetic and functional reasons, and this allows for a better mimicking of normal foot movement. In fact, the immediate forefoot contact occurs after the heel contact, promoting the ground reaction forces that secure the prosthetic knee in extension. A single-axis foot and a multi-axis foot are the two types of articulated feet. The single-axis foot allows for plantar- and dorsiflexion, which contributes to knee stability. The faster the entire sole of the foot makes contact with the ground, the more stable the prosthetic knee. It is heavier and needs to be serviced more frequently than a non-articulated foot. It is commonly used by prosthetic users who require stability around the prosthetic knee. Instead, the multi-axis foot simulates planter- and dorsiflexion as well as side-to-side movement. It absorbs some of the stresses of walking and reduces pressure in the socket, protecting both the skin and the prosthesis from wear and tear. When compared to the SACH or single axis, the function is improved, but it is heavier and more expensive. It also performs poorly in terms of shock absorption and energy return [12].

Figure 3.7 Examples of articulated foot

The dynamic response foot is another type of prosthetic foot (Fig. 3.8). The keel is designed to look like a spring-molded carbon fiber plate. Because of the shape and material of the keel, this design has a better energy response during the toe-off phase. The foot stores and releases energy while walking by absorbing energy from the keel during the "roll-over" phase of walking. This results in a push-off action. Those with an intermediate level of activity can use it because they can vary their walking speed, walk longer distances, and change direction quickly. The disadvantages of this prosthetic foot are its high cost and the presence of a stiff keel for people with low activity levels [12].

Figure 3.8 Dynamic response foot

Finally, there's the microprocessor foot, which uses a small computer and sensors to control the ankle/foot components. The computer processes information from the prosthesis, the prosthetic user's limb, and the environment before adjusting the ankle's speed and range of motion based on the action required. The ability to respond to the environment or different situations by changing the speed or range of motion is an advantage of this prosthesis. Depending on the manufacturer, these feet can be linked to a mobile device or computer to change settings and personalize the foot's actions in various scenarios. The issues are related to the battery, which must be charged, the possibility of electronic part failure, the additional weight, and the cost [12].

3.3.2. Socket

The socket represents the interface between the limb and the patient. A suitable socket should ensure proper fit, appropriate load transmission, stability, and control, and it is frequently a deciding factor in the success or failure of the prosthesis itself. Poor comfort, reduced biomechanical functionality, and hampered control are common socket-related issues. Furthermore, skin lesions affect 63-82 % of lower limb amputees, resulting in a 25-57 % abandonment rate for prostheses [26].

There are various types of sockets, and each type offers different advantages to the user. Two examples are provided below.

Patellar tendon bearing (PTB)

This is the most widely used socket in transtibial amputation. The load is applied to the patellar tendon, anterior medial tibial flare, anterior muscular compartment, and popliteal area while pressure is relieved on the fibular head, anterior tibia crest, and anterior distal tibia (Fig. 3.9). A belt that is tightened around the distal part of the thigh creates the suspension. The belt's tension restricts blood and lymphatic circulation. The PTB socket is ideal for primary amputees because it can be modified to accommodate residual limb changes that occur 12-18 months after the amputation. On the contrary, there are contraindications for active amputees who may find the PTB trim lines and

suspension methods too restrictive, as well as those who cannot tolerate patella tendon pressure [12,27].

Total surface bearing (TSB)

In the 1980s, the TSB socket was introduced. The load is distributed over the entire stump area in this system, avoiding high local stresses and improving comfort and fit (Fig. 3.9). The suspension is created by a strong adhesion between the stump and the liner, which has a pin at its distal end. This pin is installed in a blocking mechanism within the prosthetic components or via suction. A successful TSB socket fitting requires good soft tissue control and low-pressure peaks. It reduces pistoning of the socket on the residual limb by providing total contact throughout the gait cycle, and suspension appears to be superior to the PTB design because it is integrated into the socket using locking pins or suction. In addition, Safari et al. [28] stated that TSB sockets improve gait symmetry in transtibial amputees. However, they are not appropriate for primary amputees due to volume changes in the first 12-18 months post-amputation, amputees undergoing treatments such as dialysis due to volume fluctuation, or patients with short residual limbs less than 10cm long, which require higher trim lines for stability around the knee [12,26].

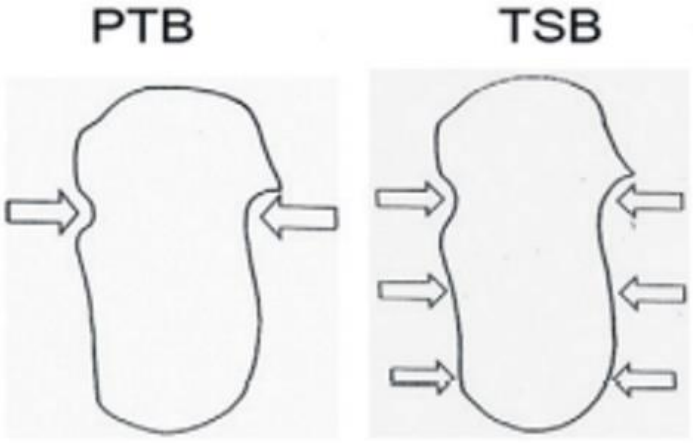

Figure 3.9 Pressure areas on PTB and TSB sockets [21]

3.3.3. Suspension

The suspension system is an important part of the design. It keeps the socket on the residual limb from falling off. The selection of a suspension system must take into account not only the amputee's functional needs, but also his or her satisfaction with the prosthesis. Indeed, as amputees' statements and research findings indicate, suspension and prosthetic fit are strongly related to functional efficiency and comfort. As a result, a good suspension will improve energy transfer, improve control of the prosthesis, and reduce any discomfort or abrasions. A poor suspension, on the other

hand, can cause skin breakdown. For suspension prescription, not only the residuum shape and length, but also overall strength, hand dexterity, eyesight, and standing balance must be assessed [12,29].

There are various types of suspension systems, and the most common will be described below.

Liner

Liners are widely used in standard practice because of their ability to adhere to the skin, form an abrasion barrier, and distribute loads. They are typically made of soft materials such as gel, urethane, and silicone, which provide shear force protection. Wear and tear issues reduce durability, necessitating replacement on a regular basis [3,26].

Cuffs, Straps and Belts

This is the traditional method of keeping the socket in place and preventing it from falling off during the swing phase. Even though it is considered an old method, it is still used today because it is a cheap, simple, dependable, and long-lasting method of suspension [12].

External Sleeve

This system consists of a sleeve that fits snugly over the socket and extends onto the user's thigh. The sleeve seals in the air in the socket to create the suspension. With an airtight seal, movement of the residuum inside the socket is reduced. Sleeves can be made of a variety of materials, including neoprene, silicone, and copolymer gel. They are usually flexible and allow the knee to bend. However, wear and tear can cause issues that reduce the effectiveness of the sleeve [12].

Pin and lock

This suspension system is made up of a silicone or gel liner with a pin at the bottom. It is based on a pin that must be inserted into a locking mechanism at the bottom of the socket when the limb is inserted. To unlock the pin, a release mechanism must be pressed. When the pin engages, it provides a positive mechanical lock with auditory feedback to the user. It is also relatively simple to put on and take off. However, due to the pulling down action of the pin on the liner, an elongation effect at the bottom of the residuum can occur, causing skin breakdown; however, newer liners are reinforced with a matrix to prevent this from happening [12].

Suction without a liner

The socket is made with an expulsion valve that will let the air out to create a seal once the residuum is in and the valve is closed. The suction is created between the bare skin and the inside of the socket. By opening or pushing on the suction valve the air will return, breaking the seal and thereby releasing the residuum to remove the prosthesis. This suspension is very good if the fit is accurate and is less expensive with respect to the options with the liner. It is an old way of suspension and donning can be complex for some individuals because it requires hand strength and dexterity as well as balance in standing [12].

Suction with a liner

This system is based on a liner that is worn on the residue and used to generate suction. These liners are typically made of silicone or gel, with silicone rings or a membrane to create a seal. As the socket is donned, air can escape through the valve, but the suction remains once the valve is closed. A lubricant or an alcohol solution on the seal will aid in the slide of the liner and the formation of a seal. Unless there are significant volume fluctuations, an external sleeve is not required [12].

Vacuum-Assisted Suspension

Direct contact between the liner and the socket wall creates suction suspension. A mechanism/pump sucks the air out between the liner and the socket, creating a uniform negative pressure across the entire surface. An external sleeve or seal is used at the top of the socket to seal off the system. When there is volume fluctuation, the mechanism creates a constant negative pressure and allows for better suspension. Furthermore, there is less pistoning and rotation within the socket. The disadvantages include an increase in the weight of the prosthesis and the possibility of mechanical component failure [12].

3.3.3.1. Prosthetic liners for lower limb amputees

Liners, as previously stated, adhere to the skin and form an interface between the stump and the socket. They were designed to help cushion the transfer of loads and reduce shock from contact between the residual limb and prosthetic socket. They also offer comfort and help to reduce shear forces. Despite the advancements, sweat remains the most serious issue [30].

More than 85% of people with transtibial amputation use a suspension system that requires a gel liner. A gel liner consists of an elastomeric polymer base that is commonly reinforced with a fabric backing. It is recognized as a relevant factor in altering pressure distribution within the socket. The gel used within prosthetic liners

increases compliance at the residual limb-prosthetic socket interface, reduces local peak pressures and creates a more uniform pressure distribution over the residual limb [31].

The following elastomeric polymers are commonly used:

- silicone
- polyurethane
- thermoplastic elastomer (TPE).

These materials can be compared using mechanical tests in terms of compressive, tensile, and shear elasticity, friction coefficient (CoF), thermal conductivity, and volumetric elasticity (Table 3.1). They exhibit viscoelastic behavior in general, as evidenced by a nonlinear toe region followed by a linear region in the stress-strain curve. In general, the compressive and shear stiffness of polyurethane and silicone liners is comparable, whereas TPE liners have lower one. For what concern dynamic CoF, polyurethane liners demonstrate relatively low values, whereas silicone and TPE liners have higher CoFs and wider ranges of CoF. Instead, thermal conductivities are comparable among the three types of materials. Finally, all materials are essentially incompressible [32,33]. Moreover, silicone elastomers and polyurethane are considered the most suitable materials for stumps with high proportion of soft tissue because they prevent the slide of the stump in the socket [34]. So, the results from ex-vivo tests on material indicated that soft liners improve cushioning over bony prominences, protect skin against breakdown and provide better suspension. However, these findings need to be confirmed by human subject experiments to establish liner prescription clinical guidelines [35].

Material	Compressive stiffness (kPa)	Shear stiffness (kPa)	Tensile elasticity (kPa)	Friction coefficient	Thermal conductivities (W/m·K)	Poisson ratio
Silicone	310 ± 100	69 ± 17	210 ± 70	1.4 - 3.1	0.16 ± 0.02	0.4929 - 0.4999
Polyurethane	300 ± 40	63 ± 3	170 ± 50	0.4 - 0.7	0.16 ± 0.02	0.4929 - 0.4999
TPE	140 ± 30	21 ± 5	1,460 ± 1,790	0.8 - 3.0	0.13 ± 0.01	0.4929 - 0.4999

Table 3.1 Liner material properties [32]

3.4. Prosthetic Prescription Algorithms for Transtibial Amputation

The components choice for transtibial prosthetic prescription depends on the individual's current or potential functional abilities and the patient's goals for prosthetic use. Therefore, the centers for Medicare and Medicaid Services introduce some functional levels which depict the mobility scale. The elements that must be present in each level are socket, interface, suspension, pylon or frame and type of foot and ankle [3].

- Functional level one (K1): patients can use a prosthesis to ambulate over level surface for short household distances. In this case the priority is safety. The socket design should be a total contact style, with special considerations for comfort during sitting. The pylon is endoskeleton and the recommended foot-ankle assembly is a non-articulated foot (e.g., SACH or SAFE foot) or a simple articulated foot (e.g., single axis foot).
- Functional level two (K2): patients can perform limited distance ambulation and traverse some environmental barriers. In this level the components should be alignable and the foot prosthesis should be multiple axis version. For what concern suspension, it can be used a pin lock, sleeve or suction suspension with a sleeve and one-way expulsion valve in the socket.
- Functional level three (K3): patients can traverse most environmental barriers and ambulate with variable cadence. Prosthetic foot is some type of energy-storing foot and depending on the activities, it can have a dynamic pylon or feature that allows ambulation over uneven terrain. The suspension system is an elevated vacuum technology.
- Functional level four (K4): patients can ambulate in conditions different from the normal ones. This may include sports or recreational activities that require high impact, high stress, or high energy levels, which are typical of the prosthetic demands of a child, high activity adult, or athlete. At this level, specialty components are running feet, waterproof foot and ankle components, and components with heel height adjustability. At this level suspension avoids disruption of the prosthetic connection during activity. This may include use of a backup or secondary suspension method [3].

3.5. Prosthesis design

There are several ways to design the socket. The traditional one depends completely on the knowledge and skill of the prosthetist. Firstly, the technician evaluates the amputee and creates a negative chalk cast working directly on patient's residual limb. Then, he realizes the positive model. This model is manually modified by adding and

removing chalk in specific zones. In fact, the internal surface of the socket is not a simple offset of the stump external surface, but it comes from the manipulation of the surface in the critical areas. In particular, in the pressure sensitive areas the technician has to add material on the positive plaster cast because there the socket does not have to press the stump; while in the pressure tolerant areas the plaster has to be removed in order to have a tighter and self-supporting socket. The amount of material added or removed depends on the characteristics of the patients. However, eight manipulation levels can be identified, from 1 to 8 mm of thickness, correlated to stump tonicity. For example, the thickness will be 3 to 4 mm when the stump has a normal tonicity, while it will be 1 to 2 mm if it is not too much toned. After this, a check socket is manufactured directly on the modified positive model and tested on the amputee. To realize a more comfortable and well-fitting final socket, the positive model is scanned searching for other necessary modifications. Finally, the definitive socket is realized, and all the prosthesis components are assembled. It is also important to highlight that normally 2 to 5 check sockets are realized before reaching the definitive one, which guarantees a good fitting and functionality (Fig. 3.10) [36].

The traditional method presents some disadvantages: lack of an objective assessment of the quality of the designed socket, modifications of the socket shape based on the knowledge and experience of the prosthetist, waste of time and material due to trial-error approach for the evaluation [37].

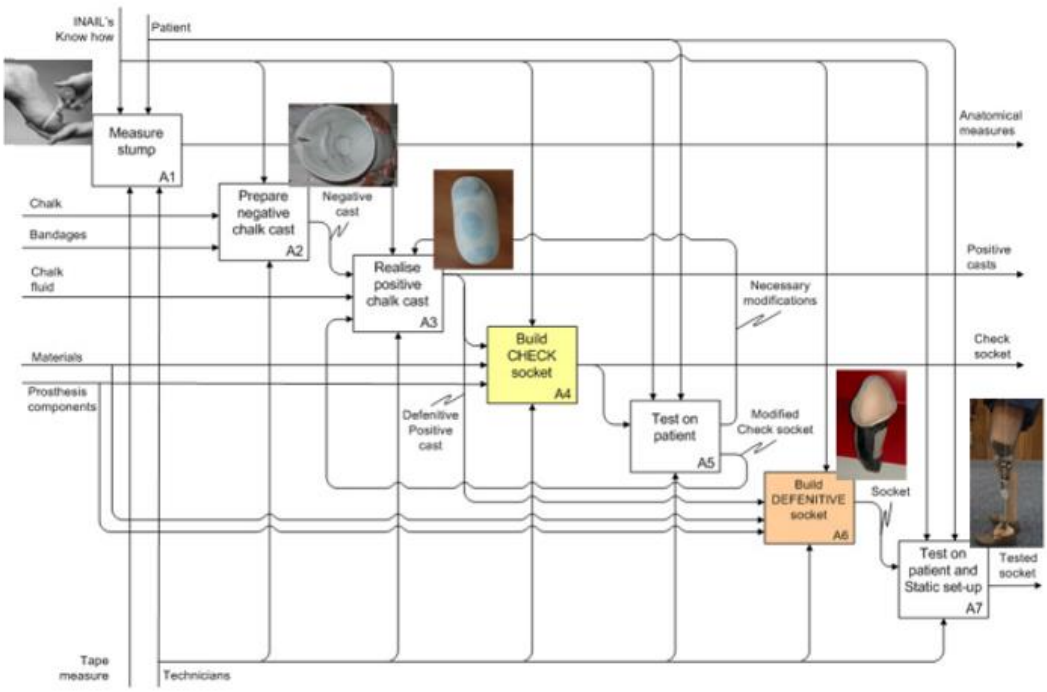

Figure 3.10 Socket traditional manufacturing process [36]

A new approach has been implemented based on the digital model of the amputee. Following the main steps [36]:

- Acquisition of patient's case history and digital model: the orthopedic technician needs to acquire all necessary information related to the patient's case history and the residual limb condition through a preliminary clinical evaluation. Then, the 3D virtual model of the patient's residual limb is acquired.
- Socket design: the 3D geometric model of the socket is created starting from the geometry of the residual limb external shape and using a modelling software. Then, using a FE system an optimal structural shape of the socket is found and studying specific situations the system suggests rules (e.g., socket thickness) and procedures (e.g., where and how make necessary changes) to the designer to improve the model.
- Prosthesis assembly: the designer choices the other components of the prosthesis from virtual catalogues containing 3D parametric models of the prosthesis parts, according to the patient's characteristics. All the parts are assembled to create the full prosthesis virtual prototype.
- Multibody analysis: kinematic and dynamic analyses of the prosthesis virtual prototype are realized to study patient's ambulation.

This new approach presents some improvements with respect to the traditional one. For example, it offers greater accuracy and precision in the manufacturing process. Moreover, the designer can modify the digital model directly from the software and these corrections would avoid waste of time and material, because the final model would be reproduced until it was fully verified [37].

3.6. Prosthesis design issues

The main complaints about prostheses relate to socket discomfort, and problems with socket fit that cause skin problems. These problems are present because the skin of the stump is exposed to several unnatural circumstances when a prosthesis is used. In particular, they may be compounded by short- and long-term residual limb volume fluctuation, and heat and perspiration caused by the enclosed socket environment. These unnatural circumstances include shear and stress forces [35]. So, design must follow some prescriptions to avoid problems. Firstly, the manufactured device tallies must be checked, and the type of prosthesis prescribed must corresponds to the user's need and give enough support in accordance with the stump length. In this way gait deviations such as lateral shift of the prosthesis, knee instability and drop off should be prevented. The prosthetist must check also that the medial, lateral, anterior, and posterior contours have adequate height and shape, and the edges are smooth and well-rounded to avoid pain to the patient. Then during prosthesis fit, it must be controlled that the socket is not too loose, small or gaping to avoid gait deviations such

as pistoning or excessive knee flexion. The length must be correct too otherwise lateral trunk bending, vaulting, abducted gait and circumduction can be present [24].

3.7. Prosthesis satisfaction

The patient's satisfaction is critical following the fitting of the prosthesis. It is the match between a patient's experience and their expectations. Satisfaction is critical for regaining mobility, optimizing use of the prosthesis, preventing rejection, and increasing compliance with the medical regimen. 40% to 60% of amputee patients are dissatisfied with their prosthesis. Over half of them are dissatisfied with the comfort of their prostheses, and more than half report pain while using them. Rejection of the prosthesis can be viewed as the ultimate expression of dissatisfaction with the prosthesis. Patients are usually given questionnaires to fill out in order to gauge their level of satisfaction. Nonetheless, they approach the goal in different ways. The Trinity Amputation and Prosthesis Experience Scales (TAPES), for example, uses a 5-point scale to assess satisfaction and includes questions about "color," "noise," "shape," "appearance," "weight," "usefulness," "reliability," "fit," "comfort," and "overall satisfaction." The Prosthesis Evaluation Questionnaire (PEQ) instead employs two visual analogue scales to assess overall satisfaction and satisfaction with walking with the prosthesis over the previous four weeks [38].

However, this is a qualitative study in which prosthesis satisfaction is defined as the patient's subjective and emotional assessment, which can be influenced by his psychological state. To quantify the impact of the prosthesis on mobility, function, and device acceptance, the amount and location of the external forces applied over the surface of the residual limb by the socket should be quantified. Pressure sensitive areas are those on the stump that have bony protuberances or tendons and cannot withstand any pressure. As a result, sockets should distribute forces as evenly as possible over pressure-tolerant areas. The pressure sensitive and pressure tolerant areas of the transtibial stump are depicted in Figure 3.11. Furthermore, pressure distribution over a larger surface reduces load and increases comfort when using a prosthesis [12].

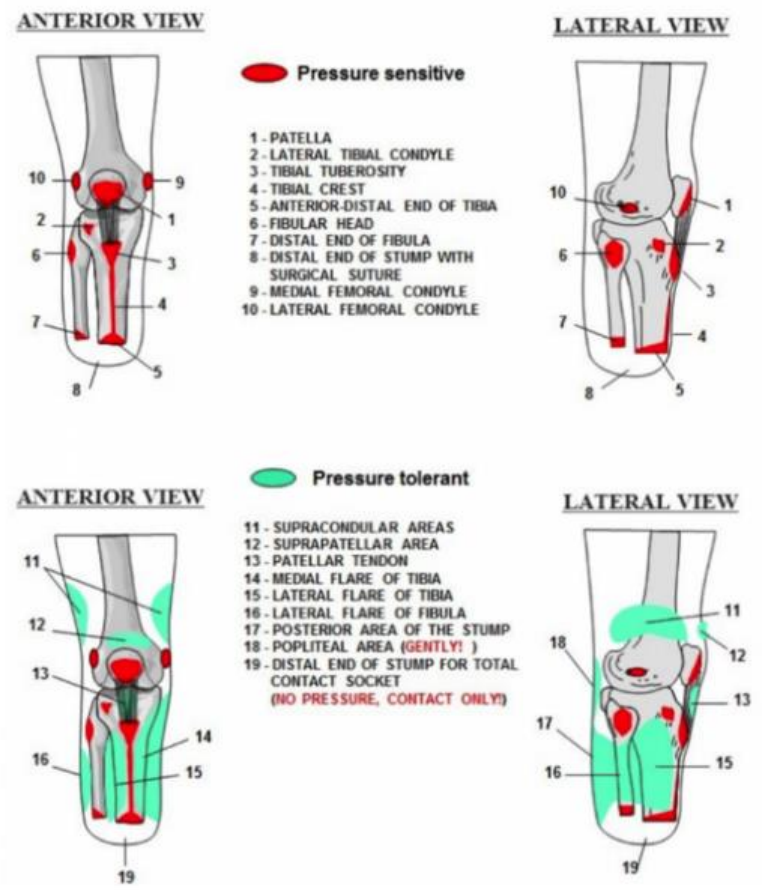

Figure 3.11 Pressure sensitive and pressure tolerant areas in a below knee amputee [12]

Even if there are pressure-tolerant areas, stress distribution at the limb-prosthesis interface can cause a variety of discomforts. Pressure ulcers, sensitive skin, irritations, and partial or total vascular occlusions can occur when high pressures are applied to the skin for an extended period of time and in a non-uniform manner. Furthermore, the friction between the limb and the socket causes shear stresses, which cause tissue deformation and increase the risk of injury. Skin problems can develop into chronic infections, necessitating re-amputation in the worst-case scenario [26]. As a result, identifying pressure threshold values and ensuring that they are not exceeded is critical. Table 3.2 depicts the pain pressure threshold and tolerance in various areas of the stump [39].

	Fibular head	**Medial condyle**	**Popliteal fossa**	**End of stump**	**Patellar tendon**
Pain pressure threshold (KPa)	599.6±82.6	555.2±132.2	503.2±134.2	396.3±154.5	919.6±161.7
Pain pressure tolerance (KPa)	789.8±143.0	651.0±111.1	866.6±77.3	547.6±109.1	1158.3±203.2

Table 3.2 Pain pressure threshold and tolerance

4. Gait analysis

4.1. Biomechanics of human movement

Human walking can be described as a cyclic pattern of body movements which advances an individual's position. Following the main phases of the gait cycle will be presented (Fig. 4.1) [24]:

1. Initial contact: moment when the foot touches the floor.
2. Loading response: the initial double-stance period. It begins with initial floor contact and continues until the other foot is lifted for swing. Using the heel as a rocker, the knee is flexed for shock absorption; ankle plantar flexion limits the heel rocker through forefoot contact with the floor.
3. Mid-stance: the first half of the single-limb support interval. The limb advances over the stationary foot through ankle dorsiflexion, while the knee and hip extend. It begins when the other foot is lifted and continues until body weight is aligned over the forefoot.
4. Terminal stance: the final stage of the single-limb support. It begins with the heel rising and continues until the other foot strikes the ground, in which the heel rises and the limb advances over the forefoot rocker. Throughout this phase, body weight moves ahead of the forefoot.
5. Pre-swing: the final phase of stance. It begins with the initial contact of the opposite limb and ends with the ipsilateral toe-off. The objective of this phase is to position the limb for swing.
6. Initial swing: approximately one-third of the swing period. It begins with a lift of the foot from the floor and ends when the swinging foot is opposite the stance foot. In this phase, the foot is lifted, and the limb is advanced by hip flexion and increased knee flexion.
7. Mid-swing: it begins as the swinging limb is opposite the stance limb and ends when the swinging limb is forward and the tibia is vertical. The knee is allowed to extend in response to gravity, while the ankle continues dorsiflexion.
8. Terminal swing: the final phase of swing. It begins with vertical tibia and ends when the foot strikes the floor. Limb advancement is completed as the leg moves ahead of the thigh. In this phase, limb advancement is completed

through knee extension. The hip maintains its earlier flexion and the ankle remains dorsiflexed.

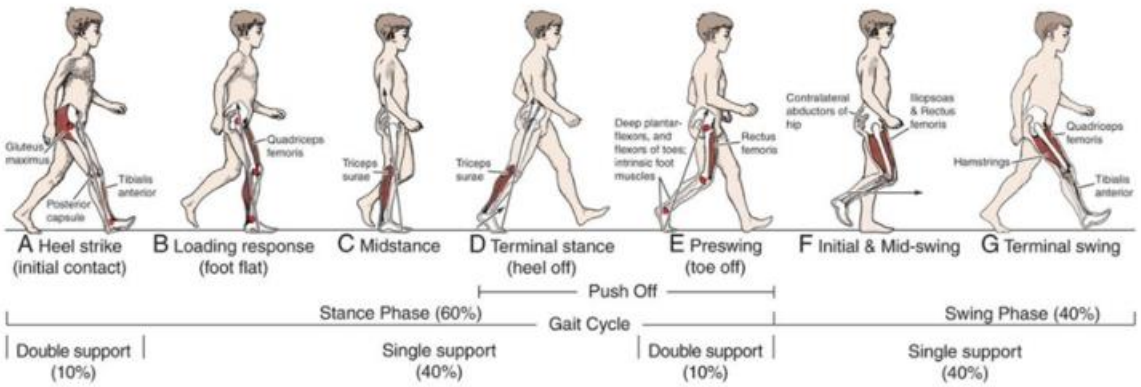

Figure 4.1 Gait cycle

4.2. Prosthetic gait

Amputation has a great impact on locomotion, and this results in a different distribution of loads and balances. An amputee's gait will depend on the quality of the prosthetic parts (socket fit and components), the condition of the stump and the interface between the body and the prosthesis. Moreover, amputees spend a greater amount of energy, that is different in case of traumatic amputation or vascular disease, as it can be noticed in Table 4.1 [12,24].

Amputation level	Increased energy requirement (%)	Increase in oxygen consumption (%)
Traumatic Transtibial	25	7
Vascular Transtibial	40	33
Traumatic Transfemoral	68	53
Vascular Transfemoral	100	87

Table 4.1 Increased energy requirement and oxygen consumption in case of traumatic amputation or vascular disease

The average gait pattern depends on the type of prosthesis used for mobility; however, some generalizations can be made. Before flat foot contact, heel strike and weight bearing through the heel are prolonged because of a reduced range of movement of the ankle of the prosthesis with respect to the anatomical one. At initial contact, knee flexion is decreased and when the foot moves to floor contact, the overall maximum flexion achieved is reduced. During swing phase of the non-prosthetic limb the body weight begins to move forward over the prosthetic limb, which is in stance phase. To gain adequate step length of the non-prosthetic limb, heel rise on the prosthesis occurs

earlier. and is greater than that of a normal gait pattern. This creates an elevation of the body and results in a greater loading force on the non-prosthetic side as the body weight drops more rapidly onto the limb. Then, greater quadriceps contraction is needed to absorb the force. The 'toe off' force generated from the prosthetic limb is reduced and it is compensated by the hip flexors. Flexion of the knee on the prosthetic limb occurs with some hamstring contraction and mainly with eccentric contraction of the quadriceps. During the stance phase, the rocker effect of the prosthesis results in increased instability and the reduced knee flexion achieved on the prosthetic side requires hip muscles to generate greater energy to ensure stability. Due to the reduced ankle movement of the prosthesis the range of extension at the hip is reduced to approximately half of that of the opposite limb. The stance time on the non-prosthetic side is also increased compared to that of the prosthetic side [12].

Generally, the walking speed of a lower limb amputee decreases in order to keep the energy expenditure to a minimum. For transtibial amputees this reduction is around 10-60%. Nevertheless, some very active transtibial amputees with a high-performance device may walk at the same speed as non-amputees [24].

Mediolateral forces

Figure 4.2 shows a front view of a below-knee amputee in a position corresponding to the midstance phase and the forces exerted. There are two types of forces represented in Figure 4.2a: the body weight W and the forces applied through contact with the socket. Figure 4.2b shows the forces acting on the prosthesis. If the prosthesis is considered as a means of supporting the body, it must be able to provide both vertical support and mediolateral balance. To simplify the analysis, the effect of the vertical components of pressure applied against the surfaces of many areas of the stump is combined in the single support force S. Considering the point of application of S as a balance point, the lateral force L times the distance b equals the body weight W times the distance a (Eq. 4.1).

$$Lb = Wa \tag{4.1}$$

However, the effect of the horizontal acceleration of the center of gravity cannot be ignored and it results in a lateral inertia force I which tends to oppose the acceleration. So, the new balance equation is:

$$L = \frac{Wa - Ic}{b} \tag{4.2}$$

This equation shows that the magnitude of the required lateral stabilizing force L can be reduced in two ways: by increasing the horizontal inertia force or by increasing the effective lever arm b [40].

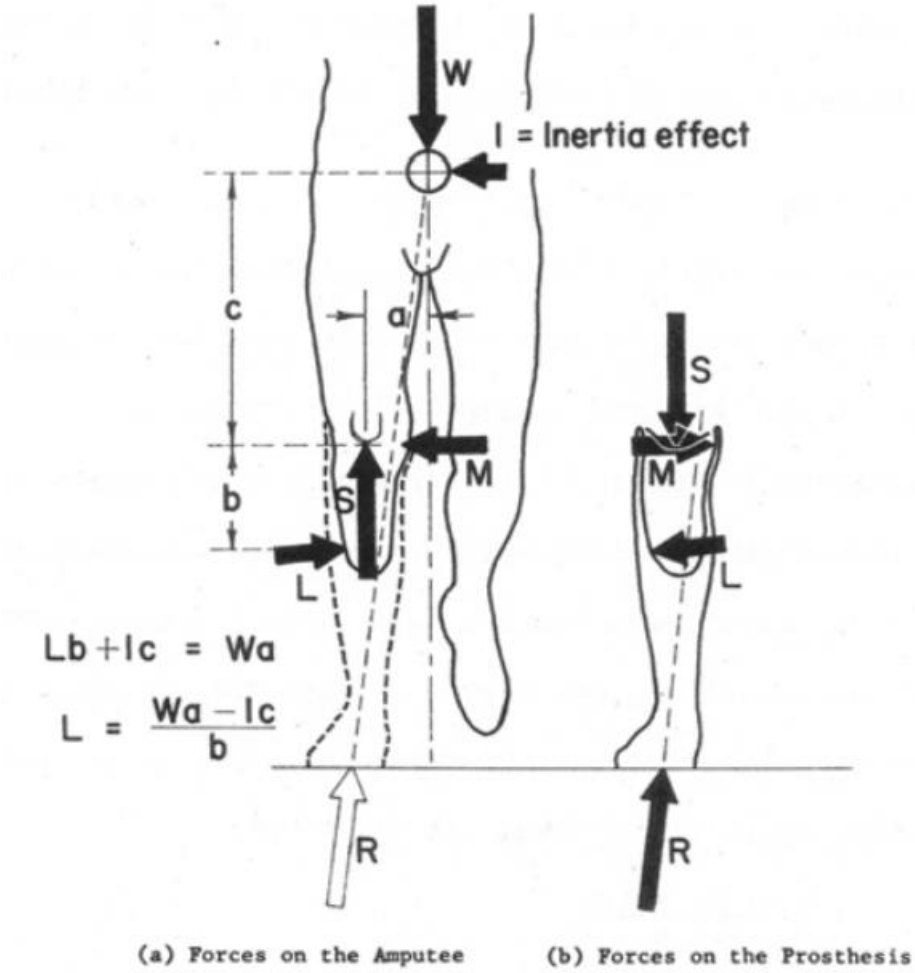

Figure 4.2 Mediolateral force diagrams. L, lateral force; S, support force; W, body weight; R, total floor reaction; I, lateral inertia force; M, medial pressure [40]

Anteroposterior forces

Figure 4.3 shows a side view of a below-knee amputee and the cuff-suspension prosthesis under three conditions of the gait: heel contact (a), shock-absorption portion of the midstance phase (b), push-off phase (c). At heel contact, for a brief period of about 5% of the walking cycle, knee stability is maintained primarily through active extension of the hip joint. The hamstring action opposes the tendency of external load on the prosthesis to cause the knee to extend. Figure 4.3 depicts the forces at work in each phase as well. The floor reaction force R acts along a line that passes posterior to the knee center during the shock-absorption portion of the midstance phase. This would cause a completely relaxed knee to buckle, but the amputee can overcome this tendency by actively extending the knee. The forces can be seen to be concentrated in three areas: the patellar tendon, the anterodistal portion of the tibia and the popliteal area. Then, during the push-off phase, the floor reaction continues to pass behind the knee and the anteroposterior forces are present in the same three areas [40].

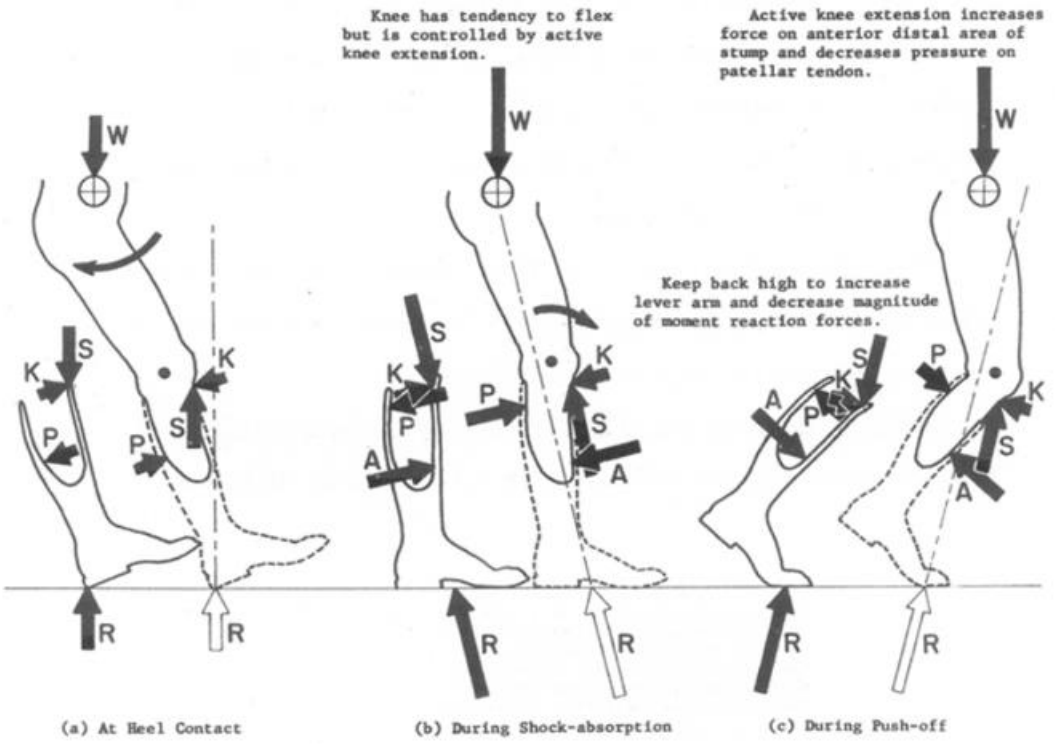

Figure 4.3 Anteroposterior force diagrams. W, body weight; S, support force; K, force on patellar tendon; P, posterior force; A, anterior force; R, total floor reaction [40]

5. State of the art in lower limb prosthesis

For lower extremity amputees, a well-fitting socket is an important element for a successful rehabilitation. The socket provides the interface between the prosthesis and residual limb, which is designed to provide comfort, appropriate load transmission, and efficient movement control. Attaining these objectives is extremely challenging, with up to 55% of lower limb amputees reporting dissatisfaction with socket comfort, residual limb pain, and/or skin breakdown [41]. So, integrating a prosthesis to the human body is a great challenge and many studies have been conducted in the last 50 years to disentangle its complexities with an exponential growth in recent decades. The number of published literature reviews on user-prosthesis interface in Figure 5.1 may give an idea [35].

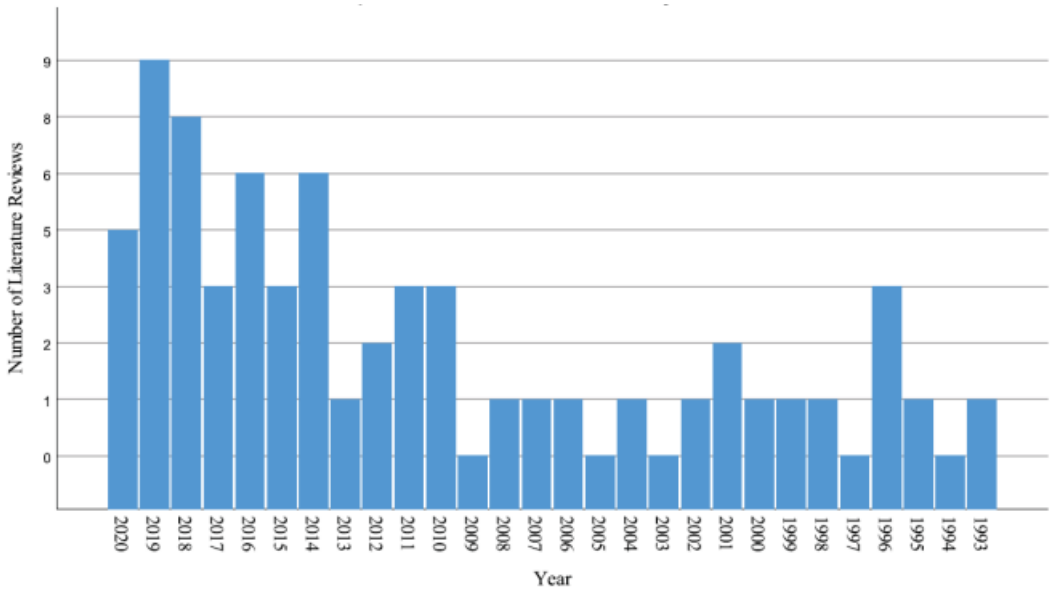

Figure 5.1 Number of literature reviews published per year on user-prosthesis interface [35]

Stresses at the residual limb socket interface can be measured, but a full-field experimental evaluation remains difficult. These difficulties associated with experimental measurements can be overcome by computational modeling. Computational models for transtibial prosthesis analysis are mainly based on finite element methods [42]. Computational models must be incorporated also to analyze deep tissue injuries, because it is not easy to measure internal stresses and strains in the soft tissue of TTA patients.

5.1. FEM

Finite element analysis is widely used in engineering to determine the distribution of structural deformations or stresses, for example. In terms of transtibial amputation, it has been identified as a potential tool to aid the prosthetist in the design process by providing a prediction of fit prior to manufacture, as well as clinicians in the evaluation of pressure on the stump. The robustness of FE models when used to inform clinical practice, as well as the extraction of relevant data, has very specific requirements. Furthermore, there are some challenges to clinical implementation of these techniques, such as difficulty obtaining imaging data, long solver times for the models, and the requirement for a trained user to develop and interpret the FE model. However, the potential use of FE to simulate the complex residuum-socket interaction is well established [43,44].

Figure 5.2 depicts the general categories on which research is based.

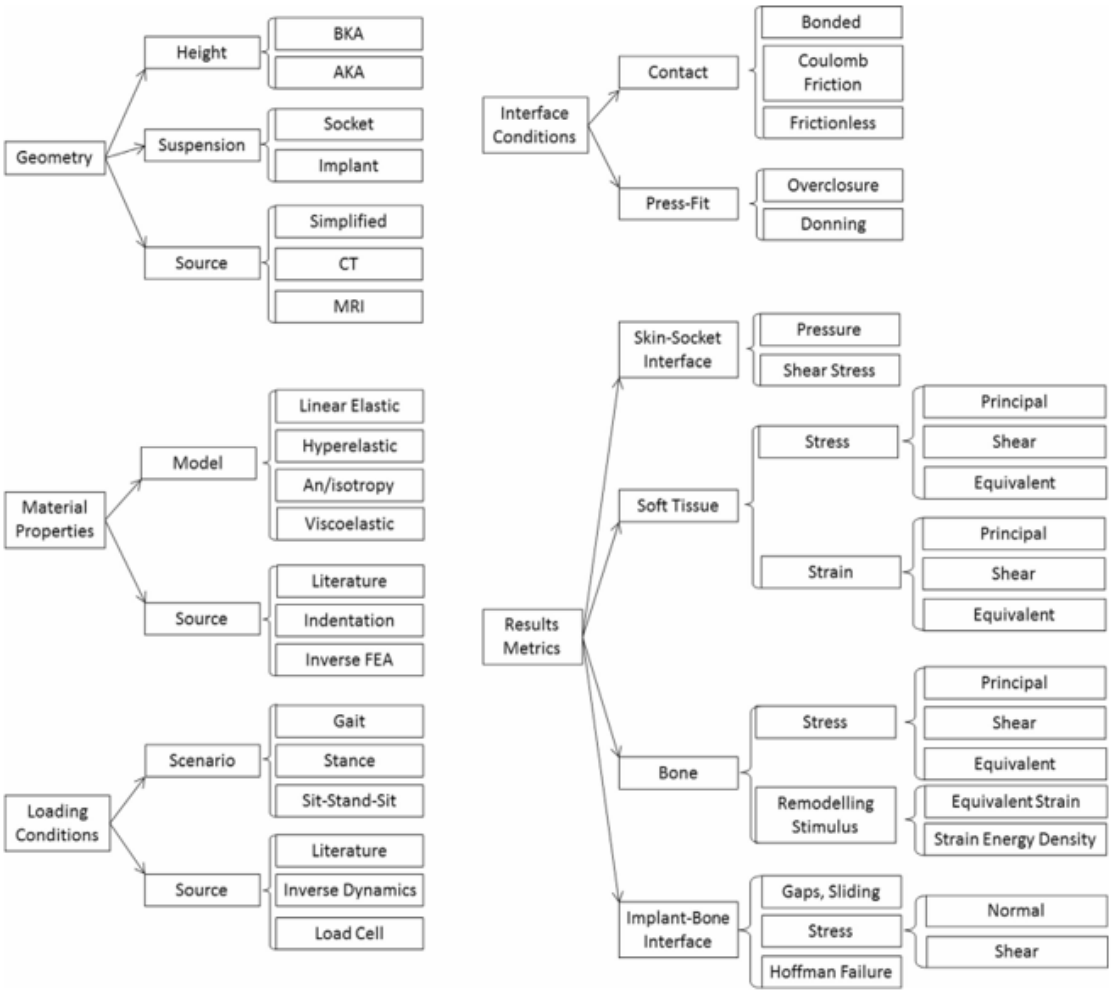

Figure 5.2 Methodological categories extracted from literature [45]

5.1.1. Geometry and mesh

Generally, the model is generated by means of imaging techniques, like MRI or CT scans. These techniques allow to have a patient-specific model of the stump. Instead, socket can be imported through an imaging technique or a CAD software. Lee et al. [46] used an unloaded MRI of limb and CAD rectified socket. Wu et al. [47] used an unloaded CT of the limb in the socket. Steer et al. [44] generated the FE model of the stump from MRI scans that were segmented into bones, soft tissue, tendon, and meniscus, while the socket was developed by copying and modifying the external shape of the residual limb.

The model of the stump has become more accurate over the years. At first elements considered are soft tissue and bones, as it was done by Zhang et al. [48]. Later, other parts have been added to the model. Cagle et al. [49] included patellar tendon in their model and Steer et al. [44] considered tendon and meniscus. For what concern the prosthesis, the kind of socket and suspension must be chosen. Recent data suggests that only 18% of sockets in clinical practice are PTB designs. Instead, the majority of contemporary sockets are total surface bearing (TSB). Then, contemporary sockets are intended to decrease peak pressures by distributing loads over the limb-socket interface, rather than focusing pressures on load-tolerant areas of the residual limb and this has been made possible through use of elastomeric liners [50].

After the geometry is imported in the software used for the analysis, it is discretized with the mesh. The type of elements and the number of nodes must be chosen. Following some examples are mentioned. Jia et al. [51] adopted a mesh with 3D 4-node tetrahedral elements for the entire model. Zachariah et al. [52] chose a 3D 8-node hexahedral elements for the soft tissue and 2D 4-node shell elements for the socket. Instead, Cagle et al. [49] used 8-node hexahedral elements for the socket (type C3D8R) and liner (type C3D8RH, a hybrid element that better emulated incompressibility), and 10-node tetrahedral elements for soft tissue (type C3D10M). For this matter, it's necessary to find a compromise between the number of nodes and the computational cost because if the number of nodes increases, the accuracy of the results improve, but also the simulation time enhances. So, order, shape and size of the element must be chosen wisely.

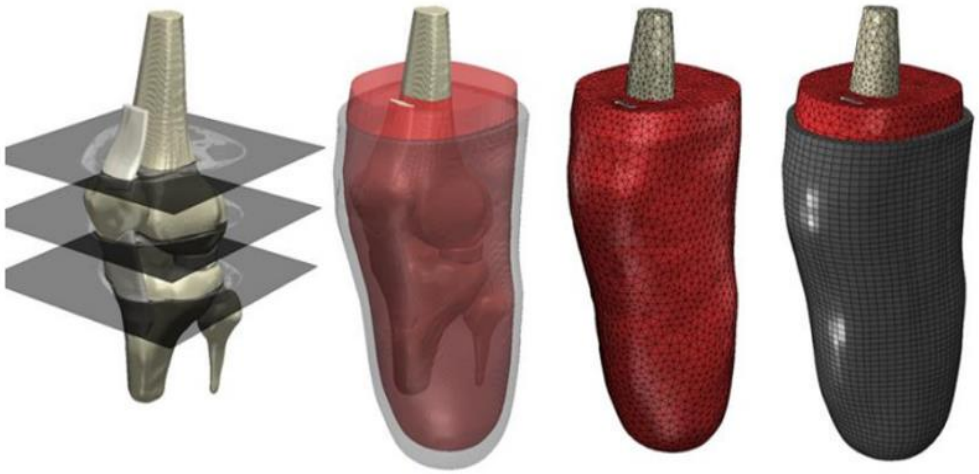

Figure 5.3 Development of the FE model from the MRI scan, involves the segmentation of the bones, the segmentation of the soft tissue and liner, the generation of the quadratic tetrahedral mesh of the limb and the hexahedral mesh of the liner [44]

5.1.2. Material properties

As a matter of simplicity, all materials are assumed as isotropic, homogeneous, and linearly elastic. Following some examples taken from the literature are reported.

Source	Bones	Soft Tissue	Liner	Socket
Zhang and Roberts, 2000 [48]	E = 15 GPa ν = 0.3	E = 160-260 kPa ν = 0.49	E = 0.38 MPa ν = 0.3	Rigid
Lee et al.,2004 [46]	E = 10 GPa ν = 0.3	E = 200 kPa ν = 0.49	N/A	E = 1.5 GPa ν = 0.3
Jia et al., 2004 [51] **Jia et al., 2005 [53]**	E = 10 GPa ν = 0.3	E = 200 kPa ν = 0.49	E = 0.38 MPa ν = 0.39	Rigid
Cagle et al., 2018 [49]	Rigid	E = 300 kPa ν = 0.45	Hyperelastic	E = 19 GPa ν = 0.1
Zachariah e Sanders, 2000 [52]	Rigid	E = 965 kPa ν = 0.45	N/A	E = 1 GPa ν = 0.35
Wu et al., 2003 [47]	E = 15.5 GPa ν = 0.28	E = 100-400 kPa ν = 0.49	E = 1 MPa ν = 0.49	Rigid
Lin et al., 2004 [54]	E = 15.5 GPa ν = 0.28	E = 60-700 kPa ν = 0.45	E = 0.4-0.8MPa ν = 0.45	Rigid

Sanders and Daly,1993 [55]	Rigid	E = 131 kPa ν = 0.49	N/A	E = 1.8 GPa ν = 0.39

Table 5.1 Mechanical properties in literature

Generally, bones are described as a linear elastic material with a Young Modulus of 10 GPa or 15 GPa and a Poisson ratio of 0.3. Characterizing bones as rigid material is another option because their stiffness is six order greater with respect to the one of soft tissue.

Material of the socket is commonly the polypropylene, with a Young Modulus in the range 1-1.8 GPa and Poisson ratio of 0.1-0.39. Another possible material is the carbon fiber, that is adopted for example by Cagle et al. [49]. It has a Young Modulus of 19 GPa and a Poisson ratio of 0.1. As a matter of simplicity and when the researcher is not interested in stresses and deformations in the socket, it can be modeled as a rigid material because its Young Modulus is also much higher with respect to that of soft tissue.

As said before, liner can be made with different materials and the most chosen is the silicone. Generally, it was adopted a linear elastic model with a Young Modulus of 0.4-1 MPa and a Poisson ratio of 0.3-0.49. Cagle et al. [49], instead, decided to use a nonlinear model. They chose the Yeoh constitutive model with material coefficients of: C10 = 2.014E+04, C20 = −1.541E+03, and C30 = 4.094E+02. Also Steer et al. [44] adopted an hyperelastic model, namely the Neo-Hookean. In this case the hyperelastic constitutive model parameters were C = 37.6 kPa and D = 0.54MPa^{-1} and they were calculated by means of the following expressions:

$$C = \frac{E}{4(1+\nu)} \tag{5.1}$$

$$D = \frac{6(1-2\nu)}{E} \tag{5.2}$$

where E is the elastic modulus, ν is the Poisson's ratio.

The last component to analyze is the soft tissue and this is the most complex material in terms of structural heterogeneity. A human soft tissue consists of skin, adipose tissue, muscle, connective tissue, veins, each with its own substructure. The result of this complexity is an anisotropic mechanical response. Each layer might also be affected by inhomogeneities, like scar tissue or fat infiltration. Soft tissues are known to exhibit highly nonlinear and time-dependent behaviors and due to high water concentration, they can be considered incompressible [56]. In most of the models in the literature all the parts that composed soft tissue are homogenized into a single soft tissue bulk, even if there are examples in which the stump is divided in different layers: both Portnoy et al. [57] and Restrepo et al. [58] considered skin, muscle, and fat to analyze the influence of each layer on the results (Fig. 5.4). However, in this case the

complexity of the model and the computational cost increased a lot. At first, linear elastic constitutive model was largely used. Generally, the Young Modulus is between 0.1 and 0.4 MPa, with some exceptions (e.g., Zachariah e Sanders, 2000 [52]), and the Poisson ratio has a value of 0.45 or 0.49. These parameters were obtained by means of indentation tests.

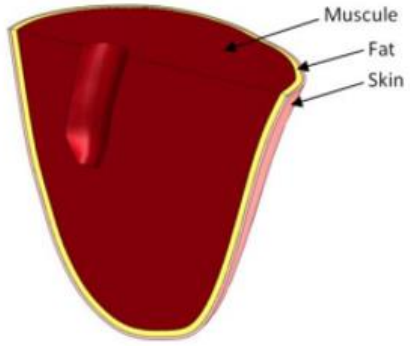

Soft Tissue	C_{10} (kPa)	C_{11} (kPa)	D_1 (MPa^{-1})
Skin	9.400	82	0
Fat	0.143	0	70.20
Muscle	8.075	0	1.243

Figure 5.4 Multilayer stump and soft tissue mechanical properties where C_{10}, C_{11} and D_1 are the hyperelastic constitutive model parameters, Restrepo et al. [58]

Linear elastic simplifications have been largely replaced by hyperelastic models, like Neo-Hookean or Mooney-Rivlin. Several hyperelastic models have been employed in modeling the soft tissues in amputated limbs, and they are formed from a strain energy density (SED) function W. This is expressed in terms of the deformation invariants of principal stretch ratios I1 and I2, and the total volume ratio J, which are calculated from the FEA predicted model deformations. The SED function contains constitutive parameters Cij and D1 which are material constants, and these are obtained by empirical fit of a selected SED function's stress–strain profile to experimental data. The identified studies used SED functions taken from general material characterization studies rather than model or patient-specific information [59]. Substantial work demonstrated the application of a Mooney-Rivlin model in a transtibial amputation FE model enabling the simulation of hyperelasticity in the bulk soft tissue [44]. Lacroix et al. [60] also used Mooney-Rivlin model with 3 coefficients: C10=4.25 kPa, C11 = 0 kPa, D1 = 2.36 MPa^{-1}. However, Steer et al. [44] demonstrated that negligible differences were noted between linear and hyperelastic models of equivalent initial stiffness and the most notable one was the increased numerical stability of the hyperelastic models.

As previously mentioned, in some studies tendons were added to the model to obtain more accurate results. The patellar tendon has been reported to have a stiffness value as low as 260 kPa [61] and as high as 2.0 GPa [62]. Such differences are likely due to different testing methods and orthotropic material composition of the tendon. Cagle et al. [49] chose a stiffness value of 150MPa for the patellar tendon. Instead, Steer et al. [44] assigned a stiffness value of 400 MPa to tendons.

5.1.3. Loading conditions

The scenario to be simulated must be chosen in terms of loading conditions. In general, the situations used in literature are donning, standing, and gait.

Socket donning applies pre-stresses to the residuum tissues. Simulating this process presents a complex, nonlinear problem for the FE model to reconcile the difference in shape between the limb and the press-fit socket. There are two ways to implement it: a simplified 'overclosure' method, where the external surface nodes of the residual limb are displaced until they contact the internal surface of the socket, and explicitly donning (Fig. 5.5). Lacroix et al. [60] compared the relative differences between these methods with transfemoral models. They found that donning introduced longitudinal shear stresses at the interface periphery, which were not captured by radial overclosure. Moreover, Steer et al. [44] found substantial differences in pressure and shear at the residuum tip. Inclusion of socket donning increases proximal interface shear, which stabilized the construct, thus protecting the residuum tip from such elevated pressure. Another possible way to implement the donning procedure was presented for example by Lee et al. [46]. They applied an axial force of 50N to approximate the force stabilizing the limb in the socket.

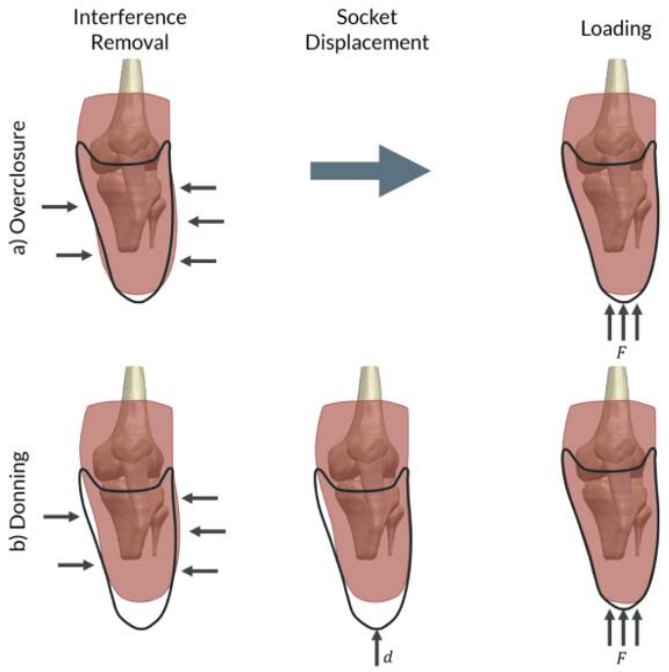

Figure 5.5 Comparison of two socket donning methods: (a) overclosure, (b) explicit donning [44]

After the donning, loads are applied to simulate the standing and the gait. Lee et al. [46] applied external loads on the knee joint as shown in Figure 5.6. Three load cases were used separately to simulate the loading conditions at foot flat, mid-stance and heel off during walking. As boundary conditions, it was assumed that the knee joint angle did not change at different loading cases and the external surface of the socket was fixed.

Jia et al. [51] applied the external forces and moments during walking at the knee joint keeping the pre-stress and the deformation due to donning and they rigidly fixed the outer surface of the liner assuming the hard socket would offer a rigid support.

Cagle et al. [49] evaluated two distinct loading profiles. The first profile had only a vertical component. Instead, the second loading profile was a simulation of heel-strike to the first peak of the gait cycle, and contained components that included: vertical load, horizontal load, and sagittal moment. Loading was applied distally with no constraints placed on the sockets' resultant displacements or rotations.

Steer et al. [44] simulated a uniaxial 400 N load case representing double leg standing, and three quasi-static load points from gait corresponding to heel-strike, mid-stance and toe-off. They constructed a coordinate system from the residual tibia's principal axes and modeled only forces and moments in the sagittal plane which are the dominant forces during gait. The Fy and Fz forces and the moment Mx were applied across a circular region of nodes at the base of the socket, representing the pylon connection. Throughout all stages of model loading, the proximal surfaces of the femur and quadriceps tendon were fixed in all directions.

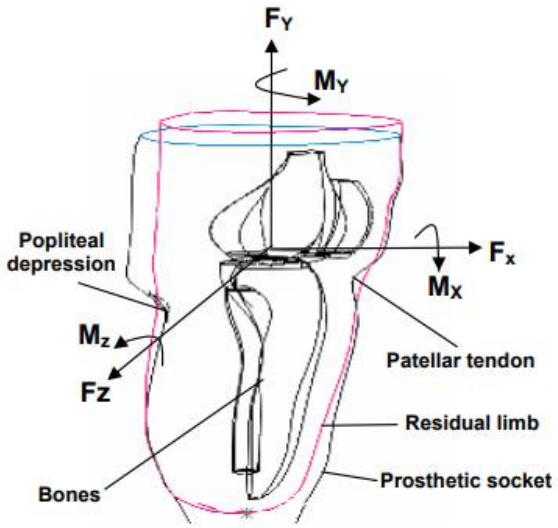

Figure 5.6 Assembled socket (black profile), limb (pink profile) and bone surfaces with forces and moments applied at the center of the knee [46]

When only the body weight is considered in the simulation, a static analysis is implemented. Then, during the gait the loads change in time, so the analysis becomes quasi-static. If also the material inertial effects are considered, a dynamic model is introduced. The simulation becomes more accurate, but it requires more computational cost [36]. However, in the stance phase the interface pressures and shear stresses don't change significantly no matter the inertia effects were considered or not, as it shown by Jia et al. [36]. Instead in the swing phase no ground reaction force is present, so the inertia plays a primary role in the calculation of equivalent loads. As a result, interface pressures and shear stresses are considerably different between two

loading cases with and without considering inertial effects. All these results are shown in Figures 5.7 and 5.8.

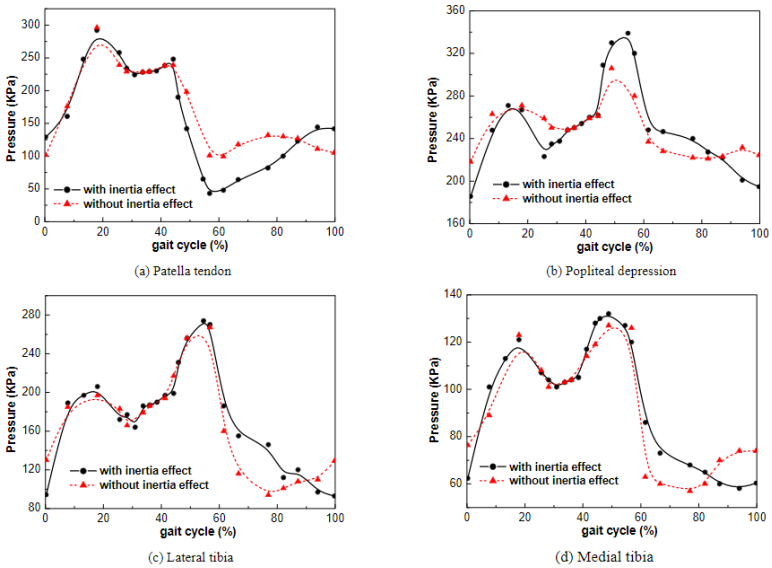

Figure 5.7 Comparison of pressures on residual limb with or without consideration of inertial effects during the whole gait cycle [36]

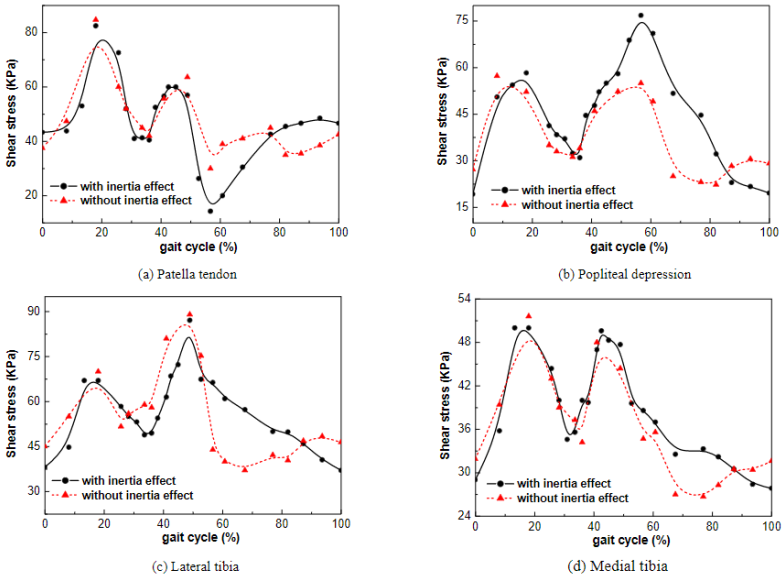

Figure 5.8 Comparison of resultant shear stresses on residual limb with or without consideration of inertial effects during the whole gait cycle [36]

5.1.4. Interface conditions

The choice of contact model is very important because it will have a substantial influence on pressure and shear stress outputs. Two different interfaces should be considered: residuum-liner and socket-liner interfaces.

Generally, a single coefficient of friction (COF) value between limb and prosthesis is chosen and it ranges from 0 (frictionless) to 1 (bonded), even if most commonly it is between 0.4 and 0.5. This indicates the use of a Coulomb 'stick-slip' friction model, whereby tangential force can be transmitted until its magnitude exceeds the product of the normal force and COF, when tangential relative displacement is permitted. Then, no difference between static and dynamic COF is considered [45].

The socket-liner interface is generally set at 0.5, that is a median value reported in the prosthetic literature. At the skin-liner interface COFs greater than 3.0 have been reported in amputee skin studies and benchtop measurements of prosthetic liners; however, preliminary simulations evaluating the effect of varying COF showed that a COF of 2.0 approximated a bonded contact. So, a simulated COF of 2.0 is suitable representation of any liner with COF greater than 2.0 [49]. In their study, Steer et al. [44] adopted a static COF at the liner-socket interface in a Coulomb slip-stick model. A baseline value of 0.5 was chosen and was varied in increments of 0.1 between 0.3 and 0.7. The residuum-liner surface was fully bonded, representing a sticky gel liner. Different friction coefficients result in different shear stresses, in particular higher friction gives reduced residuum tip pressure. Regarding the value of COF, the presence of moisture, grease or sweat at the skin surface, or the elevated temperature and humidity should be considered. Ramirez et al. [63] observed that artificial sweat and hair could produce COF values as low as 0.22. Moreover, sweat and sebum may, in sufficient quantities, produce lubricating effects and reduce the shear stress established in the skin, and they may also reduce the threshold strains sustainable before tissue damage occurs [64].

Then, to model the interaction between the residual limb and socket, the automated surface-to-surface contact is usually used. As reported by Wu et al. [47], it is better than the traditional point-to point contact pairs. Then, master and slave surfaces must be defined. The choice of slave and master surfaces must be made carefully in order to achieve the best possible contact simulation. So, some rules must be followed: the slave surface should have the finer mesh and if the mesh densities are similar, it should be the surface with the softer underlying material. The contact simulation offered in *Abaqus*/CAE is described as follows (Fig. 5.9). Normal vectors, e.g. N2, are computed for all nodes on the master surface by averaging the normal vectors of outward edges (1-2 and 2-3 segments) making up the master surface and additional normal vectors, e.g. NL/2, are computed at the middle of each segment. Those normal vectors together with the element size and function are used to define a set of smooth varying normal vectors on the whole master surface. An "anchor" point on the master surface X0 is calculated for each node on the slave surface (slave node) so that the vector formed by the slave node and X0 coincided with the normal vector N(X0) of the master surface. A tangent plane is found out at every "anchor" point which is perpendicular to the normal vector. Under the strict master-slave contact algorithm in *Abaqus*/CAE, the slave nodes are automatically constrained not to penetrate their tangent planes on the master surface when two surfaces come into contact [66]. As example, in Jia et al. [51]

the inner surface of prosthetic liner and the residual limb surface were defined as the master surface and slave surface respectively.

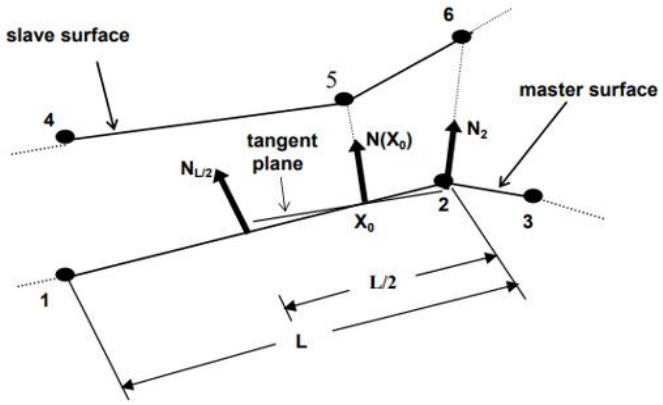

Figure 5.9 Master-Slave Surface contact algorithm [66]

5.1.5. Results

Generally, the focus of these studies is the analysis of stress in soft tissue and bones and pressure and shear stress at the skin-socket interface. In the following, some examples taken from the literature are presented. For what concern donning, Steer et al. [44] found that the inclusion of socket donning increased proximal interface shear: 22 kPa in donning versus 4 kPa in overclosure were found as values in this region. This stabilized the construct, thus protecting the residuum tip from elevated pressure (0 kPa in donning vs 41 kPa in overclosure). Figure 5.10 shows the different results obtained with the two press-fitting methods.

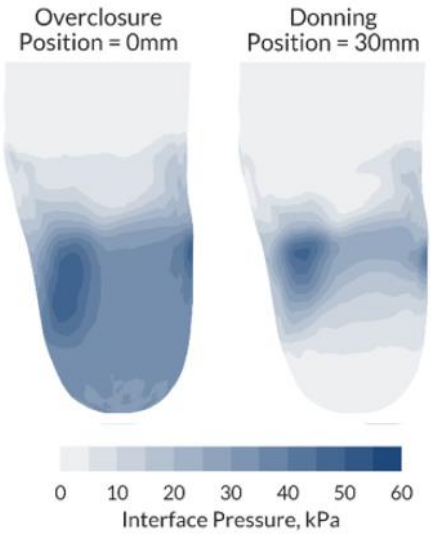

Figure 5.10 Interface pressure predictions under stance loading for different socket press-fitting methods [44]

Zhang et al. [48] worked on the comparison of FEM and experimental pressures and shear stresses, validated with triaxial force sensor. A static load of 800 N was applied to the model. They obtained a maximum value of 90 kPa of pressure at the patellar tendon and a maximum value of shear stress of 50 kPa at lateral tibia.

Lin et al. [54] applied a 600N axial load to simulate single leg stance. They obtained a maximum pressure of 783 kPa and a maximum shear stress of 373 kPa.

Lee et al. [46] analyzed the normal stress distributions when the limb was donned into the socket. High normal stress was produced at the regions of patellar tendon (96kPa), popliteal depression (147kPa), anteromedial tibial (52kPa) and anterolateral tibial (84kPa). Then they simulated three phases of the gait cycle and the maximum value reached was 300 kPa at heel-off phase in the popliteal depression. Resultant shear stress distribution at the limb/socket interface was also considered and the maximum value reached was 110kPa over the patellar tendon region at foot flat phase. The other peak values are shown in Figure 5.11.

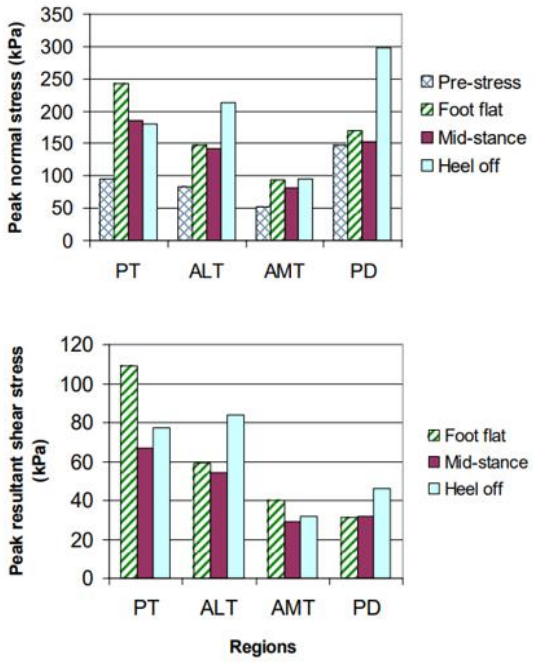

Figure 5.11 Peak normal stress and peak resultant shear stress at patellar tendon (PT), anterolateral tibia (ALT), anteromedial tibia (AMT), and popliteal depression (PD) [46]

For what concern internal stresses and strains, there are not so many results as the interface pressure. This does not mean that they are less important because they allow to evaluate deep tissue injuries. As example, Portnoy et al. [67] reported the internal stress and strain distributions at the distal ends of the tibia and fibula. Stresses under the fibula were at least one-order-of-magnitude lower than under the tibia. Peak internal strains under the tibia were 85%, 129% and 106% for compression, tension and shear, respectively. Peak internal strains under the fibula were substantially lower:

19%, 22% and 19% for compression, tension and shear, respectively. Some values are shown in Figure 5.12.

Parameter	Tibial tuberosity	Tibia end	Popliteal depression	Fibula head	Fibula end
Principal compressive strain (%)	7	85	0.2	0.2	19
Principal tensile strain (%)	6.9	129	1.8	4.5	22
Maximal shear strain (%)	8.9	106	1	1.5	19
Strain energy density (kJ/m^3)	0.04	104	0.01	0.02	1
Principal compressive stress (kPa)	3.3	240	1.1	4	8.9
Principal tensile stress (kPa)	1.4	263	0.7	7	2.2
Maximal shear stress (kPa)	0.5	23	0.4	3.2	3.3
von Mises stress (kPa)	1.3	215	0.9	6.4	7.4

Figure 5.12 Calculated strains, strain energy densities and stresses at important anatomical sites [67]

6. Preprocessing

This section is intended to present the software used prior to the simulation in *Abaqus*/CAE to acquire the model elements in an appropriate format. *Geomagic Design X* and *Meshmixer* are the names of these programs.

Meshmixer is an open-source software for working with triangle meshes. It is used to clean up a 3D scan, do some 3D printing, or design an object that fits into another [71]. This software was adopted to build the socket and the liner directly from the stump, as well as to create a model of the soft tissue.

Instead, *Geomagic Design X* is a powerful software that allows to build CAD models from 3D scan data. It requires minimal training and reduces the time necessary to process 3D scan data. Users are provided with high quality results that are unavailable through other current reverse engineering options. *Geomagic Design X* also enhances the functionality of both 3D scanning technology and existing CAD applications by sharing common technologies and processes [68]. The main use of this software in the work is the conversion of files from STL format into STEP format. STL, that is the abbreviation for STereo Lithography interface format, is an interchangeable file format that represents 3-dimensional surface geometry. It represents a surface as a series of small triangles, known as facets, where each facet is described by a perpendicular direction and three points representing the vertices of the triangle [69]. Instead, STEP stands for Standard for the Exchange of Product model data and this format is a widely used data exchange format for computer-aided design [70].

The effort began with a collection of STL files received from an MRI of an amputee transtibial patient's residual limb. The components were the femur, tibia, patella, and skin. Since the stump was so short, there was no fibula.

6.1. Geometries

The following paragraphs will describe how geometries of soft tissue, liner and socket were obtained by means of *Meshmixer*. The performed steps were necessary because no images of these parts were available. The starting point for all the operations was the STL file with the skin, that was a representation of the stump of the patient with only the outer shell. To obtain the soft tissue this part was filled and so a homogeneous bulk was obtained. So, skin, muscles, fat layers and all the other elements that formed the stump were considered as a unique part. Instead, to get the liner and socket their shapes were depicted over the skin surface and then, with an offset tool properly used, thickness was given to each part. Below all the steps will be illustrated in depth.

6.1.1. Soft tissue

Meshmixer was used to import the STL file containing the skin (Fig. 6.1). The goal of this procedure was to get a depiction of soft tissue, which is the union of skin, muscle, and fat layers into a single bulk.

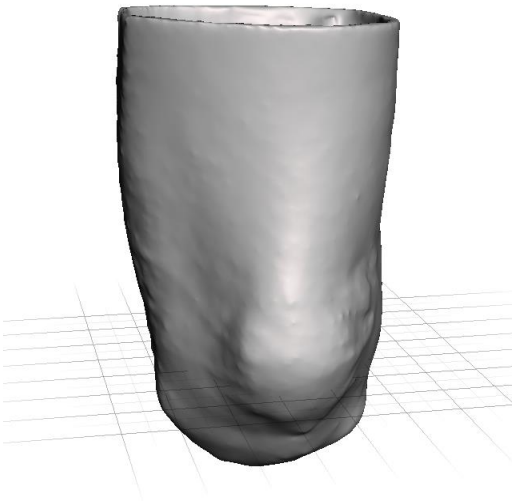

Figure 6.1 Skin part

The *Select* tool was then used to highlight all of the interior parts of the skin, which were then destroyed with the *Discard* tool. The inside section was filled with the *Inspector* tool, and soft tissue was retrieved (Fig. 6.2). This section was exported as an STL file, and the work was carried out utilizing *Geomagic Design X*.

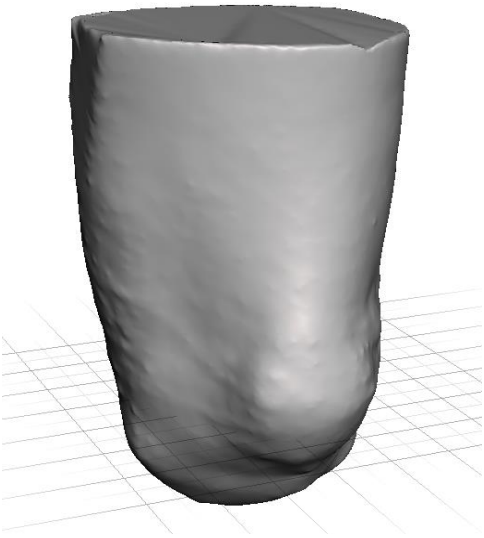

Figure 6.2 Skin part after *Inspector* tool

6.1.2. Liner

The liner was also acquired when working on the skin. The liner was sketched on the skin part through the *Select* tool (Fig. 6.3). Then, with the command *Smooth boundary* a crisp edge loop embedded in the mesh was obtained.

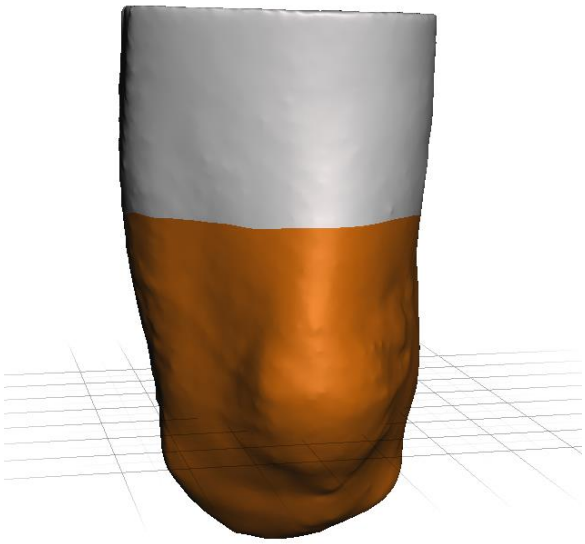

Figure 6.3 Liner shape highlighted with *Select* tool

In the *Edit* section, the thickness of the liner was created by means of the *Offset* tool. Firstly, the connected option was deselected and a zero-distance value was assigned in order to keep the liner adherent to the skin. Then, the *Offset* was used again, and the distance was chosen to be 3 mm. This value represented the liner thickness. In the *Deform* menu, the *Smooth* function was applied to smooth out the boundaries. Then, a more regular surface was obtained using the *Sculpt* tool. The resulting file was exported as STL file (Fig. 6.4). The work on this part was continued on *Geomagic Design X*.

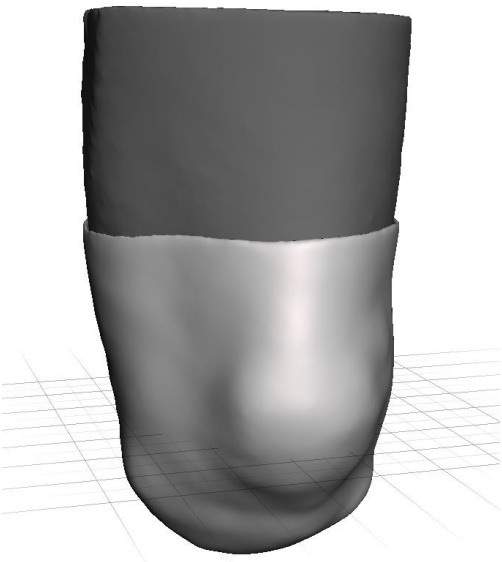

Figure 6.4 Liner STL file

6.1.3. Socket

The skin component served as the starting point for designing the socket. As a result, it was imported into the software. In terms of the liner, the form of the socket was highlighted on the skin using the *Select* tool (Fig.6.5), and a crisp edge loop embedded in the mesh was generated using the command *Smooth* boundary.

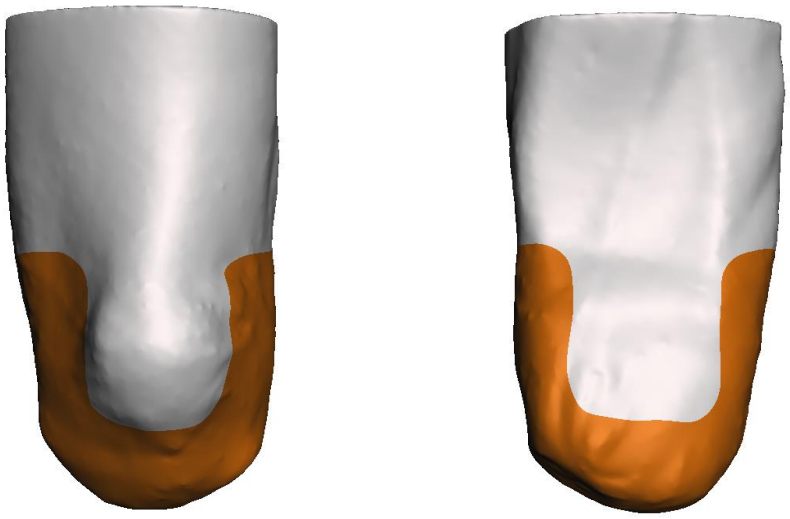

Figure 6.5 Socket shape: anterior and posterior view

The *Offset* tool was then used twice. In the first, the shape of the socket was moved 3 mm away from the skin's surface. Then, in the second stage, the connected option was selected in the *Offset* menu, and a thickness of 5 mm was assigned starting from the shifted shape of the socket. The *Smooth* feature in the *Deform* menu was enabled to smooth the boundaries. There may be errors in the mesh as well, which had to be corrected. The boundaries were examined for inaccuracies, which were identified and eliminated when they were discovered. These regions were corrected using the *Inspector* tool, filling the gaps generated and deleting the errors, and manual smoothing was performed on these parts of the model with the *Sculpt* tool. As a result, a socket that fit the residual limb was obtained. To minimize excessive pressure, a gap should be established between the bottom of the stump and the end of the socket. Indeed, the end of the stump has a pressure threshold value that can withstand. So, a cylinder was added under the stump from the element already present in the software (Fig. 6.6). This element should be integral with the socket. The top of the cylinder was removed and then the same thing happened to the bottom of the socket using the *Plane cut* and *Discard* tools (Fig. 6.7).

Figure 6.6 Cylinder element

Figure 6.7 Removal of the upper part of the cylinder and the lower part of the socket

After that, the two parts were highlighted with the *Select* tool, and in the *Edit* menu the *Join* function was activated. So, the socket and the cylinder were joined. Then, the *Smooth* tool allowed to have a better union. To improve the outside surface, the *Sculpt* tool was used. Other adjustments were required. The thickness of the socket is not uniform because the prosthetist generally modifies it adding or removing material in the critical and tolerant zones. In this work, this procedure was simulated by means of the *Offset* tool. The popliteal area and the sub-patellar region were highlighted through the *Select* tool and then the *Offset* was activated (Fig. 6.8). A negative value of 3 mm was given because these areas are pressure tolerant. Finally, with the *Sculpt* tool, a smoothing operation was realized on these regions to avoid great changes over the surface.

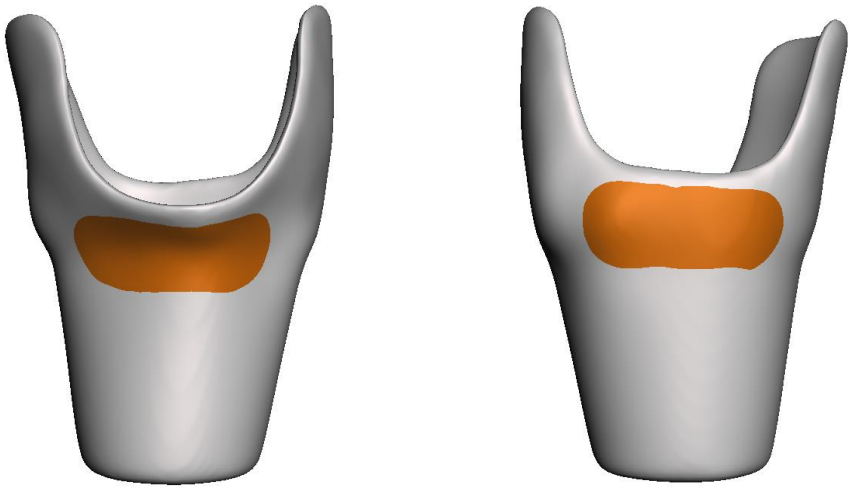

Figure 6.8 Modification of sub-patellar and popliteal areas

The final file was saved as an STL file (Fig. 6.9), and the work was resumed in *Geomagic Design X*.

Figure 6.9 Socket STL file

6.2. Geomagic Design X

After getting the parts, the subsequent step was to transform the models into solid versions. This action was performed because all the parts must be imported in *Abaqus*/CAE that does not allow to use STL file. So, to achieve this goal *Geomagic Design X* was used. This software was also utilized to improve the shape of the part for example removing sharp edges because they could be a source of problems in *Abaqus*/CAE.

Following, the general processes executed in *Geomagic Design X* for each section will be outlined. The Femur is used as an example.

The STL file was imported in *Geomagic Design X*. The first steps were executed in the *Polygons* section of the menu bar. *Mesh Buildup Wizard* command was activated to create a defect-free and watertight mesh models from raw 3D scan data. It consists of 3-5 stages that enable the speedy creation of optimized mesh (Fig. 6.10) [68].

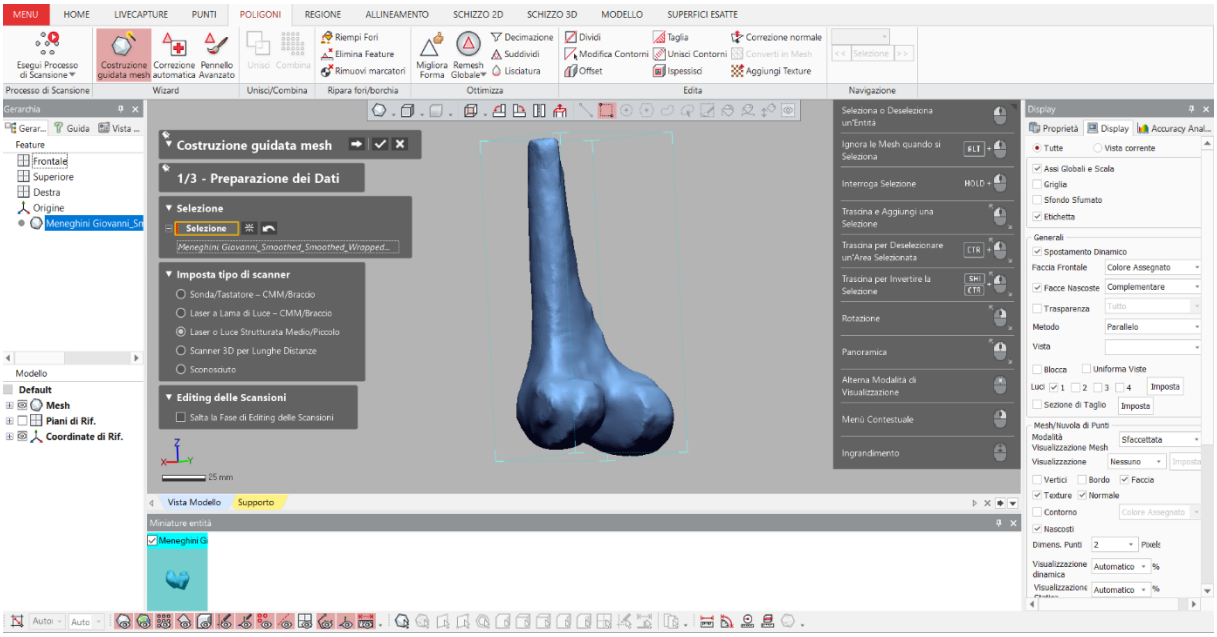

Figure 6.10 *Mesh Buildup Wizard*

After that, some holes were formed on the surface. Using the *Fill holes* tool, a manually filling in of the holes with poly-faces based on geometric feature shapes was performed (Fig. 6.11). Then, the *Healing Wizard* command was used (Fig.6.12). It was useful to create an optimal mesh model without any abnormal poly-faces and healing defects [68].

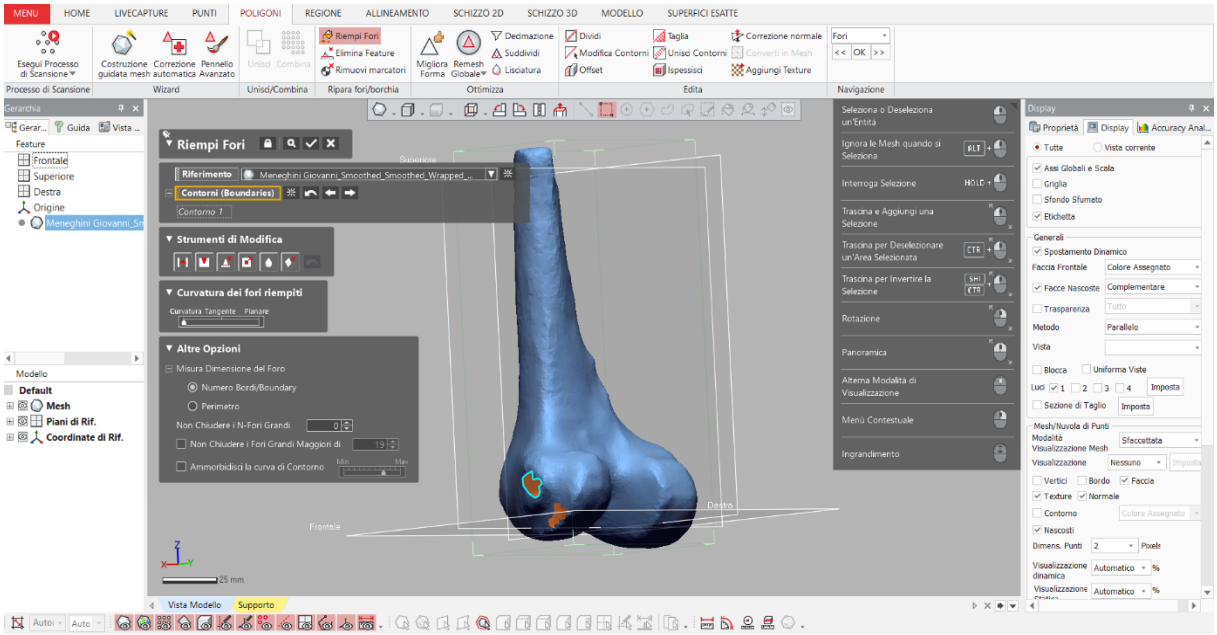

Figure 6.11 *Fill holes*

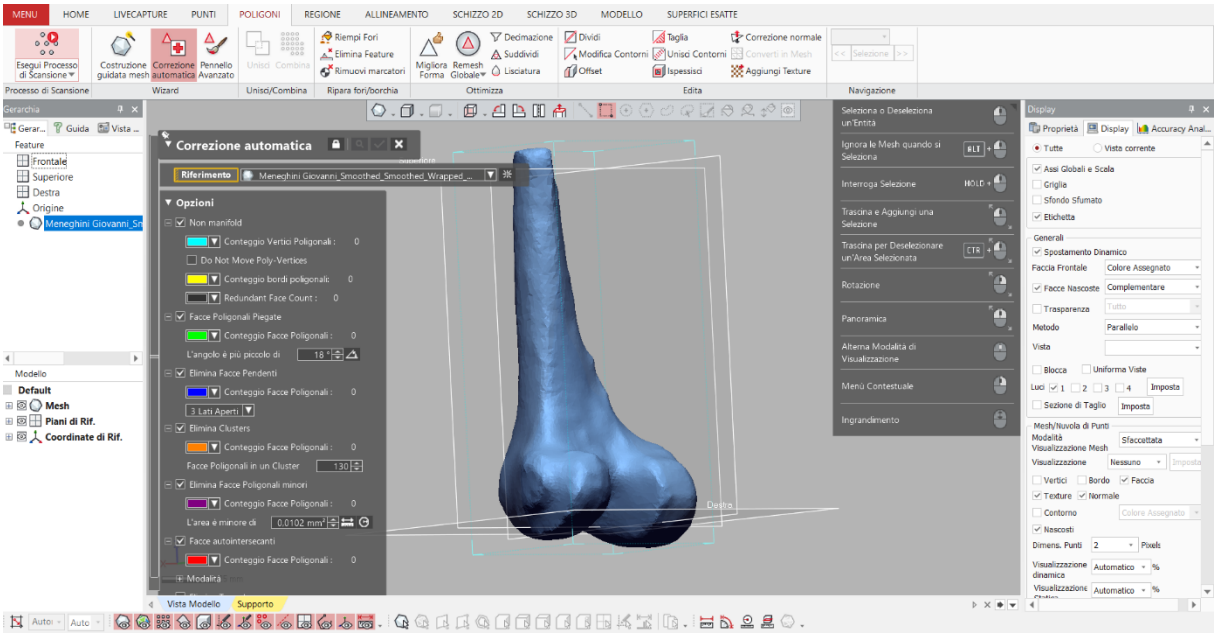

Figure 6.12 *Healing Wizard*

To improve the model, the commands *Smooth* and *Enhance shape* were used. The *Enhance Shape* command enhanced feature shapes by characterizing sharp areas and smoothing rounded corner areas. Instead, the *Smooth* command reduced the effect of noise and roughness in a mesh. Then, the *Thicken* command was adopted. It changed the volume of a mesh by giving a constant thickness to each face to create a completely closed mesh with no boundaries. This action was performed because sharp edges must be removed. Hence, the shape was no more the same, but the difference is minimal, and the geometry was preserved, so it was acceptable. It was important also for the liner-socket interface because it allowed to create overlaps between these two surfaces. The last step was performed in the *Surfacing* section and *Auto Surface* command was activated. It generated surfaces that mathematically fit CAD surfaces to mesh. During this process, the application automatically created a curve network that enveloped the entire mesh and filled fitting surfaces for each patch of the curve network [68]. Finally, the result was exported as a STEP file (Fig. 6.13).

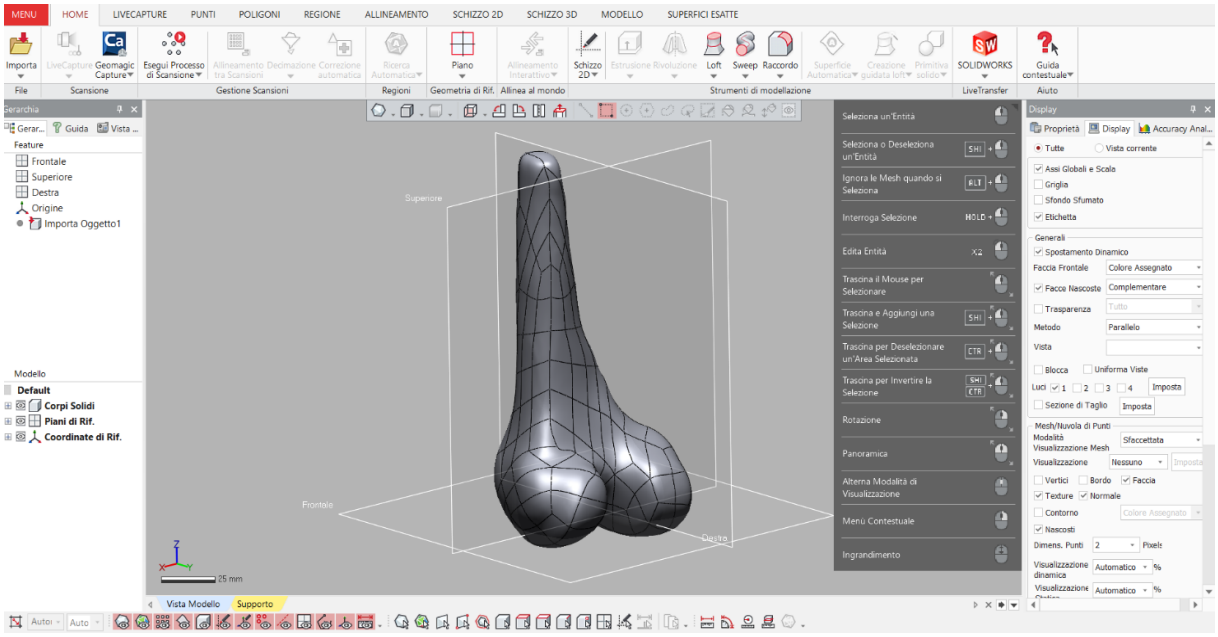

Figure 6.13 STEP format file for femur

Moreover, an additional step was performed but only on the soft tissue part. Before computing the *Auto Surface* command, the *Split* tool was activated (Fig. 6.14). Indeed, the upper region of this part was not so relevant for the aim of this work because there was no pressure tolerant or pressure sensitive areas, and so it could be neglected. In this manner, the computing cost of the final simulation was also decreased.

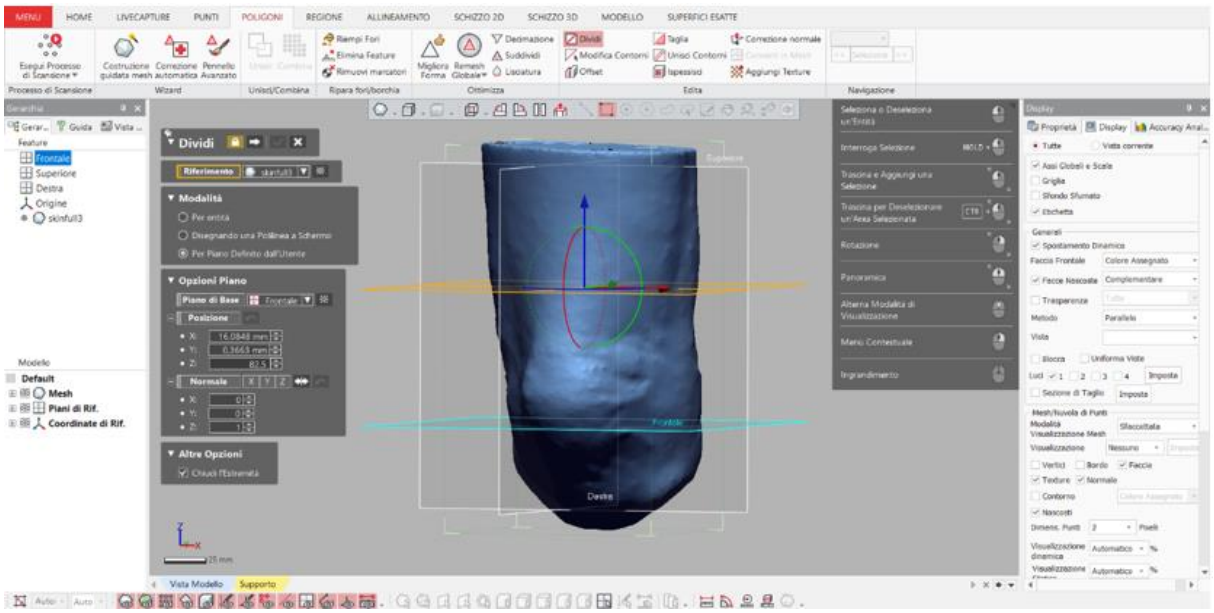

Figure 6.14 *Split* tool on soft tissue part

The other STL file format parts, including the femur, patella, soft tissue, liner, and socket, must follow the same technique. Figure 6.15 depicts the converted STEP format file results.

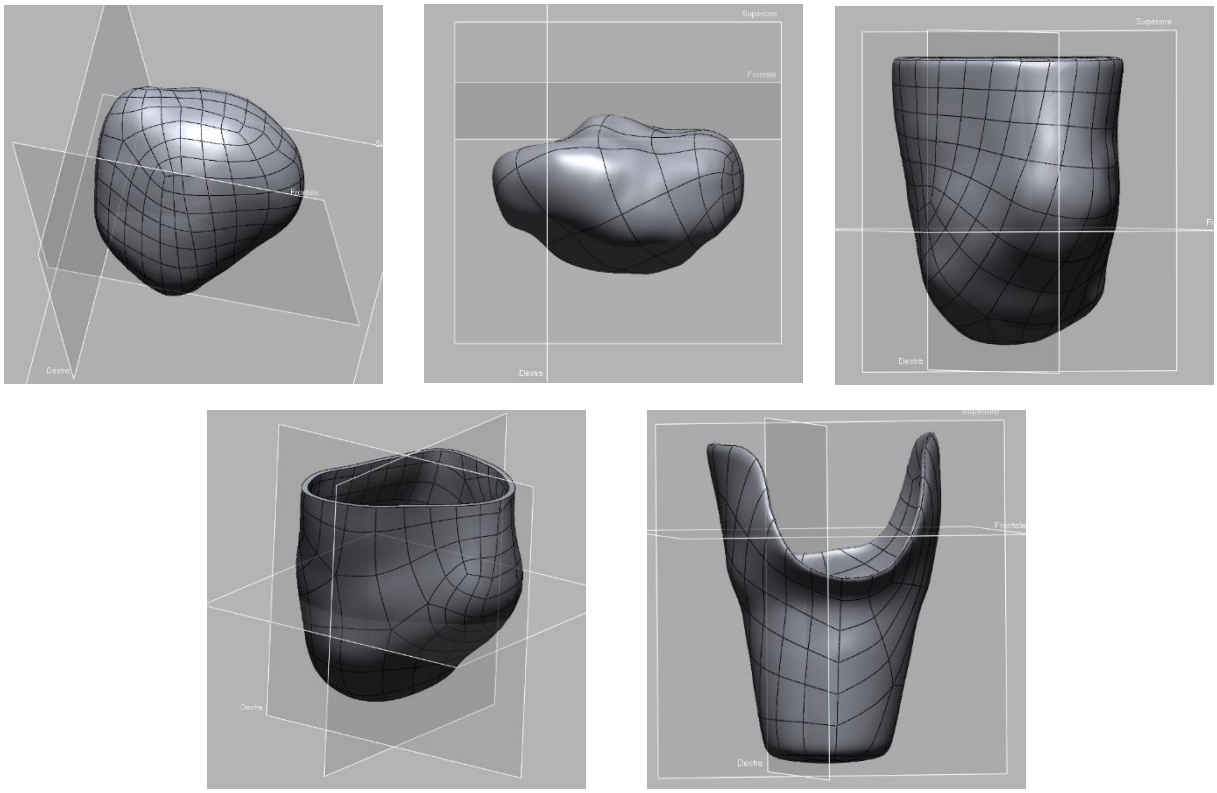

Figure 6.15 STEP format file of patella, tibia, soft tissue, liner and socket from left top to right bottom respectively

7. Materials and methods

This chapter will go over the processes utilized in *Abaqus*/CAE to achieve the final results. The work consisted in the creation of an input file with all the information of the model, as the geometries, material properties, interactions, etc. Then, this file was submitted for the analysis and when it finished, the results were examined.

The below description is structured into subsections, each of which represents a single module of the program, allowing for a step-by-step approach to problem description. In particular, the work was divided in the subsequent modules:

1) Part: parts of the model were imported in *Abaqus*/CAE.
2) Property: material definitions were defined and assigned to a section.
3) Assembly: part instances were created and assembled.
4) Step: analysis steps were created and defined.
5) Mesh: a finite element mesh was created.
6) Interaction: interactions between regions of the model were specified.
7) Load: loads and boundary conditions were identified.
8) Job: a job was submitted for the analysis and its progresses were monitored.

7.1. Part module

The STEP files generated by the Geomagic Design X software were imported into *Abaqus*/CAE using the *Import part* command. As a result, the following parts were examined in the final model:

- Femur
- Patella
- Tibia
- Soft tissue
- Liner
- Socket.

They were regarded as 3D deformable objects, as illustrated in Figure 7.1.

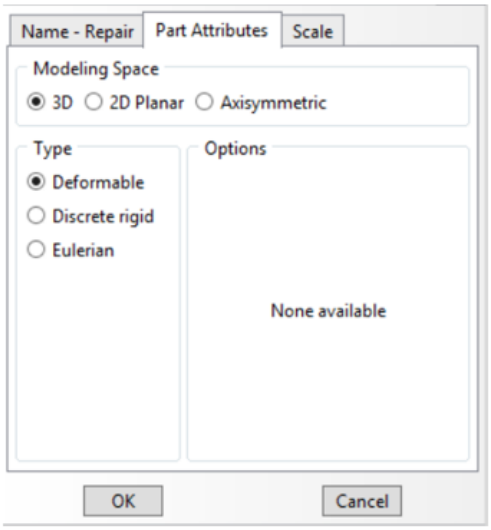

Figure 7.1 Part options

7.2. Property module

In the *Property* module materials of each part of the model were created. Then, a homogeneous solid section was created for each kind of material and all of them were associated to the relative component by means of the *Section Assignment* tool.

In *Abaqus*/CAE the system of units must be defined before defining the model. There is no built-in system of units, but all input data must be specified in consistent units [66]. Some common systems of consistent units are shown in Figure 7.2. In this work the SI (mm) was chosen. Stiffness values are generally expressed in terms of MPa or GPa, so this choice proved to be appropriate.

Quantity	SI	SI (mm)	US Unit (ft)	US Unit (inch)
Length	m	mm	ft	in
Force	N	N	lbf	lbf
Mass	kg	tonne (10^3 kg)	slug	lbf s^2/in
Time	s	s	s	s
Stress	Pa (N/m^2)	MPa (N/mm^2)	lbf/ft^2	psi (lbf/in^2)
Energy	J	mJ (10^{-3} J)	ft lbf	in lbf
Density	kg/m^3	$tonne/mm^3$	$slug/ft^3$	lbf s^2/in^4

Figure 7.2 Consistent units [66]

Bones were set to be a linear elastic isotropic material with a very high stiffness equal to 15E03 MPa and a Poisson ratio of 0.3 (Fig. 7.3) [48]. A density value was required to deal with dynamic step; therefore, it was set to 2E-09 tonne/mm^3 [18].

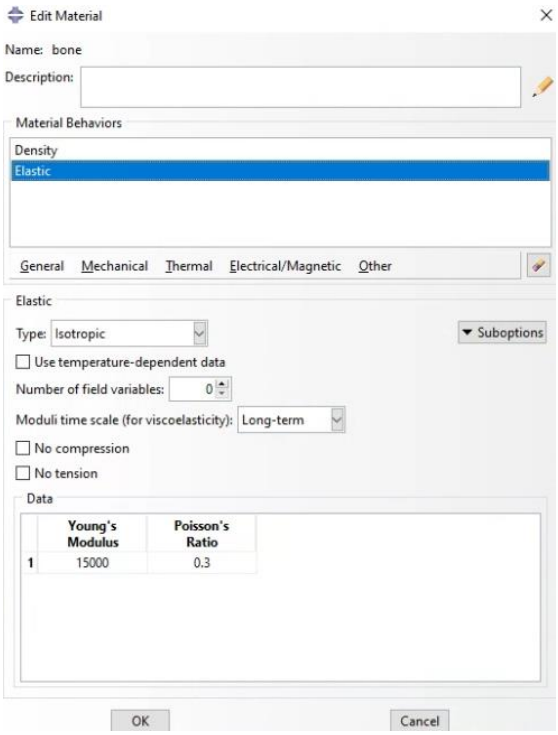

Figure 7.3 Material parameters for the bones

For what concern the soft tissue, different scenarios were taken into consideration. As previously mentioned, it is the most complex material in terms of structural heterogeneity. Moreover, mechanical properties change with different patients. So, two material models obtained from literature [44] were evaluated and the Neo-Hookean constitutive model was chosen. This model has two parameters to be defined: C and D. It is simple to use and can make good approximation at relatively small strains. The strain energy function is expressed as followed [72]:

$$W = C(\bar{I}1 - 3) + \frac{1}{D}(J - 1)^2$$

where C and D are hyperelastic constitutive model parameters, $\bar{I}1$ is the first invariant of the isochoric part of the right Cauchy-Green deformation tensor and J is the volume ratio.

Two material properties were implemented and the designations flaccid and contracted were given to distinguish them. Associated parameters are shown in Table 7.1.

Structure	C (kPa)	D (MPa^{-1})
Soft tissue - flaccid	6.2	1.62
Soft tissue - contracted	8.075	1.234

Table 7.1 Material parameters for the soft tissue

In this case the density was set to 1.48E-09 tonne/mm^3 [18].

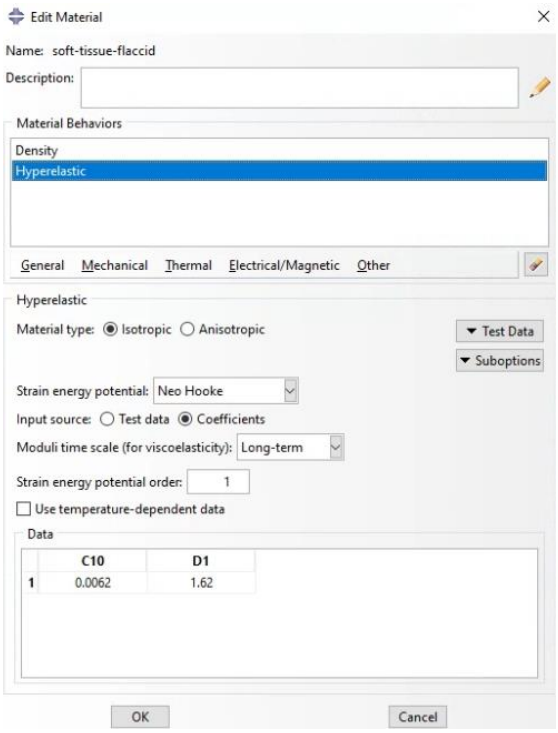

Figure 7.4 Material parameters for the soft tissue (soft tissue-flaccid)

The liner was set to be a linear elastic isotropic material, and, also in this case, different material properties were considered. The elastomeric polymers commonly used are silicone, urethane, and thermoplastic elastomer. Reasonable values were taken from a research study of Cagle et al. [32] and are shown in Table 7.2.

Material	Stiffness (MPa)	Poisson ratio
Silicone	0.384	0.4992
Urethane	0.318	0.4997
TPE	0.144	0.4998

Table 7.2 Material parameters for liner

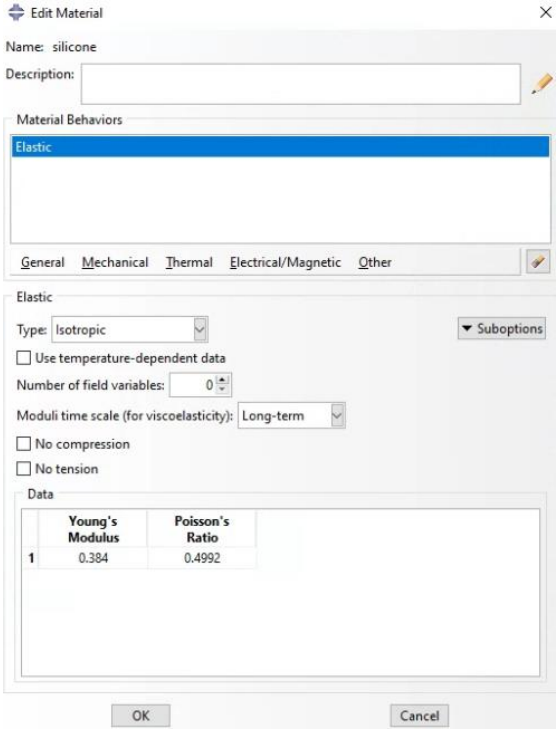

Figure 7.5 Material parameters for the liner (silicone)

For the socket the selected material was the Polypropylene, with a Young Modulus of 1.5E03 MPa, a Poisson ratio of 0.39 (Fig. 7.6) [44] and a density of 7.8E-09 tonne/mm^3 [18].

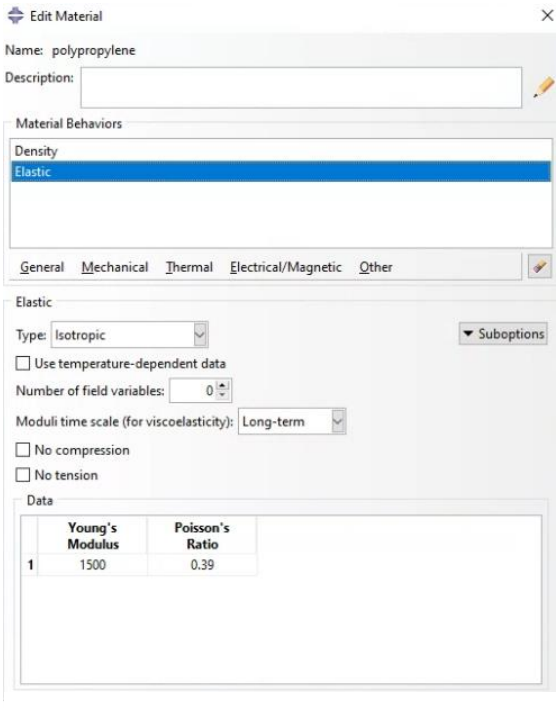

Figure 7.6 Material parameters for the socket

7.3. Assembly module

In order to create the assembly, six instances were created. They were independent, so the mesh was created in the assembly and not directly on the part. For what concern the soft tissue part, the space occupied by bones must be removed to avoid any kind of overclosure. So, the *Merge/Cut* tool was used to cut it away. Then, when the instance of the socket was created it was already in the right position because it was designed directly on the soft tissue. But in this work the donning procedure was simulated, so the instance was translated of -60 mm along the longitudinal axis (z-direction) and 5 mm on frontal axis (x-direction), as it shows in Figure 7.7. Generally, only a displacement along the longitudinal direction is given to simulate the donning, but in this case movements in a different direction was provided to avoid excessive penetration of the part, as will be explained below in the paragraph "Load module".

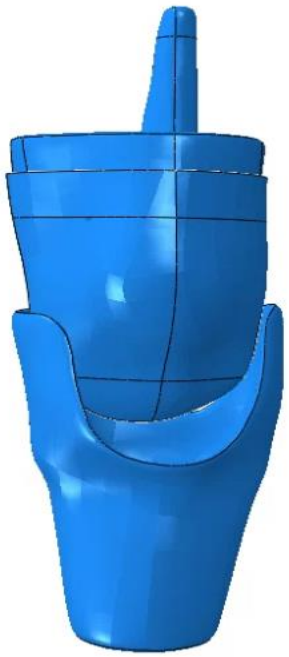

Figure 7.7 Model before donning

7.4. Step module

In the *Step* module the problem was divided into steps, that are any convenient phase of the history. The step definition includes the type of analysis to be performed and optional history data, such as loads, boundary conditions, and output requests. All the values specified in this module had second as unit of measure [66].

Static general steps were created for donning and standing simulation. During a static step the time period i.e., the time for solving the problem, must be assigned. This is necessary for cross-references to the amplitude options, which can be used to determine the variation of loads and other externally prescribed parameters during a

step. Then, the *Nlgeom* option was selected to ensure a better convergence of the simulation. This choice was made due to a complex geometry, the presence of contacts and interactions, nonlinear material properties and large deformations. Abaqus/Standard uses Newton's method to solve the nonlinear equilibrium equations. Many problems involve history-dependent response; therefore, the solution usually is obtained as a series of increments, with iterations to obtain equilibrium within each increment. Increments must sometimes be kept small to ensure correct modeling of history-dependent effects. Most commonly the choice of increment size is a matter of computational efficiency: if the increments are too large, more iterations will be required. Furthermore, Newton's method has a finite radius of convergence; too large an increment can prevent any solution from being obtained because the initial state is too far away from the equilibrium state that is being sought [66]. In this work the minimum and maximum time increments were respectively 1E-09 and 0.1 in each step (Fig. 7.8).

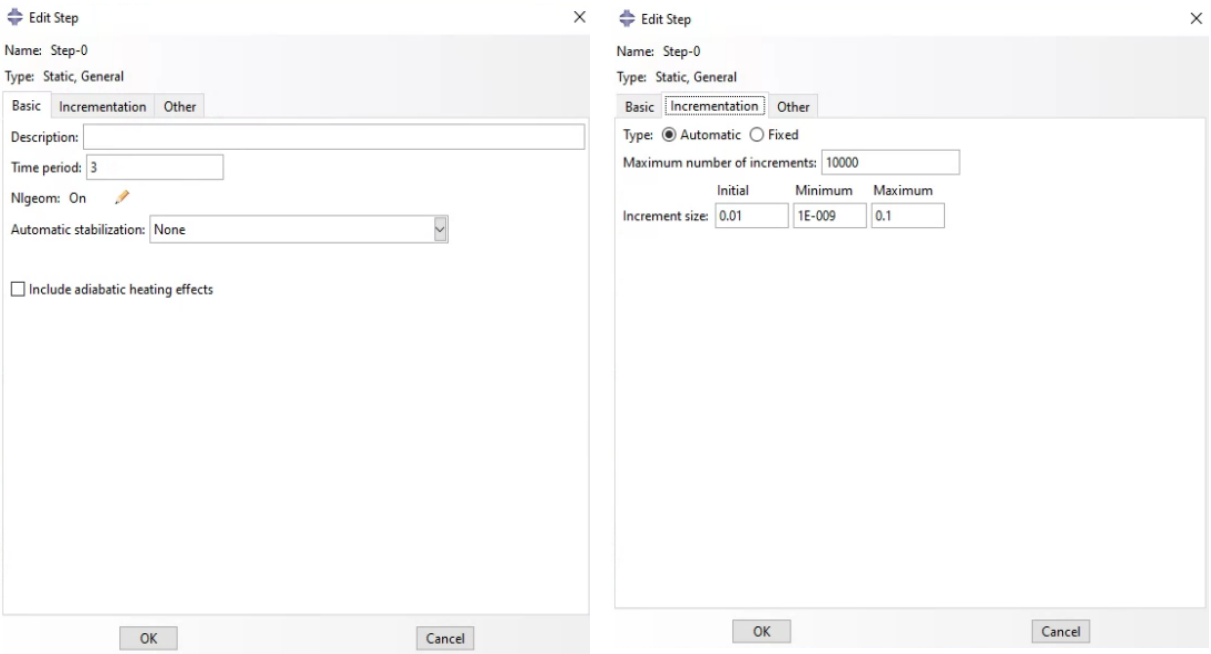

Figure 7.8 Static general step options

Instead, to simulate the gait a dynamic implicit type of step was chosen (Fig. 7.9). A direct-integration dynamic analysis in Abaqus/Standard must be used when nonlinear dynamic response is being studied and can be fully nonlinear or can be based on the modes of the linear system. It can be used to study a variety of applications, including:

- dynamic responses requiring transient fidelity and involving minimal energy dissipation;
- dynamic responses involving nonlinearity, contact, and moderate energy dissipation;

- quasi-static responses in which considerable energy dissipation provides stability and improved convergence behavior for determining an essentially static solution.

The quasi-static application was chosen to capture the intended behavior of this analysis most efficiently and accurately. Quasi-static applications introduce inertia effects primarily to regularize unstable behavior in analyses whose focus is a final static response. Large time increments are taken when possible to minimize computational cost, and considerable numerical dissipation may be used to obtain convergence during certain stages of the loading history [66]. As minimum time increment the value 1E-09 was chosen, whereas for the maximum one the *Analysis application default* option was selected to set the maximum time increment size automatically based on the application setting option. For quasi-static applications, the default maximum time increment is the time period of the step. Then, it is important to mention that for this kind of analysis a material's mass density must be defined because inertia effects are introduced. During this phase the *Nlgeom* option was selected again due to the presence of a complex geometry, contacts and interactions, nonlinear material properties and large deformations [66]. This choice of the step was considered acceptable because Jia et al [36] showed that during the stance phase of the gait the interface pressures and shear stresses don't significantly change no matter the inertia effects were considered or not. The number of steps necessary to conclude the simulations were 13 for Foot Flat and 11 for Mid Stance.

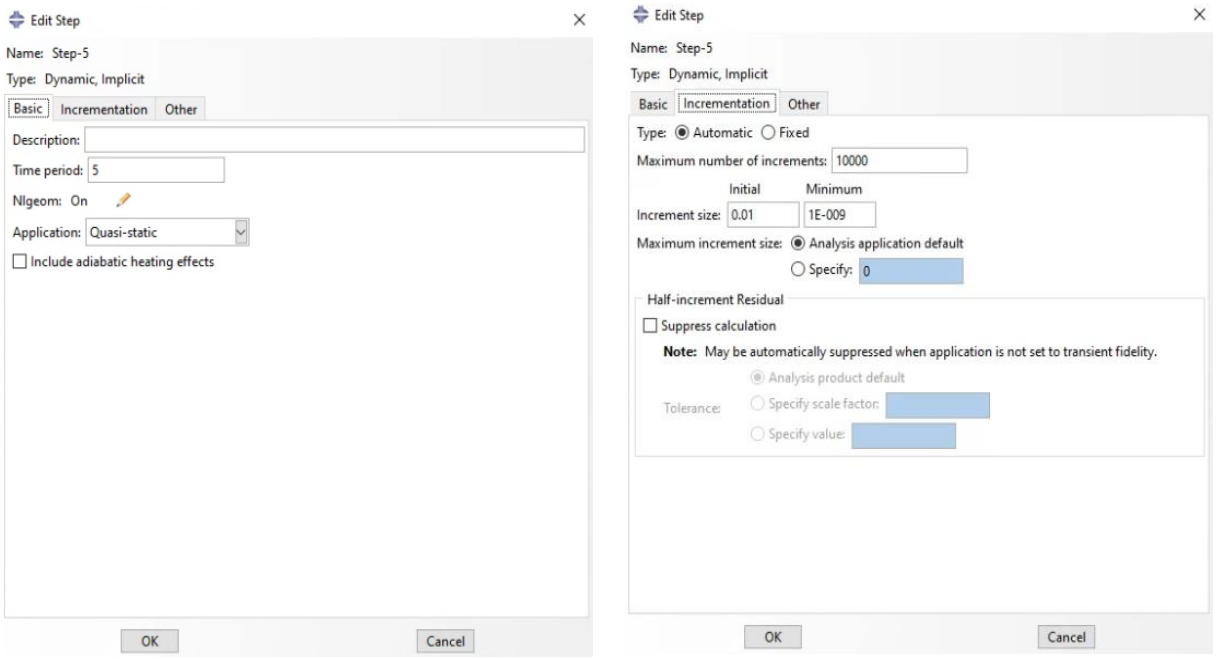

Figure 7.9 Dynamic implicit step options

7.5. Mesh module

Before creating the mesh, the *Virtual Topology* tool was used to combine the whole surfaces together (Fig. 7.10). In fact, instances are composed by many surfaces patched together, due to the Geomagic step that converted the model from a cloud of point to a solid one. Then, a clever partition allowed to divide a complex, three-dimensional part into simpler regions and to obtain a better-quality mesh. So, planes were created for each part and the *Partition* tool was used (Fig. 7.11, 7.13, 7.15, 7.17).

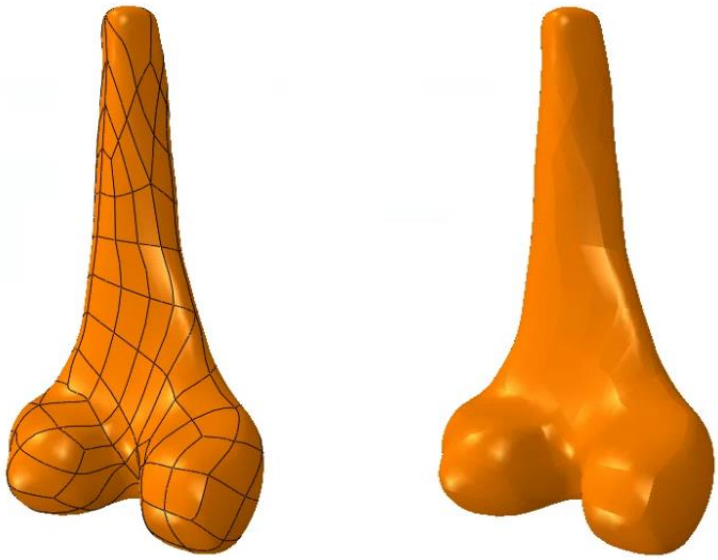

Figure 7.10 Femur before and after Virtual Topology

After that, the process for the creation of the mesh started. The ideal case would be having a hexahedral mesh for all the instances because it usually provides a good accuracy of the solution, but this could not happen. The problem was that the geometry was very complex and so it was very difficult to have a good partition that allowed to obtain this feature. Hence, triangular and tetrahedral elements were used because they are geometrically versatile and require a lower computational cost.

The first tool used to create the mesh was the *Seed*. Seeds are markers placed along the edges of a region to specify the target mesh density in that region. The values for the *Seed* were taken from a previous work on a transtibial amputee [25]. Then, the element type was decided. Five aspects of an element characterize its behavior: family, degrees of freedom, number of nodes, formulation, integration. The first letter of an element's name indicates which family the element belongs to. In this model all the parts had continuum elements, except the socket that had shell elements. The degrees of freedom are the fundamental variables calculated during the analysis. For a stress/displacement simulation the degrees of freedom are translations and rotations at each node. Then, the number of nodes used in the element usually identified the order of interpolation and this number is clearly identified in the element name. C3D4 and C3D6 indicate respectively a 4-node linear tetrahedron element and a 6-node linear triangular prism.

Instead S3 means 3-node triangular shell. An element's formulation refers to the mathematical theory used to define the element's behavior. Generally, for a stress/displacement analysis in Abaqus standard elements are based on the Lagrangian formulation, that describes the behavior of the element which deforms with the material. Moreover, there are some alternative formulations. In this work, to deal with incompressible or very close to incompressible behaviors the hybrid formulation was adopted. These elements are identified by the letter H at the end of the name. This was the case of liner and soft tissue because they both had a Poisson ratio that was very close to the value of 0.5. If this choice wasn't made, *Abaqus*/CAE would not have allowed the simulation. For what concern the integration, *Abaqus*/CAE uses Gaussian quadrature for most elements and evaluates the material response at each integration point in each element [66].

Finally, the mesh was examined with the *Verify mesh* tool to see whether the results were acceptable. The aspect ratio i.e., ratio of an element's longest and shortest edges, was the parameter under control, and its value must not be greater than 10. The ideal value is 1 and it represents a perfectly shaped element. However, when the geometry is complex as in this work a greater aspect ratio is consider acceptable if it is below a certain threshold, that in this case corresponded to the default value of 10. On the contrary, if the aspect ratio is too high the mesh has a low quality and should be improved, for example modifying seed distribution, partition or mesh technique [66].

Values chosen for each part in the analysis are reported in Table 7.3 and the results are shown in Figures 7.12, 7.14,.7.16, 7.18.

Part	Seed	Element type	Number of elements	Worst aspect ratio
Femur	5	C3D4	17562	3.37
Patella	5	C3D4	2348	2.78
Tibia	5	C3D4	8721	2.73
Soft tissue	5.5	C3D4H	80004	3.47
Liner	5.5	C3D6H	4173	3.09
Socket	6	S3	9653	3.17

Table 7.3 Mesh features

Figure 7.11 Bones partition

Figure 7.12 Bones mesh

Figure 7.13 Soft tissue partition

Figure 7.14 Soft tissue mesh

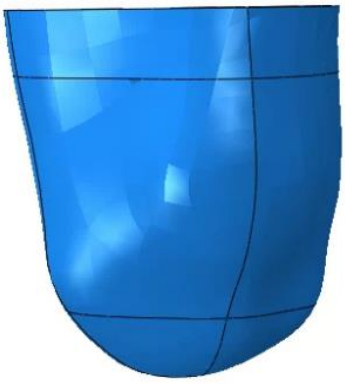

Figure 7.15 Liner partition

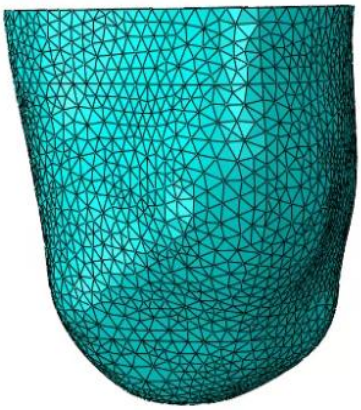

Figure 7.16 Liner mesh

Figure 7.17 Socket partition

Figure 7.18 Socket mesh

7.6. Interaction module

The mechanical interaction between two regions of a model can be described in the *Interaction* module. The relationships used in this study will be discussed below.

7.6.1. Constraint

A Tie Constraint was constructed between the bones and the soft tissue to avoid adding to the model's already high complexity (Fig. 7.19). It connects two independent surfaces so that there is no relative motion between them and permits the fusion of two areas even if the meshes formed on the surfaces of the regions are different. The specification of the master and slave surfaces is necessary for this form of interaction. The first is generally picked as the tougher one, and it was represented by the bones in the model, whereas the slave surface is usually chosen as the softest, and it was represented by soft tissue. As a result, the slave surface was compelled to follow the movement of the master one [66].

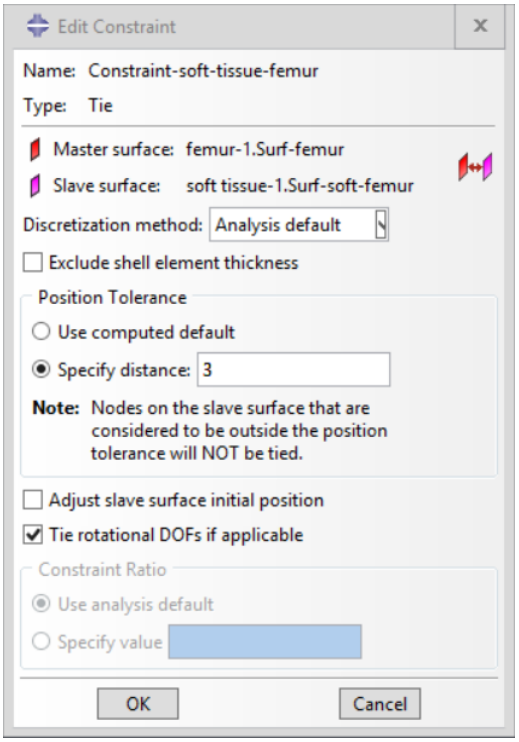

Figure 7.19 Tie Constraint options between bones and soft tissue

Another type of constraint was the coupling, which was applied in this study as *Kinematic Coupling* and *Continuum Distributing Coupling*. *Kinematic coupling* restricts the motion of the coupling nodes to the motion of the reference node's rigid body. The restriction is enforced by removing degrees of freedom at the coupling nodes and can be applied to user-specified degrees of freedom at the coupling nodes with respect to a global or a local coordinate system [66]. It was utilized in the model to confine the bottom surface of the socket to a reference point (RP1) positioned below the same surface (Fig. 7.20). As a result, the degrees of freedom of all selected nodes were constrained to the degrees of freedom of the reference point. During the donning simulation, the displacements were applied to this point in order to move the socket and position it correctly.

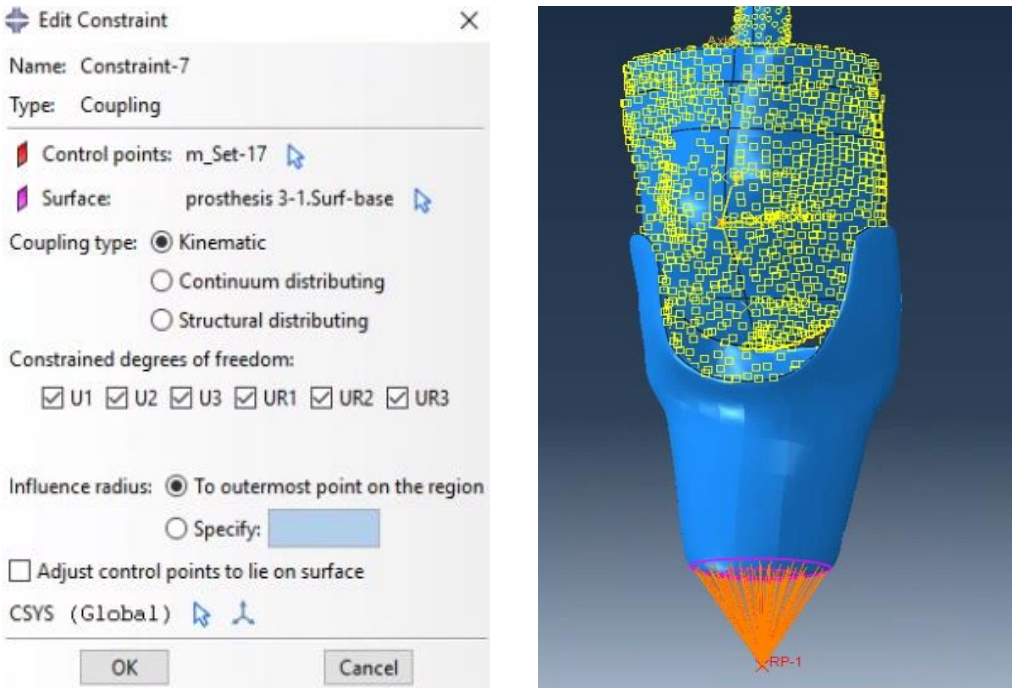

Figure 7.20 Kinematic coupling at the base of the socket

Another reference point (RP2) was constructed above the femur and was linked to the proximal surface of this bone using a *Kinematic coupling* (Fig. 7.21). The reference point avoided all translations and rotations in each simulation to maintain the femur's location in space. The existence of a set of encastres held the other bones in place, as indicated in the "Load module" paragraph.

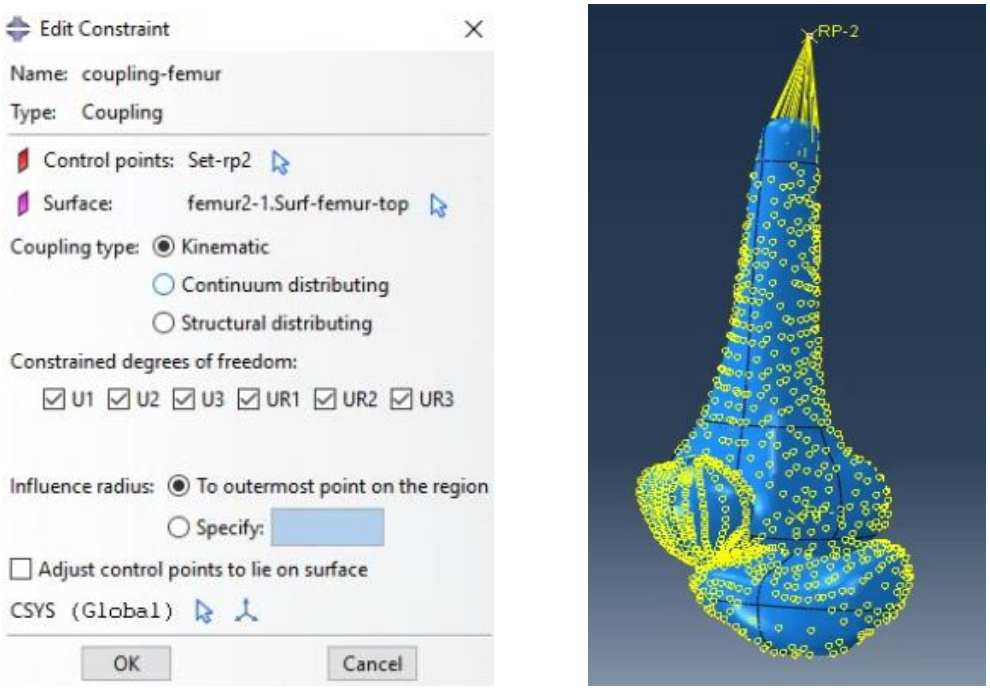

Figure 7.21 Kinematic coupling on the femur

A reference point (RP-condyle) was additionally attached to the surface of the femoral condyles through the *Kinematic coupling* constraint. It was utilized to imitate the rotation of the femur during various periods of walking.

Instead, *Continuum Distributing coupling* constraints the motion of the coupling nodes to the translation and rotation of the reference node. This constraint is enforced to enable control of the transmission of loads through weight factors at the coupling nodes. The constraint distributes loads such that the resultants of forces and moments at the coupling nodes are equivalent to the forces and moments at the reference node [66]. For this type of constraint, a reference point (RP3) was created at the center of the knee and was connected to a circular portion of the socket base that resembled the area occupied by the pylon (Fig. 7.22). Loads that simulated the phases of the gait were applied to this reference point.

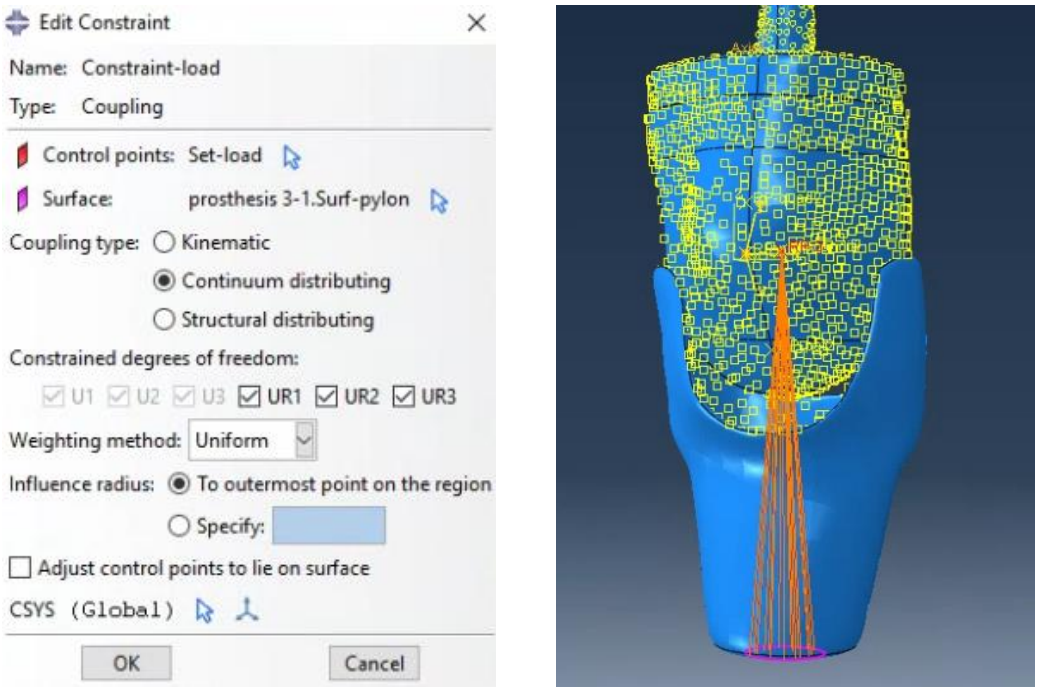

Figure 7.22 Continuum distributing coupling for the application of the loads

7.6.2. Interaction

A Surface-to-surface interaction type was chosen for the other contacts, which were soft tissue-liner and liner-socket interactions. In this situation, master and slave surfaces must also be specified. The master surface was the inner section of the liner in the soft tissue-liner interaction, while the slave surface was the soft tissue's outside surface. In the opposite contact, the socket was designated as the master surface and the liner as the slave. For both contacts, the option Finite sliding, which is the most generic and permits any arbitrary motion of the surfaces, was chosen as the Sliding formulation. The slave node adjustment option was then specified: No adjustment was selected for both soft tissue-liner and liner-socket interactions (Fig. 7.23, 7.24).

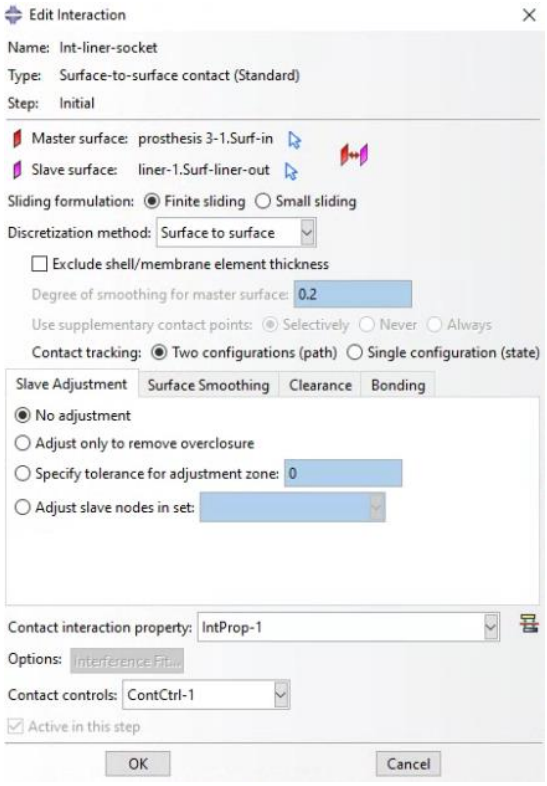

Figure 7.23 Interaction parameters between liner and socket

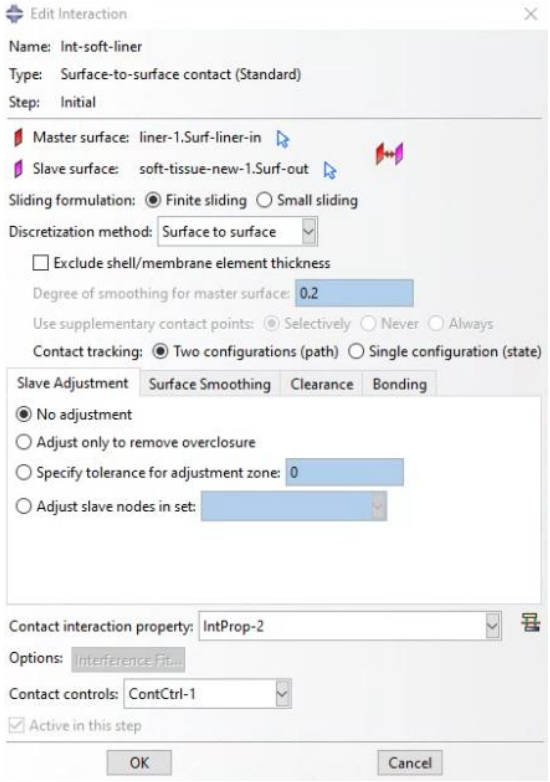

Figure 7.24 Interaction parameters between soft tissue and liner

Moreover, in the first step the *Interference fit* tool was adopted. It occurs by default when the contact formulation computes overclosures between surfaces in the initial configuration of a model and can be gradually resolved over multiple increments. The default contact constraint imposed at each constraint location the current penetration $h(t) \leq 0$. Penetration is present when $h(t)$ is positive. To alter this constraint, an allowable interference, v, should be specified and it will be ramped down over the course of a step. The specified allowable interference modifies the contact constraint as follows:

$$h(t) - v(t) \leq 0$$

where h is the penetration and v is the allowable interference. Thus, specifying a positive value for v(t) causes to ignore penetrations up to that magnitude. There are different ways to specify the allowable interference: a time-varying allowable contact interference can be defined by creating an amplitude curve, a single allowable interference v can be specified for every node on the slave surface, or a uniform allowable interference v and a direction n can be stated and the relative shift vector vn is applied to the slave nodes. However, some features are common for all of them. By default, in all cases the value of the specified allowable interference is applied instantaneously at the start of the step and then ramped down to zero linearly over the step, unless an amplitude reference that defines a particular allowable interference-time variation is specified [66].

In this work the option *Gradually remove slave node overclosure during the step* was selected and the automatic "shrink" fit method was used. It does not require any interference value but assigns the same value of v, corresponding to the maximum penetration of the contact pair, to all constraints that are initially closed (Fig. 7.25) [66].

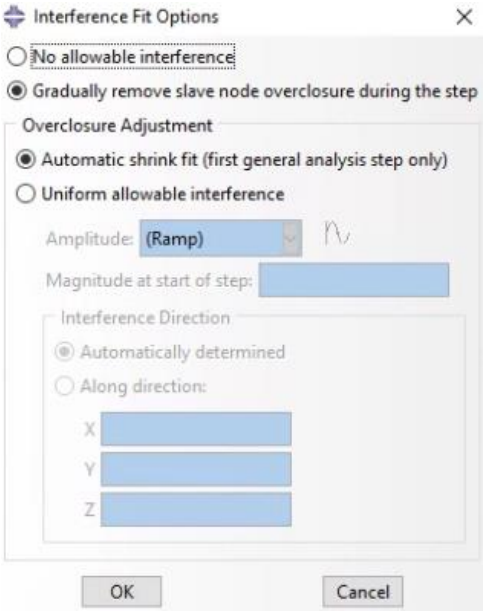

Figure 7.25 Interference Fit

Finally, the contact controls were set, and the automatic stabilization was selected. The parameters present in the default configuration were maintained (Fig. 7.26). This tool allowed to control body motions in static problems before contact closure and friction restrain such motions [66].

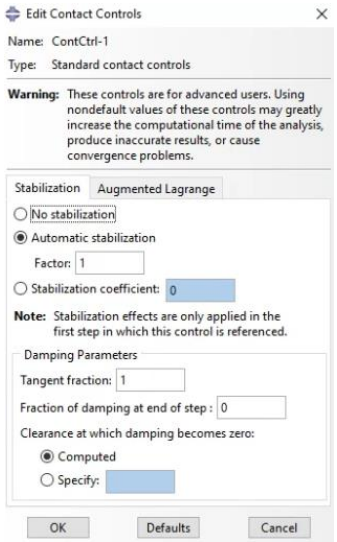

Figure 7.26 Contact Controls

7.6.3. Contact properties

When editing interactions, the contact interaction characteristics must also be specified. As a result, the mechanical contact properties, specifically the tangential and normal behaviors, were identified. It was described in this way how two things mechanically interact in two directions: tangentially with regard to the plane tangent to them and orthogonally to the same plane. In terms of tangential behavior, the Penalty friction model was chosen because it employs a stiffness technique that allows for some relative motion of the surfaces even when they should be sticking. *Abaqus*/CAE will continually adjust the magnitude of the penalty constraint to enforce this condition. Then a uniform friction coefficient was assigned. In the liner-socket interaction it was equal to 0.5 (Fig. 7.27). Instead, in the soft-tissue-liner contact the friction coefficient value changed based on the material of the liner. Below the Table 7.4 shows the values corresponding to each material taken from a research study of Cagle et al. [32].

Material	Friction coefficient
Silicone	2
Urethane	0.5
PTE	1.5

Table 7.4 Friction coefficient in liner-soft tissue contact

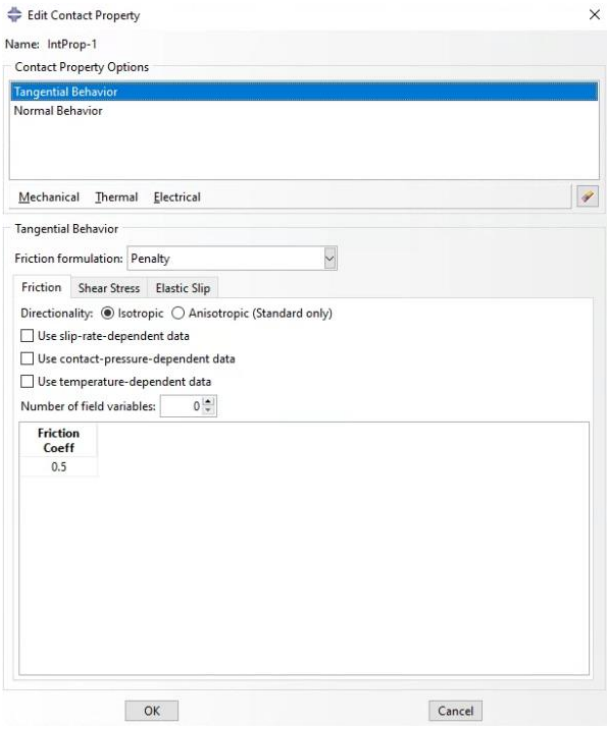

Figure 7.27 Tangential behavior in liner-socket interaction

For the normal behavior, the *Hard contact*, a contact relationship that minimizes the penetration of the slave surface into the master surface at the constraint locations and does not allow the transfer of tensile stress across the interface, was selected. When surfaces are in contact, any contact pressure can be transmitted between them, while there is no exchange of contact pressure if the surfaces do not touch each other. Separated surfaces come into contact when the clearance between them reduces to zero (Fig 7.28) [66].

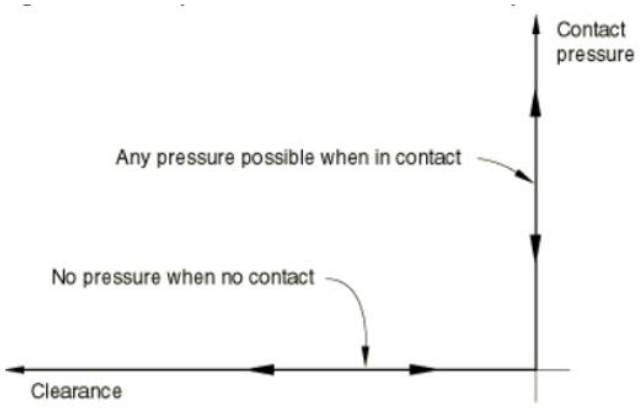

Figure 7.28 Relation between clearance and contact pressure in the Hard contact [59]

Penalty method was chosen as constraint enforcement method. Abaqus/Standard offers linear and nonlinear variations of the penalty method. With the linear penalty method, the so-called penalty stiffness is constant, so the pressure-overclosure relationship is linear. With the nonlinear penalty method, the penalty stiffness increases linearly between regions of constant low initial stiffness and constant high final stiffness, resulting in a nonlinear pressure-overclosure relationship (Fig 7.29) [66]. In this work, relation between the contact pressure and overclosure resulted to be linear and a stiffness scale factor of 1.67 was used for the socket-liner contact, as it was shown in a previous work [25], whereas for the liner-soft tissue interaction the default value 1 was chosen.

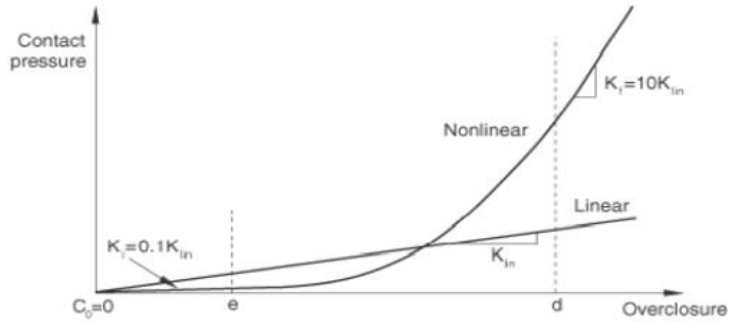

Figure 7.29 Relation between overclosure and contact pressure in the Hard contact (K_i: initial penalty stiffness, K_f: final penalty stiffness, K_{lin}: stiffness in the linear case, e, d: percentage of a characteristic length computed by Abaqus/Standard to represent a typical facet size, C_0: clearance) [59]

7.6.4. Connectors

There are some elements present in the anatomy of the knee joint that should be represented for the accuracy of the model, but their geometry was not given. They are tendons and ligaments. As suggested in the thesis of Gandolfi and Giudici [25], adding the main ligaments, tibiofemoral and patellofemoral articulations can be stabilized. Moreover, including these elements in their work they could fix the position of the bones and created the kinematic chain that allowed the passage of loads from a bone to another one.

In this work patellar tendon and quadriceps tendon were modeled and they were considered as two separate entities, even if physiologically their bundles join at the level of the anterior face of the patella. For the area of insertion, in the *Mesh* module a surface was created on the bones as shown in Figure 7.30. Then, a reference point was generated in the center of this area few millimeters away, and it was associated to the surface with a *Continuum Distributing Coupling* constraint.

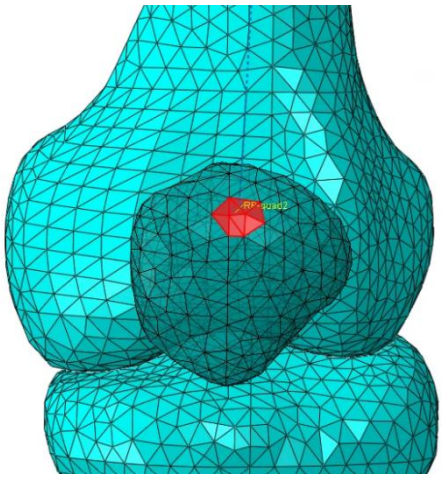

Figure 7.30 Distal insertion area of quadriceps tendon

The only exception was the proximal end of the quadriceps tendon. For this element a reference point was created but it was not connected to any bone surface because it represented the quadriceps muscle end and the beginning of the quadriceps tendon.

To create the tendons the reference points were joined through a connector, that is one-dimensional element which relates two nodes (Fig. 7.31). In this work the coupled nodes were positioned in places shown in Table 7.5.

	Proximal end	**Distal end**
Patellar tendon	Inferior aspect of patella	Tibial tuberosity
Quadriceps tendon	Terminal part of quadriceps	Superior aspect of patella

Table 7.5 Insertion zones of patellar tendon and quadriceps tendon

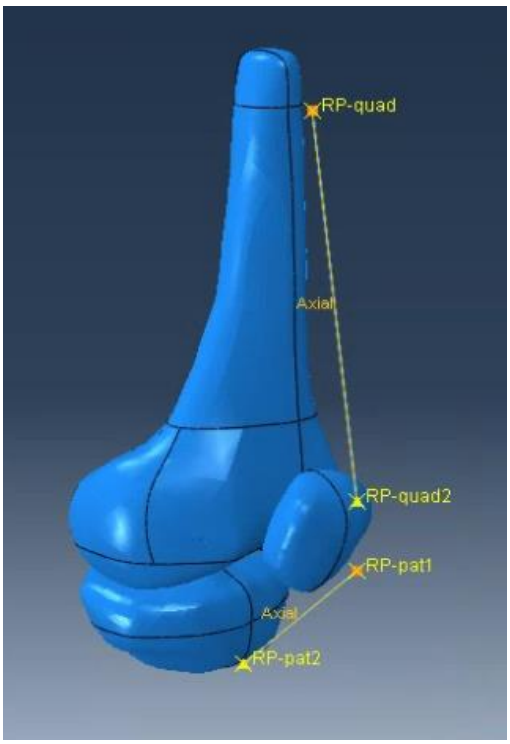

Figure 7.31 Axial connectors that represent quadriceps and patellar tendons

To create these connectors a point-to-point wire feature was generated to link the two ends of the tendon. Then, a connector section must be generated. Basic connection was chosen and in particular the axial one, that provides a connection between two nodes that acts along the line connecting the nodes (Fig 7.32). The axial connection does not constrain any component of relative motion and the available component of relative motion acts along the line connecting the two nodes. An elastic behavior was also assigned to this connector and a stiffness value of 400 MPa was chosen (Fig 7.33) [44]. After that, the connection section was assigned to the wire through the *Connector Section Assignment*.

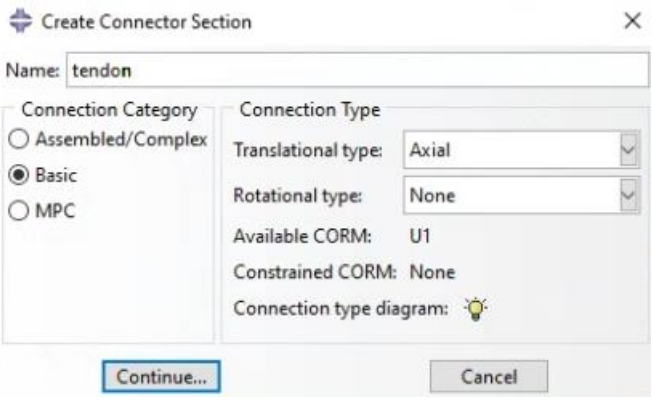

Figure 7.32 Assignment of axial connection section

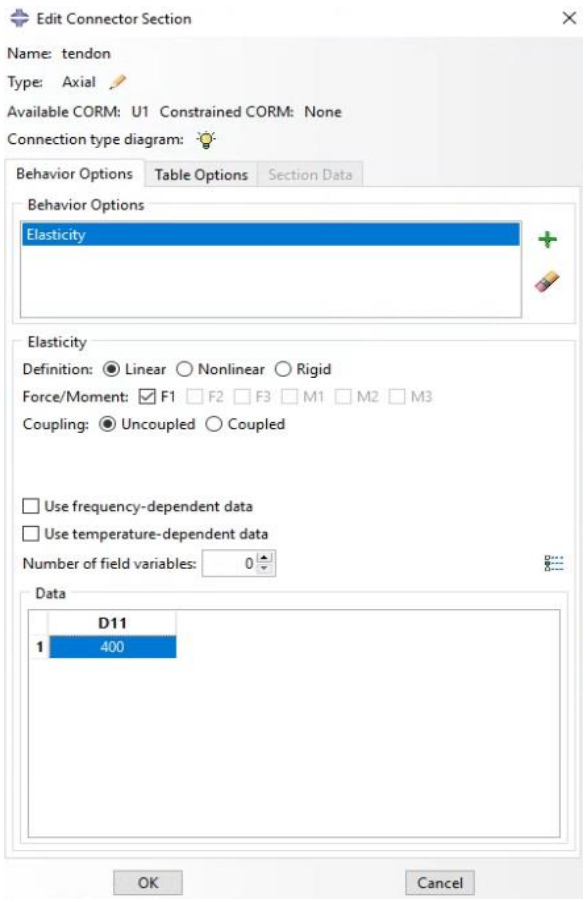

Figure 7.33 Assignment of elasticity property to the connector section

7.7. Load module

In this module loads and boundary conditions were assigned. The modeled scenarios were the donning, the standing and two phases of the gait: Foot-Flat and Mid-Stance. The loads used for the gait were taken from the thesis work of Gandolfi-Giudici [25]. They were referred to a patient of 70 kg with a transtibial amputation and came from Centro Protesi INAIL of Budrio. They are shown in Table 7.6.

	Foot-Flat	**Mid-Stance**
Angle	8°	5°
Medio-lateral F_x (N)	-25	-13
Anterior-posterior F_y (N)	129	2
Superior-inferior F_z (N)	631	537
Flexion-extension M_x (Nmm)	-6500	0
Abduction-adduction M_y (Nmm)	8600	12988
Internal-external rotation M_z (Nmm)	1630	-2138

Table 7.6 Applied load cases [25]

As previously said, the starting point was the donning. First, a set of 4 nodes was created on both patella and tibia and then a *Mechanical Encastre* was associated to the same set (Fig. 7.34) as suggested by a previous analysis on a transtibial amputee [11]. A minor number of nodes would have made the simulation less stable. To hold in space the femur, the reference point associated to its proximal surface was kept in position by means of a *Mechanical Encastre.* In this way the bones were not allowed to move with respect to each other. These boundary conditions persisted throughout all the simulation of the donning.

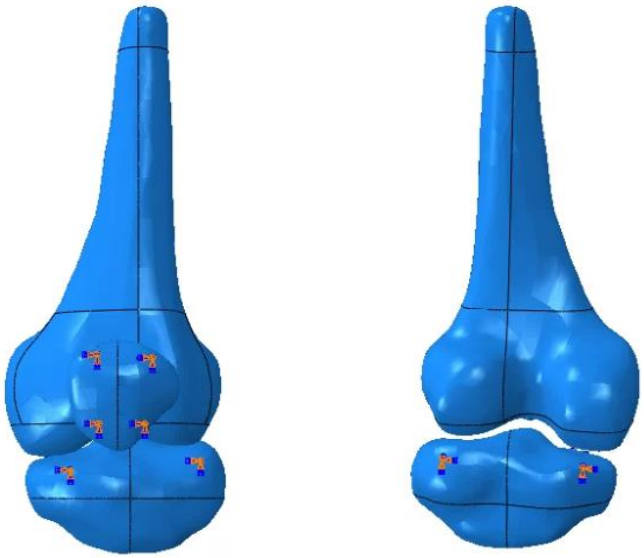

Figure 7.34 Encastres on patella and tibia

Then, to simulate the donning explicitly, displacement controls were chosen. A first step was used to resolve the interference between the liner and soft tissue by means of the *interference fit* tool. In this case, no boundary conditions were assigned to the socket. Then, the simulation of the donning started. So, a displacement of 60mm in the z direction (U3) and one of -5mm in the x direction (U1) was given to the reference point RP1 that was associated with the base of the socket. In general, only longitudinal displacement was used to simulate this procedure, but transversal displacement was allowed to avoid penetration that would result in an abortion. This choice was made after working with the *Job diagnostic* tool in the *Visualization* module, because it allowed us to identify the region where the penetration was excessive. This displacement could also represent the adjustments that were made in the real donning performed by the amputee. After this step, the socket has reached the correct position.

Then, the boundary condition on the socket was gradually removed. In the first step, U1, U2, and R3 were suppressed, and in the subsequent one, all the other displacement controls were released. In the same step, a load of 200N was applied along the longitudinal direction to the reference point at the center of the knee that was connected to the portion of the socket base that corresponded to the pylon. After that, the load was increased to 350N, which corresponded to half the weight of the patient,

in order to simulate standing. The boundary conditions on the bones were the same as those used to simulate the donning. So, to obtain the results, five steps were required in total.

Instead, to simulate the gait, the boundary conditions changed. First, after the socket reached the correct position, the femur was rotated by means of a *displacement/rotation* boundary condition applied to the reference point at the center of the knee connected to the femoral condyles. So, a rotation around the frontal axis was imposed (UR1). Rotation was expressed in radians and was equal to -0.14 rad (approximately 8°) in Foot Flat and -0.09 rad (about 5°) in Mid Stance. The patella and tibia were kept in position by means of the same set of encastres present in the donning, while the boundary condition activated at the top of the femur was removed during this step. After the flexion, the encastres on the bones were removed. Then, each end of the connectors that simulated the tendons was fixed for all translations and rotations. In this way, the bone position did not change over the simulation. Moreover, the outer surface of the liner was rigidly fixed along the z-direction, assuming the socket would offer rigid support and excessive movements of the liner were avoided in this direction. After that, the simulation could start. The boundary conditions at the base of the socket were gradually removed following the application of the loads. The loads were applied to the reference point created at the center of the knee that was linked to the portion of the socket base that simulated the pylon. All the loads were not applied completely in a single phase, but they were subdivided in different portions and applied progressively to avoid convergence problems that would cause abortion of the simulations. Tables 7.7 and 7.8 show how loads were divided into different portions during the Foot Flat and Mid Stance phases. In particular, the first column shows forces and moments in each direction, where the numbers 1, 2 and 3 represent frontal, sagittal and longitudinal axes respectively. Instead, the first row shows the number of load increments necessary to complete the simulations.

Steps / Loads	1	2	3	4	5	6	7	8	9	10
F1 (N)	-	-	-	-	-25	-25	-25	-25	-25	-25
F2 (N)	-	-	-	-	-	129	129	129	129	129
F3 (N)	200	400	500	631	631	631	631	631	631	631
M1 (Nmm)	-	-	-	-	-	-	-3250	-3250	-6500	-6500
M2 (Nmm)	-	-	-	-	-	-	-	4300	4300	8600
M3 (Nmm)	-	-	-	-	-	-	-	815	815	1630

Table 7.7 Loads distribution in Foot Flat simulation

Loads \ Steps	1	2	3	4	5	6	7	8
F1 (N)	-	-	-	2	2	2	2	2
F2 (N)	-	-	-	-13	-13	-13	-13	-13
F3 (N)	200	400	537	537	537	537	537	537
M1 (Nmm)	-	-	-	-	-	-	-	-
M2 (Nmm)	-	-	-	-	-	5000	10000	12988
M3 (Nmm)	-	-	-	-	-2138	-2138	-2138	-2138

Table 7.8 Loads distribution in Mid Stance simulation

7.8. Job module

Once all the tasks involved in defining the model were finished, the *Job* module was used to get the results.

The *Job* module allows to create a job, to submit it for analysis, and to monitor its progress. After submitting the job, information appears next to the job name indicating its status. There are four possible statuses:

- Submitted while the analysis input file is generated.
- Running while the model is analyzed.
- Completed when the analysis is complete, and the output are written to the output database.
- Aborted if a problem with the input file or the analysis is found and aborts the analysis. In addition, problems are reported in the message area

When the job was completed successfully, the results of the analysis could be viewed in the *Visualization* module [66].

8. Results

The outcome was an *.odb* file containing the field output results. The *Visualization* module was used to read the output database that *Abaqus*/CAE generated and to view the results of the analysis.

The variables of interest were CPRESS, CSHEAR for stresses at the liner-soft tissue interface, and Von Mises stress in the soft tissue's interior volume. CPRESS denoted the normal-direction contact pressure between two surfaces. CSHEAR, on the other hand, referred to the frictional shear stress caused by the existence of a friction coefficient at the interface. CSHEAR1 and CSHEAR2, i.e., stresses along the two slip directions, were produced by Abaqus/CAE. The following law was used to calculate the resulting shear stress:

$$CSHEAR = \sqrt{CSHEAR1^2 + CSHEAR2^2}$$

As a result, the region of interest was the soft tissue part, which was isolated from the overall model in the Visualization module using the *Display Group* tool. Furthermore, *Abaqus*/CAE allows to customize the contour plots, that display the variation of a variable across the surface of a model, in the *Contour Plot Options* menu. So, the maximum value of each simulation was changed in order to have the same upper limit and improve the display of the findings. In this manner it was easier to compare the various situations. The figures with CPRESS and CSHEAR findings in the next paragraphs represent the anterior part of the residual limb in the frontal plane where the most intriguing results were obtained. Instead, for the Von Mises stress two sections of the stump on the transverse plane were analyzed.

8.1. Donning procedure

Donning is the motion of the socket in the correct position on the residual limb. In this work it was simulated explicitly and so, some pre-stresses are applied on the stump before any loads are applied. The comparison was made after the step in which socket computed the displacements to reach the best fit and before it was completely released. If it had been done after that passage, the socket would have changed position due to elastic return, but the new location would have been different for each combination of liner and soft tissue material properties.

Considering the flaccid soft tissue, the peak contact pressures are 98.13 kPa, 84.43 kPa and 75.57 kPa with silicone, urethane and TPE. Instead, with contracted soft tissue they are 116.4 kPa, 98.15 kPa and 85.57 kPa. These higher values are concentrated in the sub-patellar region and tibial medial flare. Results are shown in Figures 8.1 and 8.2. Then, peak shear stresses with flaccid soft tissue are 28.17 kPa, 34.07 kPa and 33.96 kPa

for silicone, urethane and TPE; with contracted soft tissue they are 31.2 kPa, 42.64 kPa and 42.06 kPa. They are observed more in tibial lateral flare and lateral femoral condyle. Results are depicted in Figures 8.3 and 8.4. All the figures depict stresses over the stump in the frontal plane for each kind of liner.

CPRESS

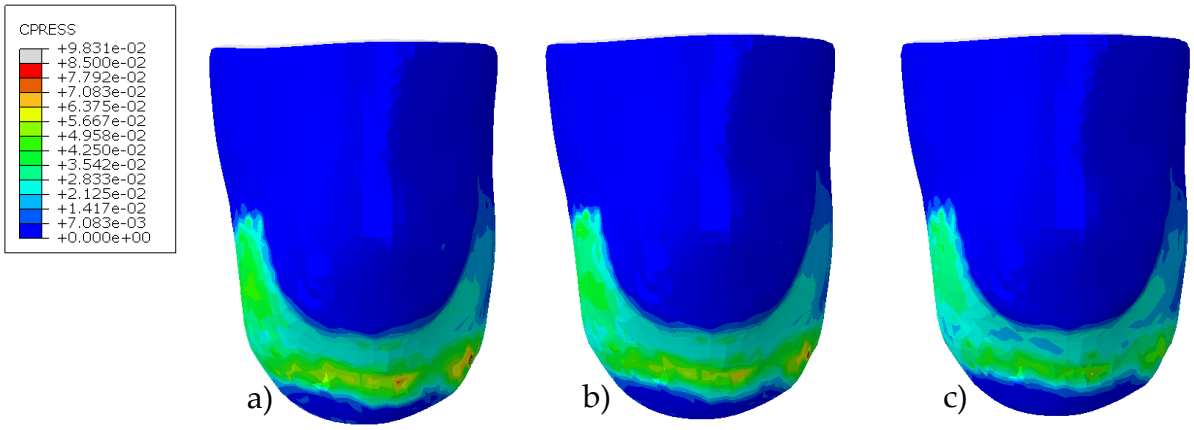

Figure 8.1 CPRESS on flaccid soft tissue with a) silicone, b) urethane, c) TPE liner in donning

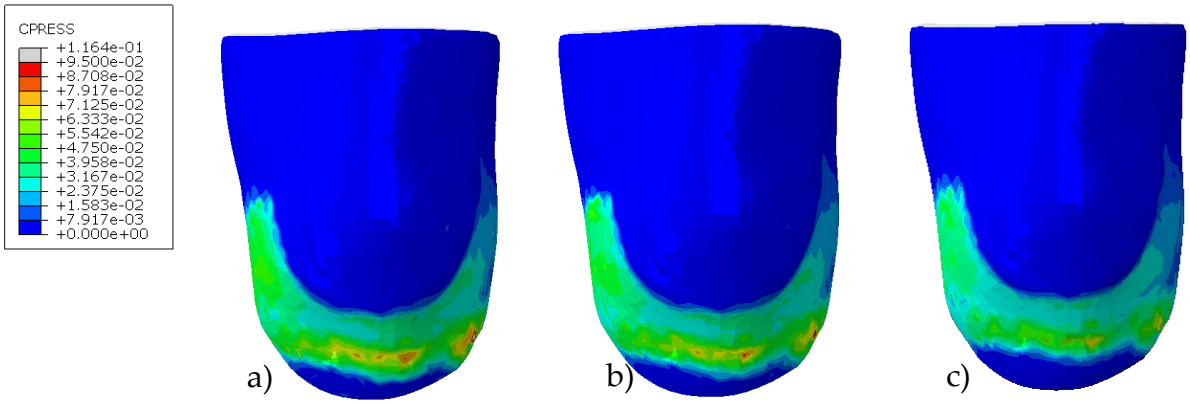

Figure 8.2 CPRESS on contracted soft tissue with a) silicone, b) urethane, c) TPE liner in donning

CSHEAR

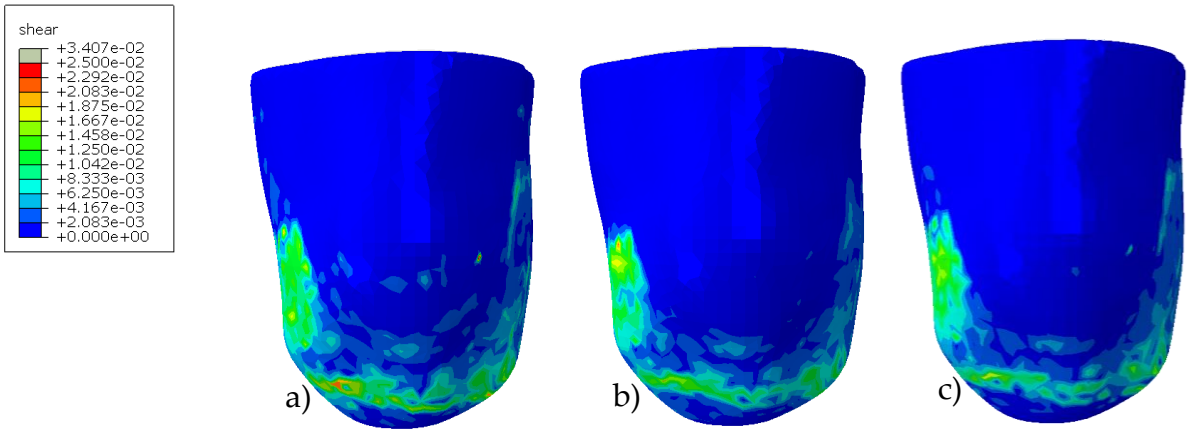

Figure 8.3 CSHEAR on flaccid soft tissue with a) silicone, b) urethane, c) TPE liner in donning

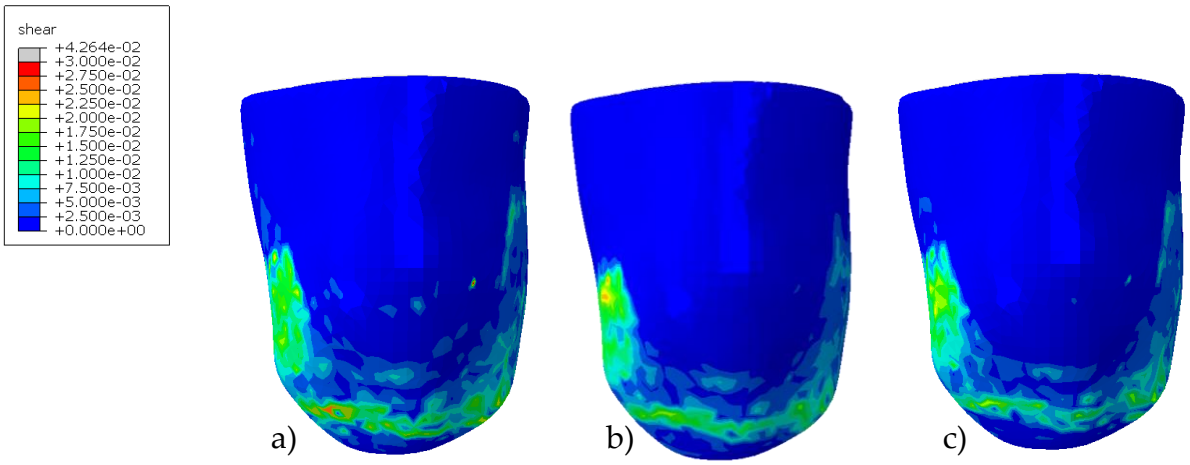

Figure 8.4 CSHEAR on contracted soft tissue with a) silicone, b) urethane, c) TPE liner in donning

8.2. Standing

The standing phase was simulated applying solely a vertical force of 350N. Even when diverse materials were examined, pressures were distributed uniformly throughout the surface. Because the end of the stump and the region with the patella are pressure sensitive regions, the socket was designed to have the lowest possible pressure value there. Because of the shape of the socket, these features are present in all of the simulations performed in this work.

Starting with flaccid soft tissue, the highest values of CPRESS are 120.8 kPa, 109.4 kPa, and 104 kPa with silicone, urethane, and TPE liner, respectively. Higher pressures are located in tibial medial flare and sub-patellar region. Instead, the maximal CSHEAR values are 29.87 kPa, 39.7 kPa, and 55.84 kPa, and they are more concentrated on the later tibial condyle. The greatest results with the stiffer soft tissue are 115 kPa, 103.3 kPa, and 96.75 kPa for CPRESS and 31.43 kPa, 36.56 kPa, and 49.21 kPa for CSHEAR. The regions of interest are the same as for the flaccid soft tissue. Figures 8.5 and 8.6 depict the CPRESS variable distribution across the stump in the frontal plane with flaccid soft tissue and contracted soft tissue for all liner materials. Figures 8.7 and 8.8 show the same thing for CSHEAR.

CPRESS

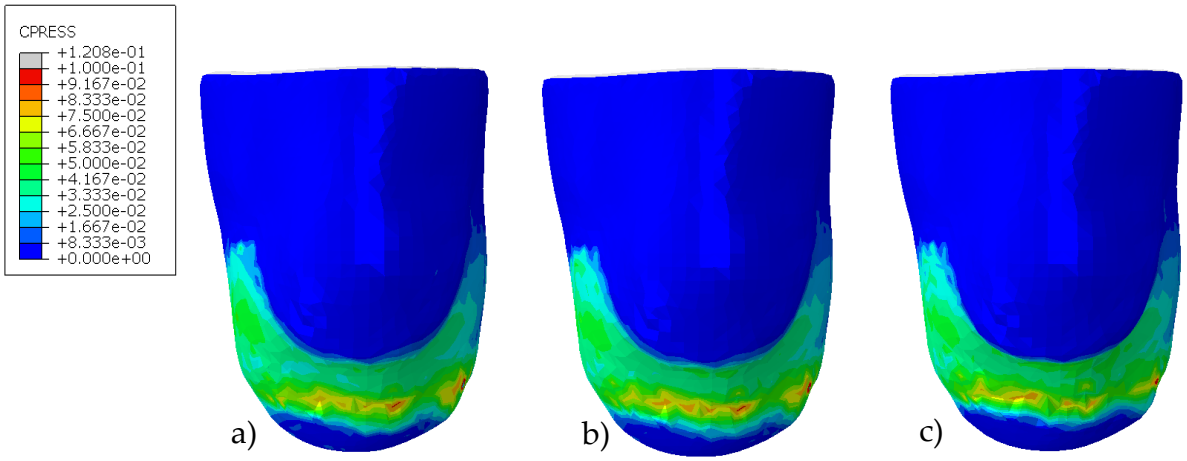

Figure 8.5 CPRESS on flaccid soft tissue with a) silicone, b) urethane, c) TPE liner in standing

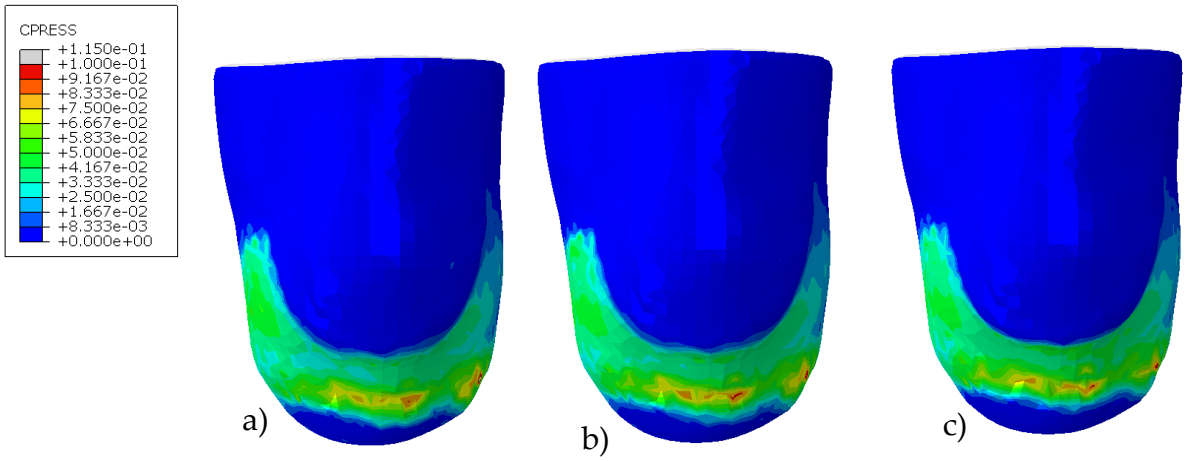

Figure 8.6 CPRESS on contracted soft tissue with a) silicone, b) urethane, c) TPE liner in standing

CSHEAR

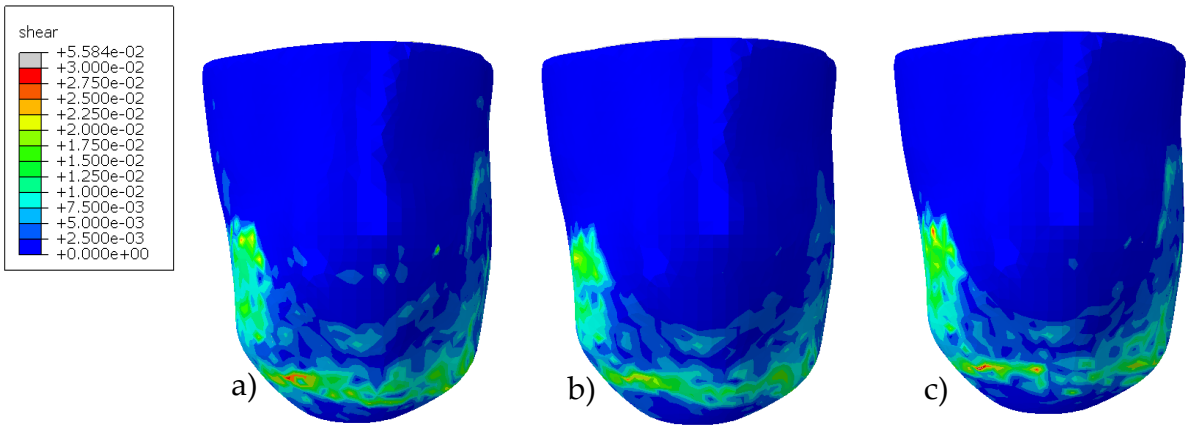

Figure 8.7 CSHEAR on flaccid soft tissue with a) silicone, b) urethane, c) TPE liner in standing

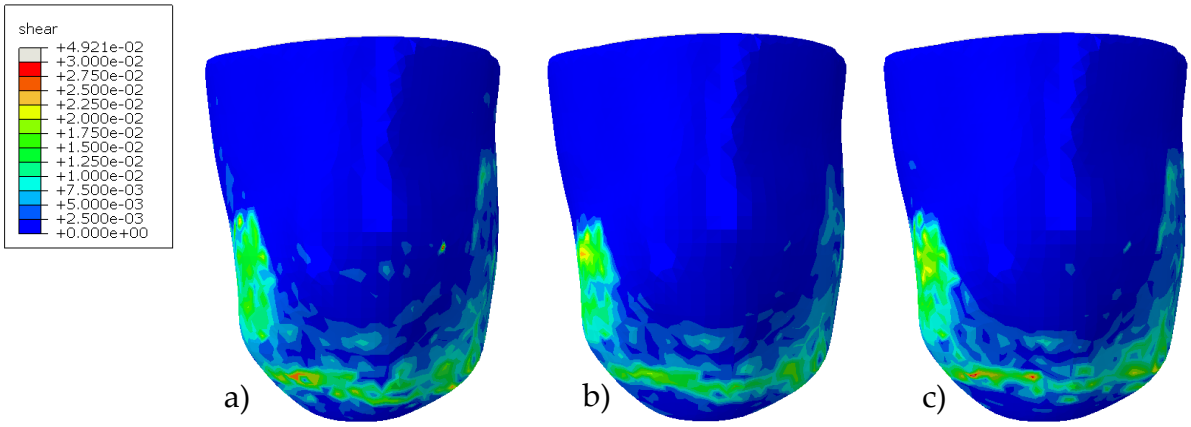

Figure 8.8 CSHEAR on contracted soft tissue with a) silicone, b) urethane, c) TPE liner in standing

8.3. Foot Flat

Regarding Foot Flat, with flaccid soft tissue the maximum values reached by CPRESS are 237.4 kPa, 178.4 KPa, and 170.2 KPa for silicone, urethane and TPE respectively. Instead with contracted soft tissue they are 206 kPa, 181.7 kPa and 170 kPa for silicone, urethane and TPE respectively. These values are concentrated in a small area of the lateral flare of the tibia and the sub-patellar region in this case. Pressures are not as evenly distributed as in the standing phase, but they are more concentrated in the patellar tendon area. These might be explained by the existence of femoral rotation and moment on the socket. In fact, just a vertical load was applied in the standing. Instead, there were forces and moments in each direction in Foot Flat. Figures 8.9 and 8.10 illustrate the results. With flaccid soft tissue, the greatest values are 61.57 kPa, 30.82 kPa, 51.13 kPa. With contracted soft tissue, the highest results are 62.67 kPa, 32.89 kPa, 44.94 kPa. They are more prevalent in the sub-patellar area. Figures 8.11 and 8.12 show the results on the stump.

CPRESS

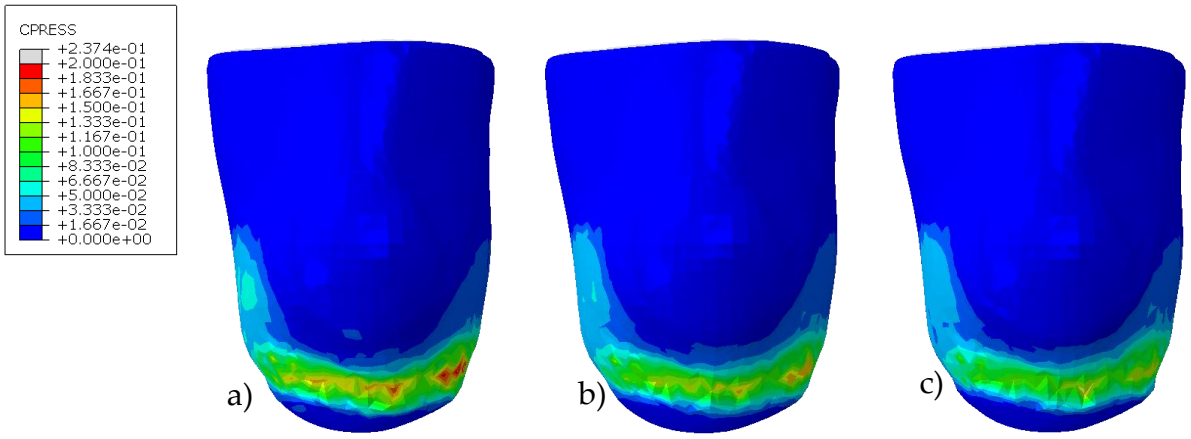

Figure 8.9 CPRESS on flaccid soft tissue with a) silicone, b) urethane, c) TPE liner in Foot Flat

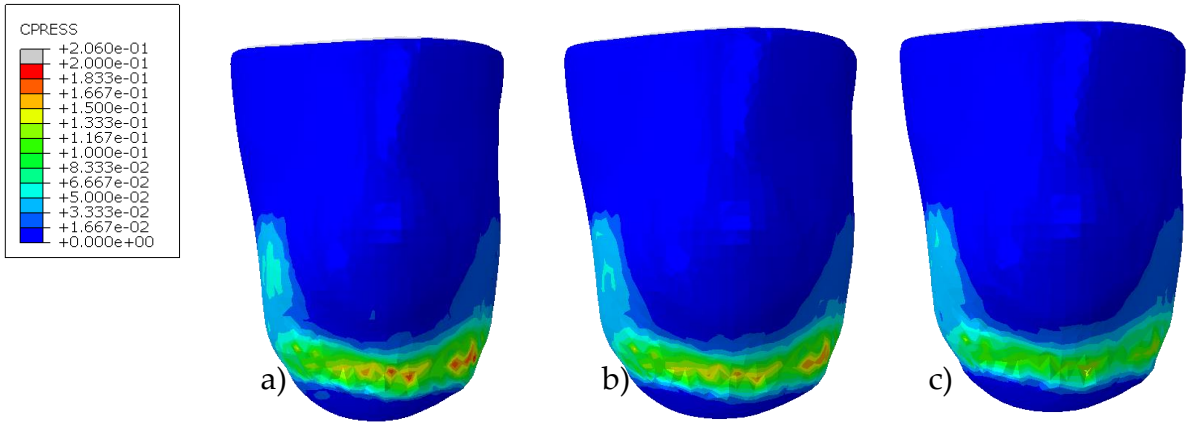

Figure 8.10 CPRESS on contracted soft tissue with a) silicone, b) urethane, c) TPE liner in Foot Flat

CSHEAR

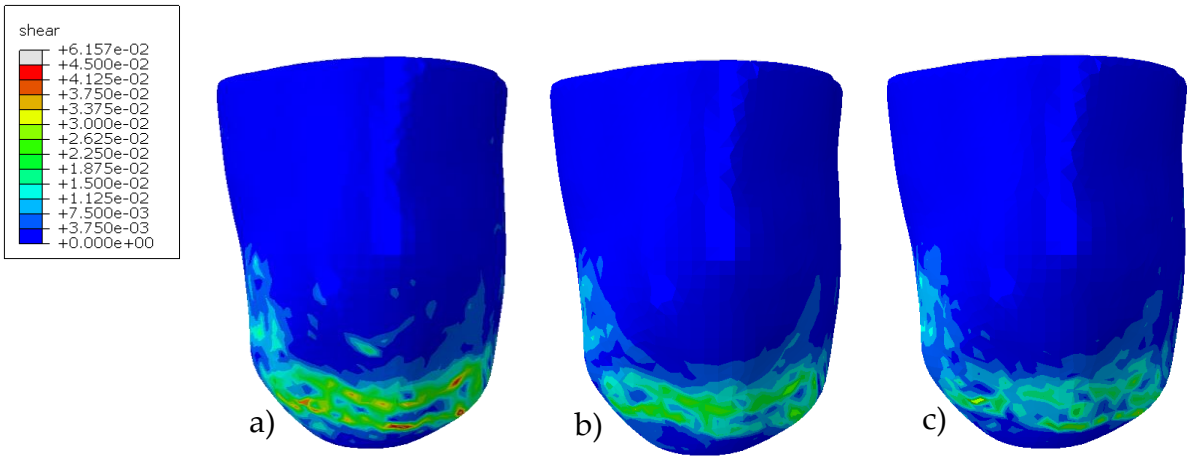

Figure 8.11 CSHEAR on flaccid soft tissue with a) silicone, b) urethane, c) TPE liner in Foot Flat

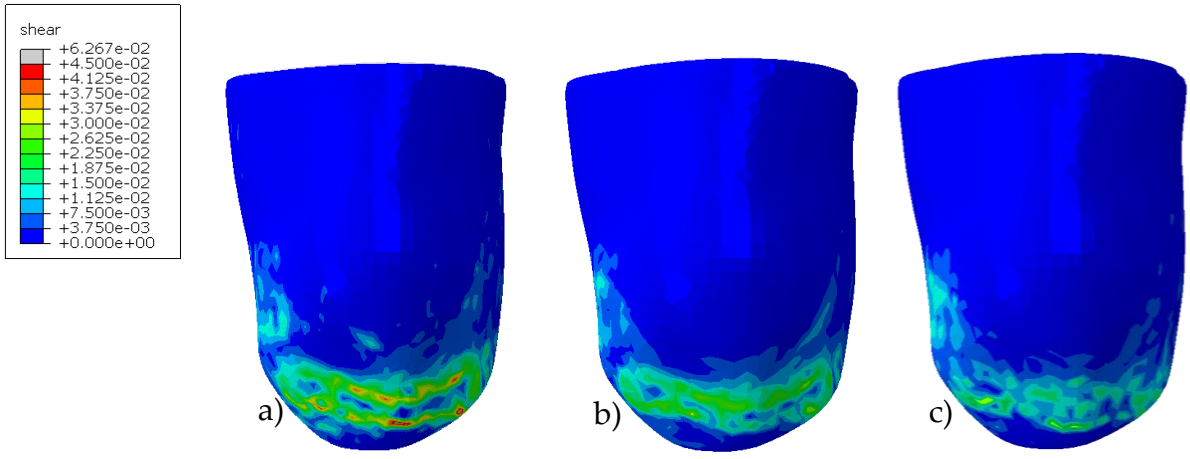

Figure 8.12 CSHEAR on contracted soft tissue with a) silicone, b) urethane, c) TPE liner in Foot Flat

8.4. Mid Stance

Maximum values of CPRESS on flaccid soft tissue at the conclusion of Mid Stance simulation are 207.3 kPa, 189.2 KPa, and 185.6 KPa for silicone, urethane, and TPE respectively. Instead, for contracted soft tissue, the values are 201.6 kPa, 171.9 KPa, and 177.3 kPa for silicone, urethane, and TPE respectively. Peak pressures are concentrated in the tibia's medial flare. Pressures are highest in the sub-patellar area and the lateral flare of the tibia, as in Foot Flat. Figures 8.13 and 8.14 illustrate the results. With flaccid soft tissue, the maximum shear stresses are 57.16 kPa, 36.76 kPa, and 57 kPa, whereas with contracted soft tissue, the highest shear stresses are 58.91 kPa, 39 kPa, and 45.15 kPa. They occupy the lateral tibial condyle and sub-patellar region. Figures 8.15 and 8.16 show the results.

CPRESS

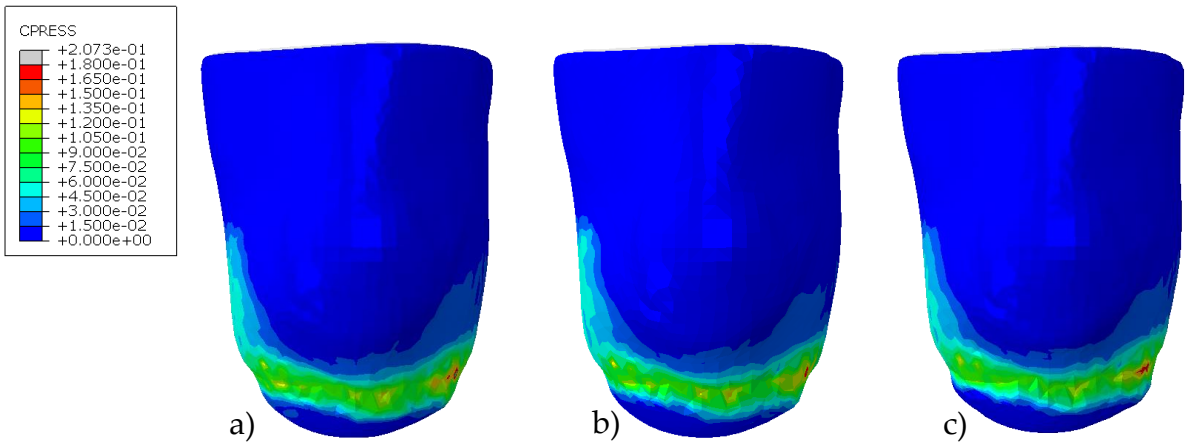

Figure 8.13 CPRESS on flaccid soft tissue with a) silicone, b) urethane, c) TPE liner in Mid Stance

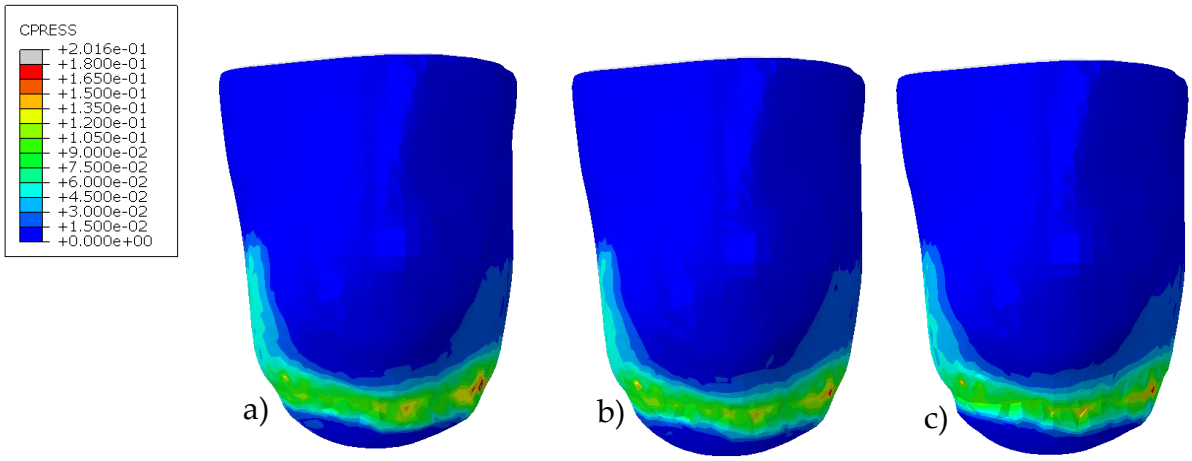

Figure 8.14 CPRESS on contracted soft tissue with a) silicone, b) urethane, c) TPE liner in Mid Stance

CSHEAR

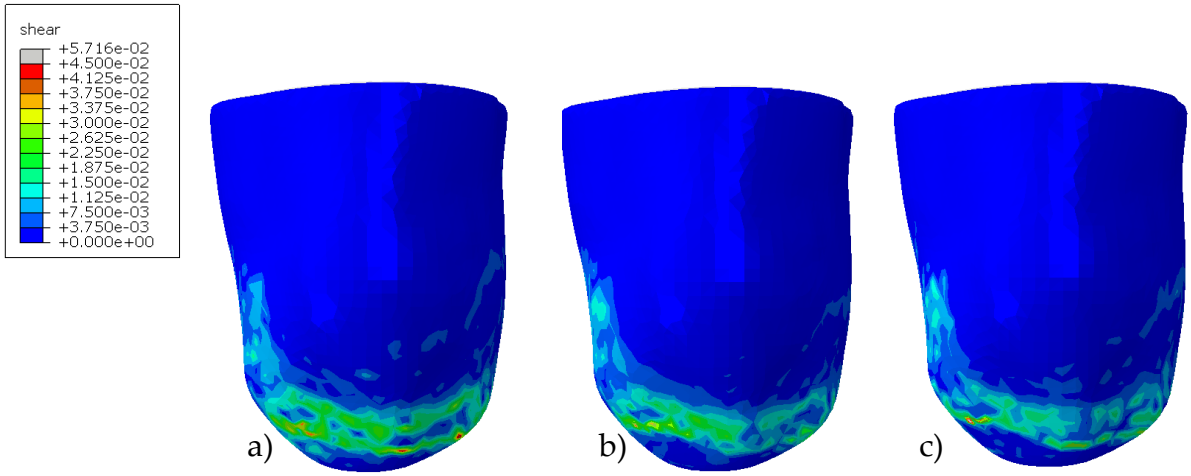

Figure 8.15 CSHEAR on flaccid soft tissue with a) silicone, b) urethane, c) TPE liner in Mid Stance

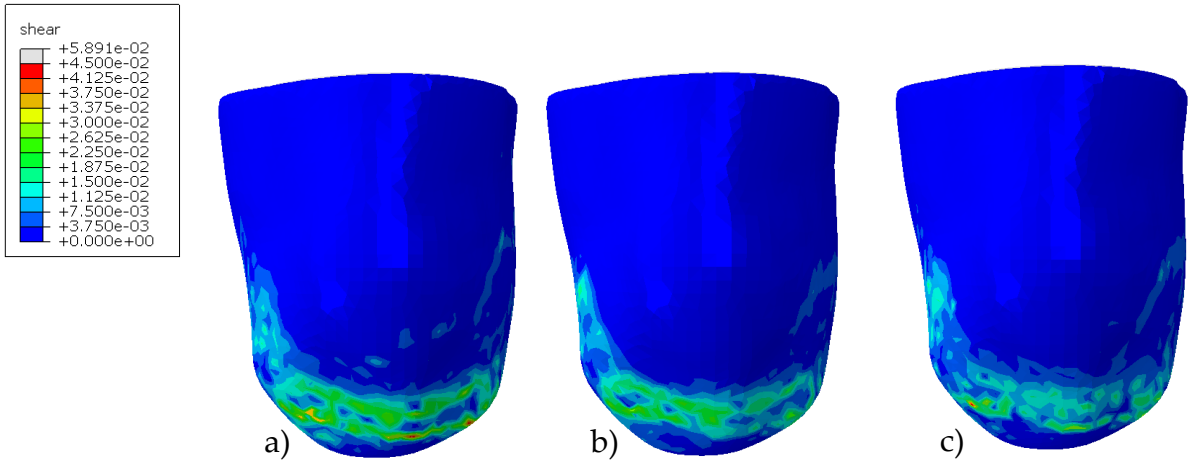

Figure 8.16 CSHEAR on contracted soft tissue with a) silicone, b) urethane, c) TPE liner in Mid Stance

8.5. Internal stresses in the soft tissue

Von Mises stresses were used to evaluate the stresses inside the residual limb. Sections of soft tissue were obtained using the *View cut* tool in order to analyze what transpired within. The cut on Z-planes, i.e. take the longitudinal axis as the normal to the plane, was chosen for this task. Two cuts were performed: one allowed to visualize the stress distribution at the level of femur and patella, and the other showed what happened in tibia. Furthermore, in each simulation the peak stress was concentrated in a single element, and it was significantly higher with respect to all nearby elements. So, to improve display of the findings and compare the results, a value was specified as the upper limit in the *Contour Plot Options* menu: 80 kPa for standing and Mid Stance, and

180 kPa and 80 kPa for Foot Flat at the level of femur and tibia respectively. Using this tool, the higher pressures appear behind the tibia in standing, and between femur and patella in Foot Flat and Mid Stance. The contracted soft tissue is examined in Figures 8.17, 8.18, and 8.19 to represent the distribution of stresses in standing, Foot Flat and Mid Stance, and to compare the differences when the liner material changes. In this analysis donning is not shown because it was added to evaluate pre-stresses at the interface with the liner, whereas here the focus is to find regions inside the stump where higher pressures are applied. In all the three phases studied they are all greater with respect to those obtained in donning simulation.

STANDING

a) *Silicone*

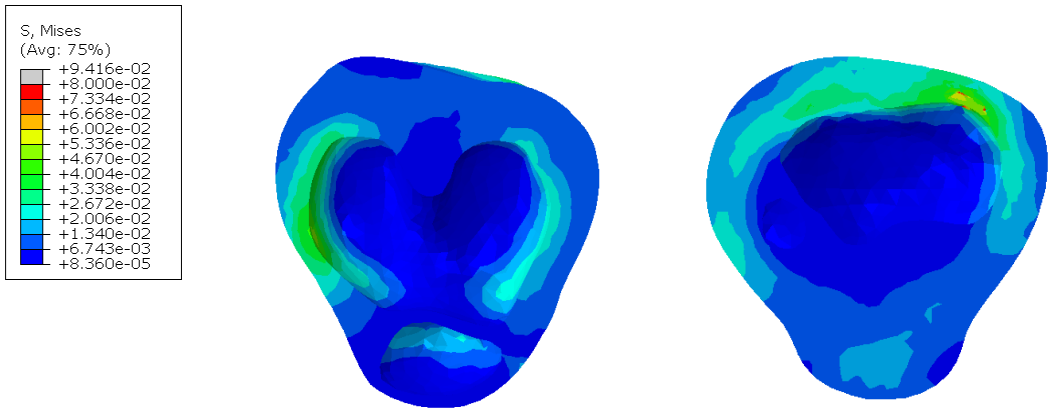

b) *Urethane*

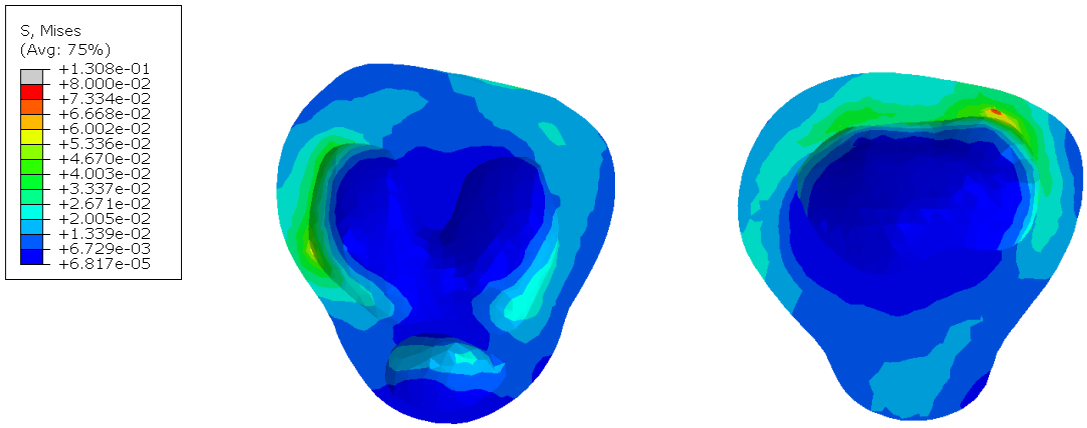

c) TPE

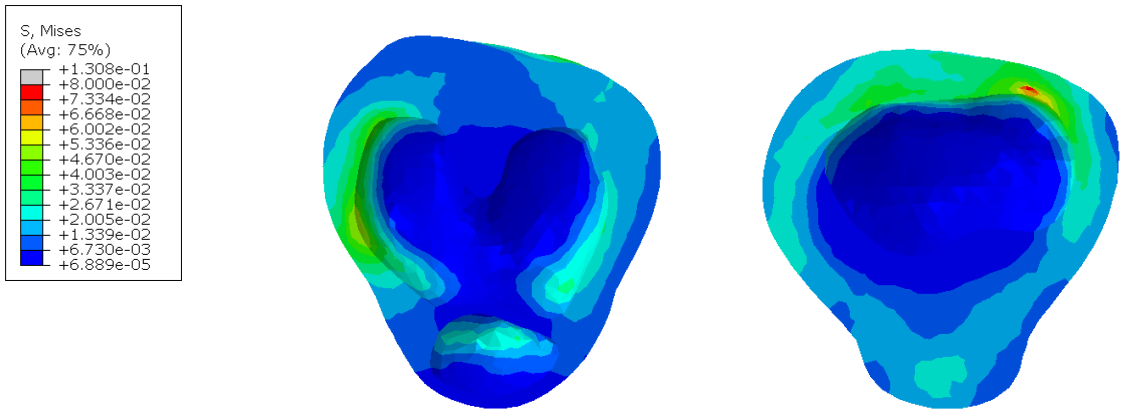

Figure 8.17 Von Mises stresses in soft tissue at the level of femur and patella on the left and of tibia on the right with a) silicone, b) urethane, c) TPE liner in standing

FOOT FLAT

a) Silicone

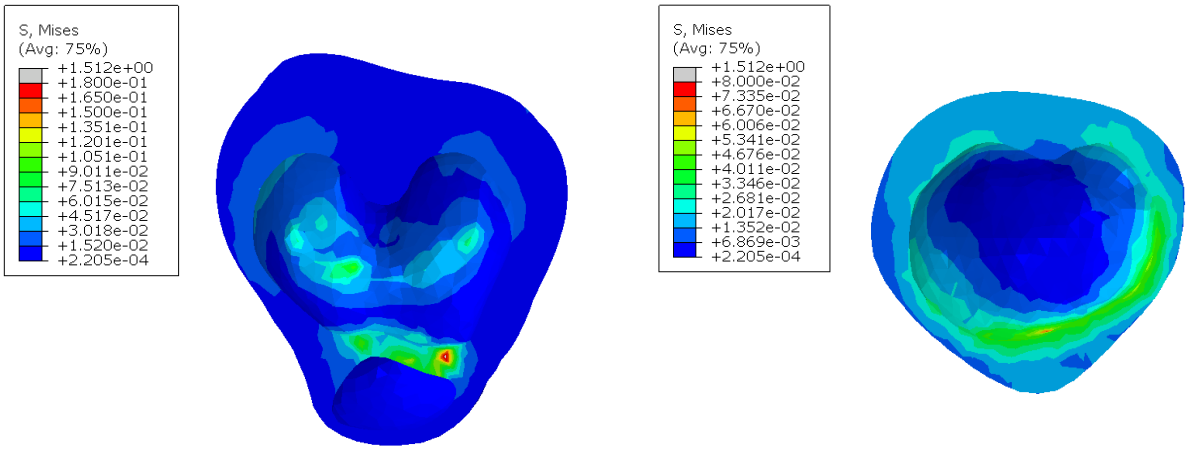

b) *Urethane*

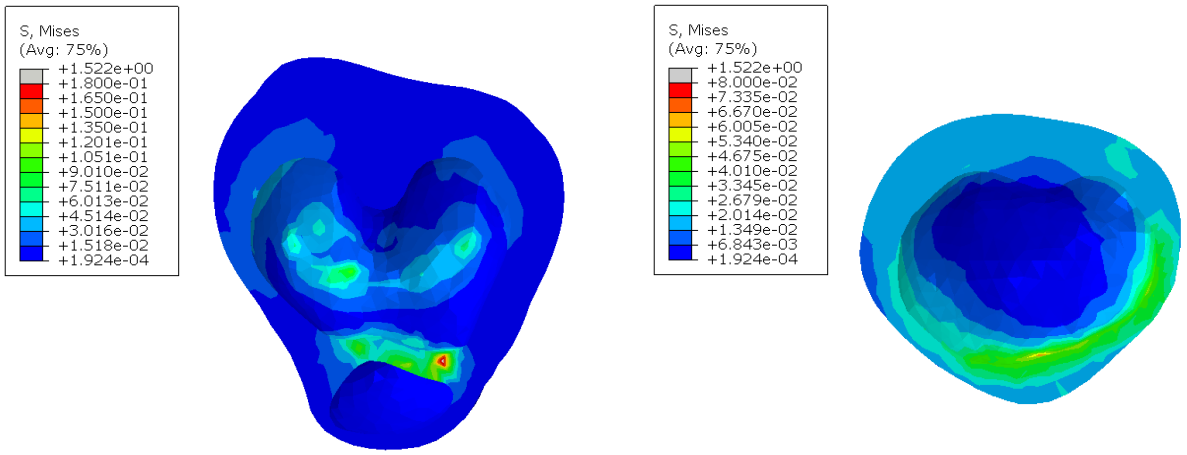

c) TPE

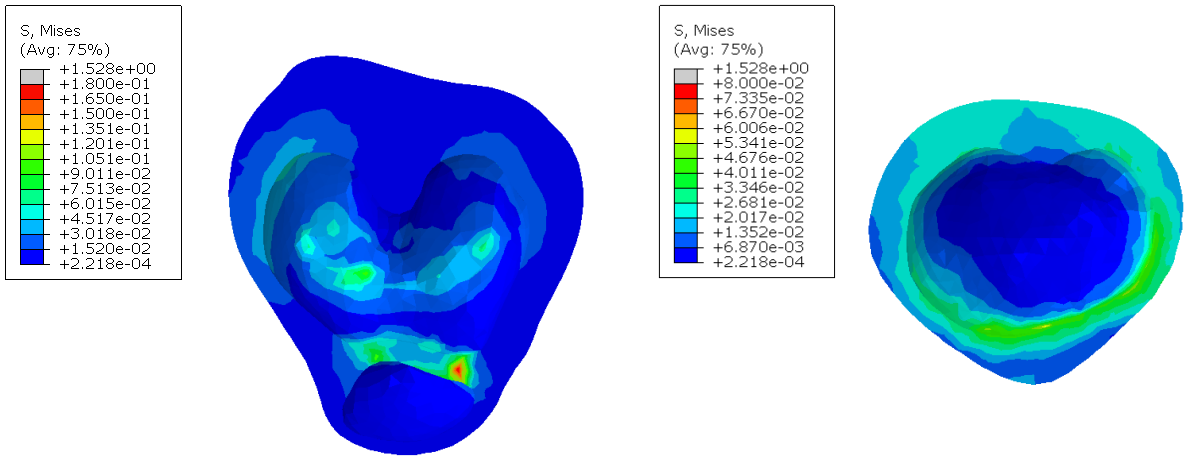

Figure 8.18 Von Mises stresses in soft tissue at the level of femur and patella on the left and of tibia on the right with a) silicone, b) urethane, c) TPE liner in Foot Flat

MID STANCE

a) Silicone

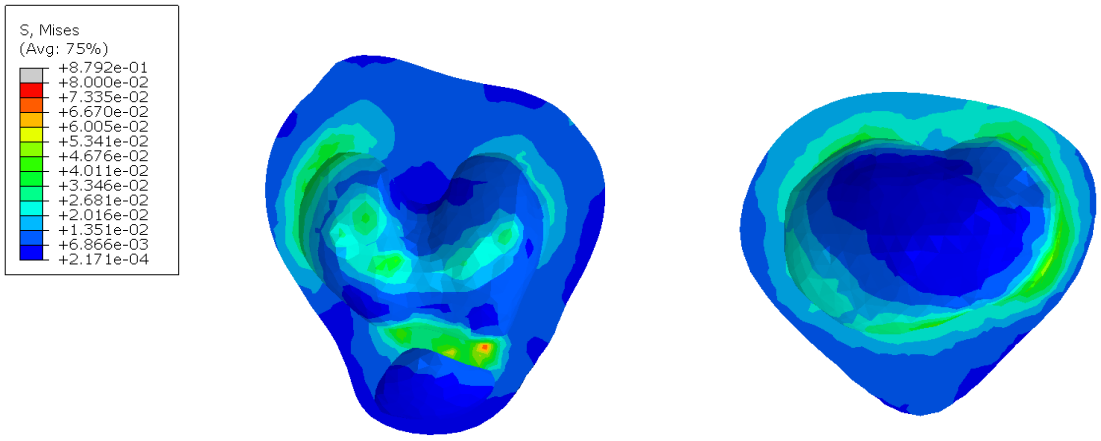

b) *Urethane*

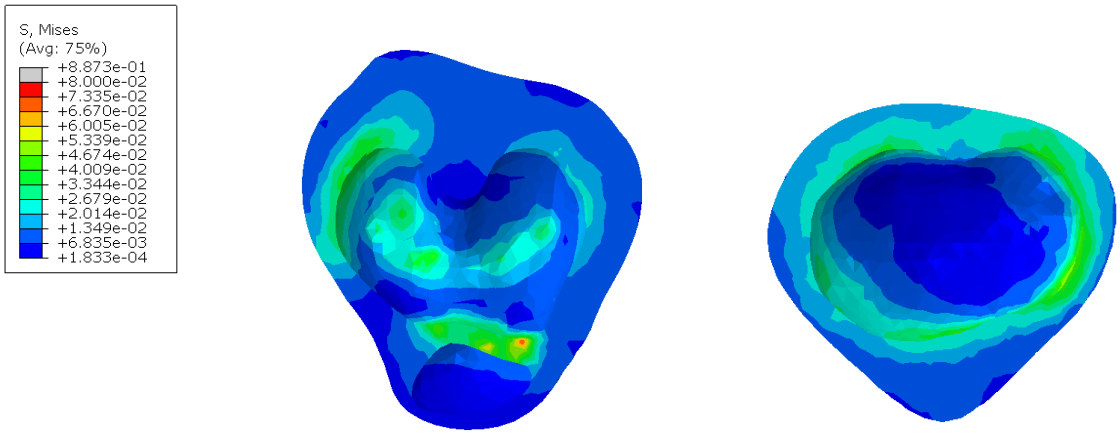

c) TPE

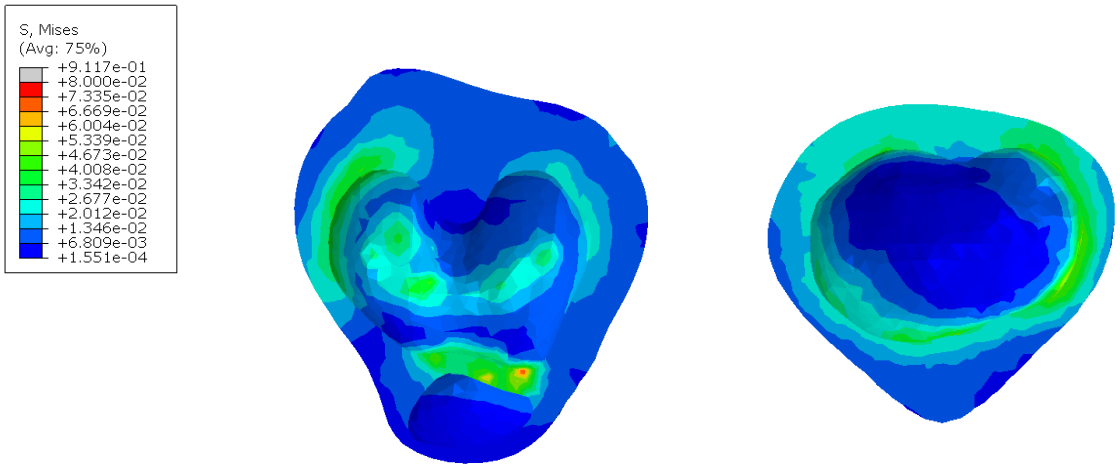

Figure 8.19 Von Mises stresses in soft tissue at the level of femur and patella on the left and of tibia on the right with a) silicone, b) urethane, c) TPE liner in Mid Stance

After that, a comparison between the two material properties of the soft tissue were performed in the same sections used before. So, to better understand the differences, a *path* was created in the *Visualization* module. It is a line defined by specifying a series of points through the model. To identify the *path*, the method "*by shortest distance*" was chosen. It allows selecting an element edge and a node and then *Abaqus/CAE* choosing the shortest distance path along the element edges between them [66]. This method was chosen because it was not easy to select nodes inside the soft tissue manually. Figures 8.20 and 8.21 show the *paths* used for standing and gait phases. They were taken where the value difference was evident, and in particular in the posterior part of the tibia for the standing, and between the femur and patella in Foot Flat and Mid Stance.

Figure 8.20 *Path* on the soft tissue section for double leg standing

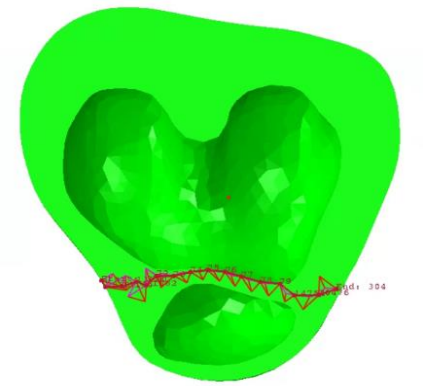

Figure 8.21 *Path* on the soft tissue section for gait phases

After creating the *path*, an XY plot was generated with the stresses on the y axis and the position along the *path* on the x axis. In particular, X-values correspond to each point's actual distance along the *path* in model space coordinates, starting with zero [66]. Figures 8.22, 8.23 and 8.24 show the graph obtained in standing, Foot Flat and Mid Stance respectively.

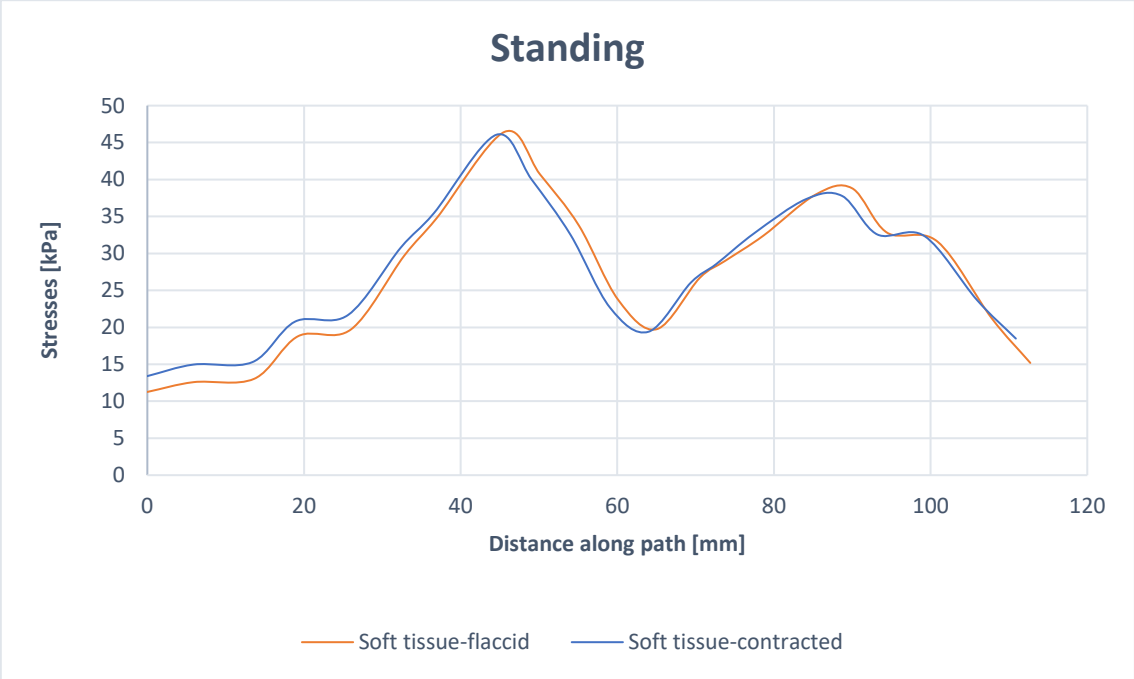

Figure 8.22 Comparison of Von Mises stresses along the *path* in double leg standing with flaccid soft tissue and contracted soft tissue

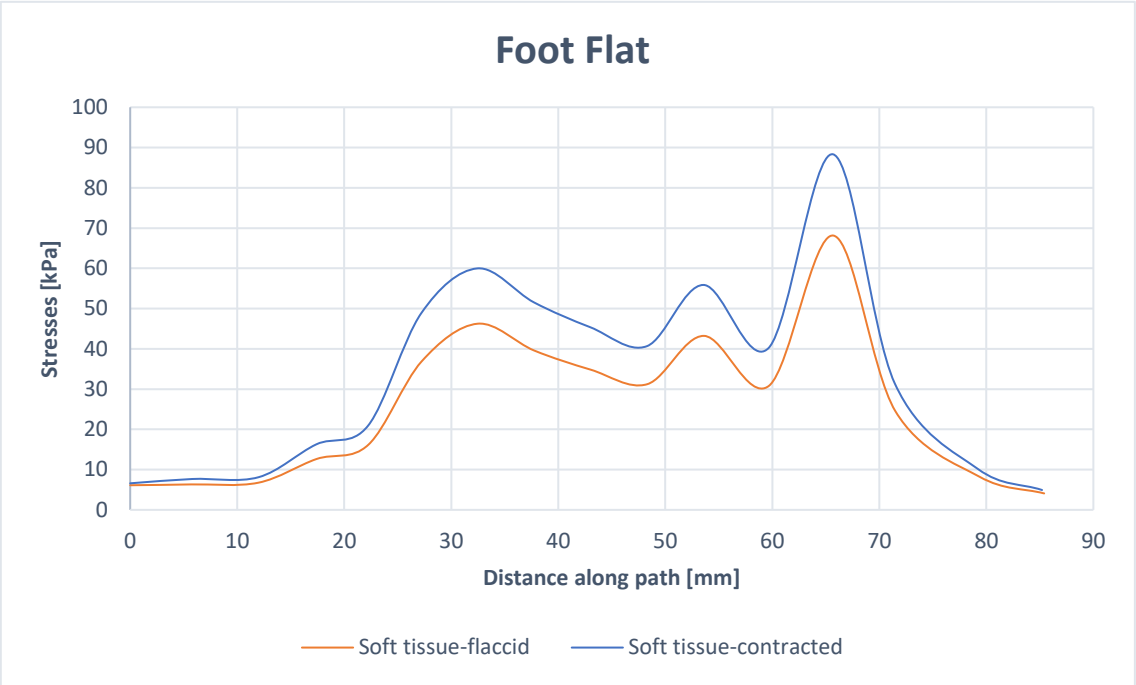

Figure 8.23 Comparison of Von Mises stresses along the *path* in Foot Flat with flaccid soft tissue and contracted soft tissue

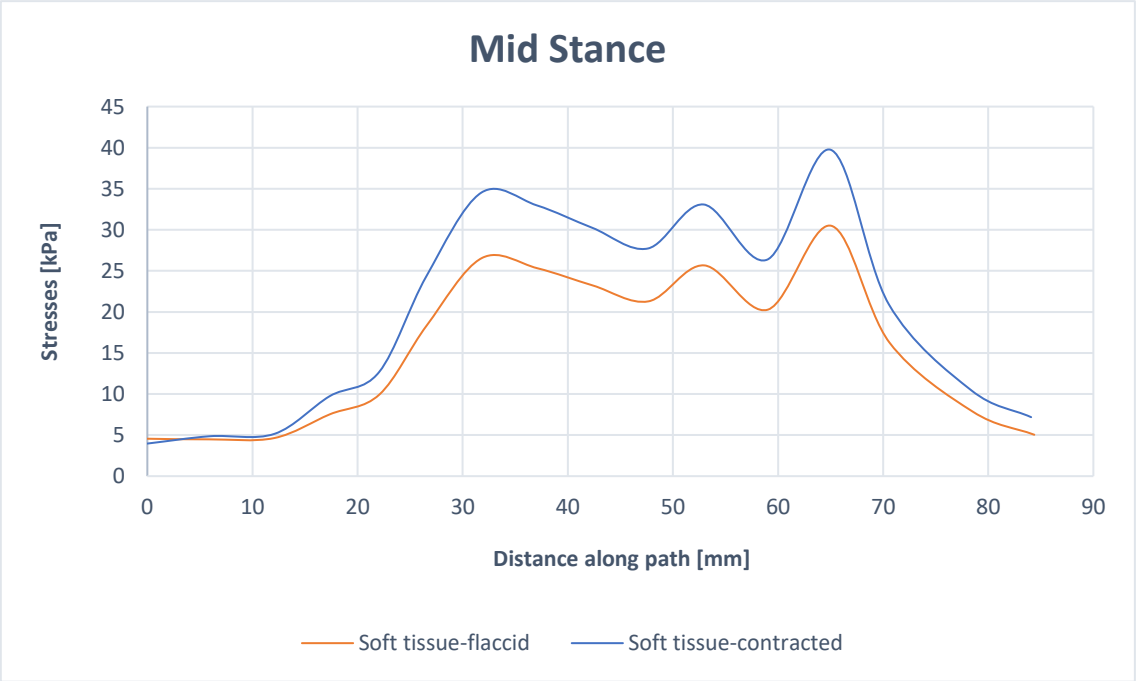

Figure 8.24 Comparison of Von Mises stresses along the *path* in Mid Stance with flaccid soft tissue and contracted soft tissue

9.Discussion

The investigation is separated into two stages. The first compares the peak normal and shear stresses on the stump, concentrating on the differences between liner materials and soft tissue material properties. The analysis then shifts its emphasis to the internal stresses in the soft tissue.

9.1. Analysis of pressure and shear stress on the residual limb

The first analysis is a comparison of all data to the pain pressure tolerance and threshold shown in Table 9.1 [39]. As described in the "Prosthesis satisfaction" paragraph, this is a critical issue because if the pressures on the stump surpass certain values, the patient would have significant complications. However, when the highest results from each simulation are compared to the threshold values, contact difficulties should be avoided because all outcomes are lower all over the stump. In fact, the highest pressure value was detected during the simulation of the Foot-Flat phase with the coupling of the silicone liner with the flaccid soft tissue in the region of medial flare of the tibia and is equal to 237.4 kPa, which is significantly lower than all pain pressure tolerances and thresholds.

	Fibular head	**Medial condyle**	**Popliteal fossa**	**End of stump**	**Patellar tendon**
Pain pressure threshold (KPa)	599.6±82.6	555.2±132.2	503.2±134.2	396.3±154.5	919.6±161.7
Pain pressure tolerance (KPa)	789.8±143.0	651.0±111.1	866.6±77.3	547.6±109.1	1158.3±203.2

Table 9.1 Pain pressure threshold and tolerance [39]

Following this first examination, a comparison of the outcomes obtained from the different coupling of liner and soft tissue material properties is made. The discussion focuses mainly on the sub-patellar region and lateral and medial part of the tibia because they presented the higher pressures. Instead, there are no significant variations in popliteal depression, and the contact pressures in this area are lower than those present in the other parts of the stump.

First, donning is analyzed. It is important to study because it adds pre-stresses all over the stump. The peak contact pressure decreases passing from silicone to urethane to TPE liners for both types of soft tissue. This trend can be clearly observed in the sub-

patellar region in “Results” chapter. Instead, considering peak shear stress urethane and TPE show higher values with respect to silicone. The comparisons are depicted in Figures 9.1 and 9.2. From these figures it is possible to notice that peak values for both CPRESS and CSHEAR are higher with contracted soft tissue with respect to the other one. This could be explained by the fact that a greater force is needed to reach the same position on the stump with the stiffer soft tissue.

The outcomes of the donning simulation are compared with a work of Steer et al. [44], that simulated donning explicitly. They obtained a peak contact pressure around 70 kPa and a peak shear stress of 30 kPa. The first one is comparable with the TPE liner and is lower with respect to the others. Instead, considering the shear stress it is similar to the silicone case and lower compared to the others. Differences can be justified by the presence of variations in the models, as the geometries or boundary conditions. Then, a comparison with work of Lee et al. [46] is made. In this case they did not simulated donning explicitly, but an axial force of 50N was applied to approximate the force stabilizing the limb in the socket. They obtained a peak pre-stress of 147 kPa in the popliteal depression that is higher with respect to those found in this work. However, if the patellar tendon area is considered, more comparable results are observed. The differences could be explained with the variations in the method used to simulate the donning and in the geometries of the socket.

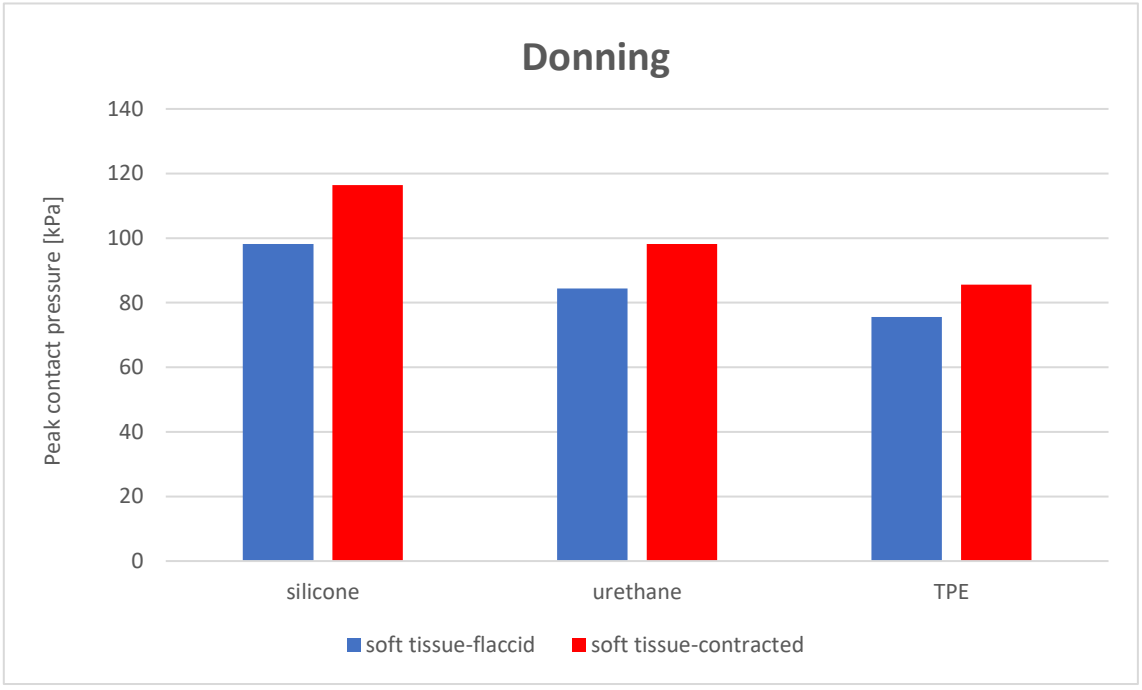

Figure 9.1 Comparison of CPRESS in donning

Figure 9.2 Comparison of CSHEAR in donning

When evaluating the standing phase, the peak pressure on the stump reduces from silicone to urethane to TPE liner for both kinds of soft tissue. Instead, in terms of shear stresses, the opposite trend is evident. Figures 9.3 and 9.4 depict a comparison of CPRESS and CSHEAR peak values. When it comes to CPRESS peak values, it is worth noting that they are usually higher in flaccid soft tissue. Instead, when the distribution of contact pressures is studied, TPE displays lower values again, even if the silicone liner shows a higher decrease in the lateral flare of the tibia.

These findings are comparable to those of Cagle et al. [49], who examined three patients by means of FEA. The maximum peak pressure and shear stress were around 90 kPa and 45 kPa, respectively. The pressure is somewhat lower in comparison to the findings of this work, but the shear stresses are lower in the case of silicone and urethane, and greater in the case of TPE liner. They are, however, of the same order, and there isn't much of a distinction between them. These inconsistencies can be explained by the fact that various factors, such as geometries, material characteristics, interactions, and boundary conditions, were used to simulate the model and change between the two works. Therefore, we can say that our results are in reasonable agreement with those found in the literature.

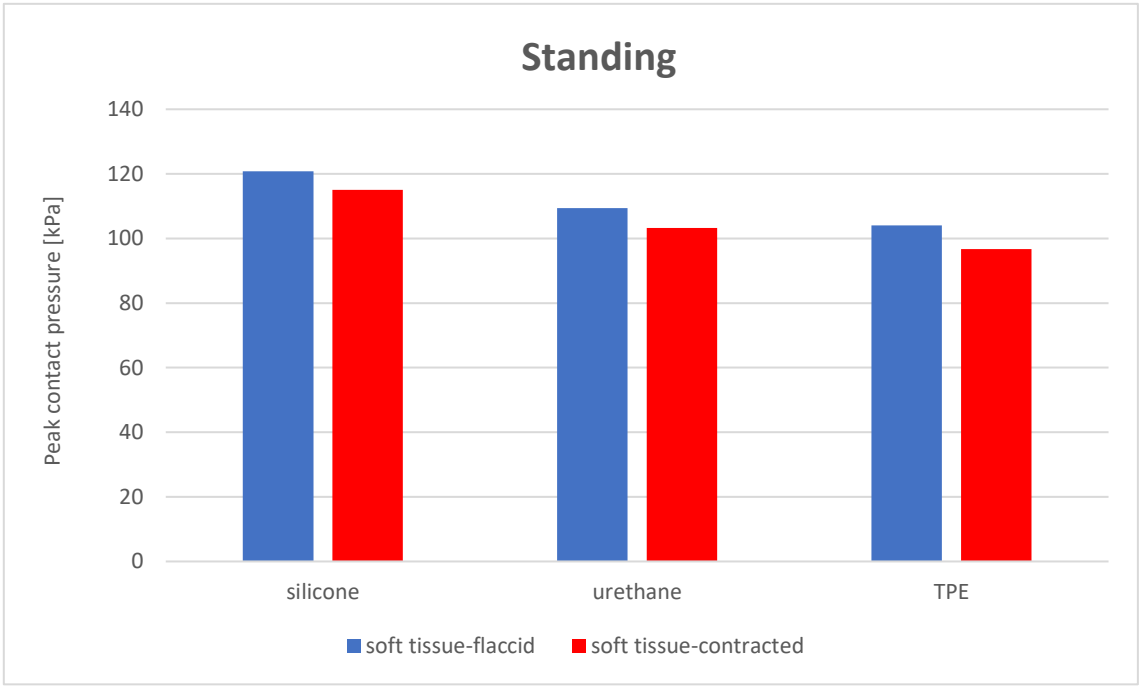

Figure 9.3 Comparison of CPRESS in standing

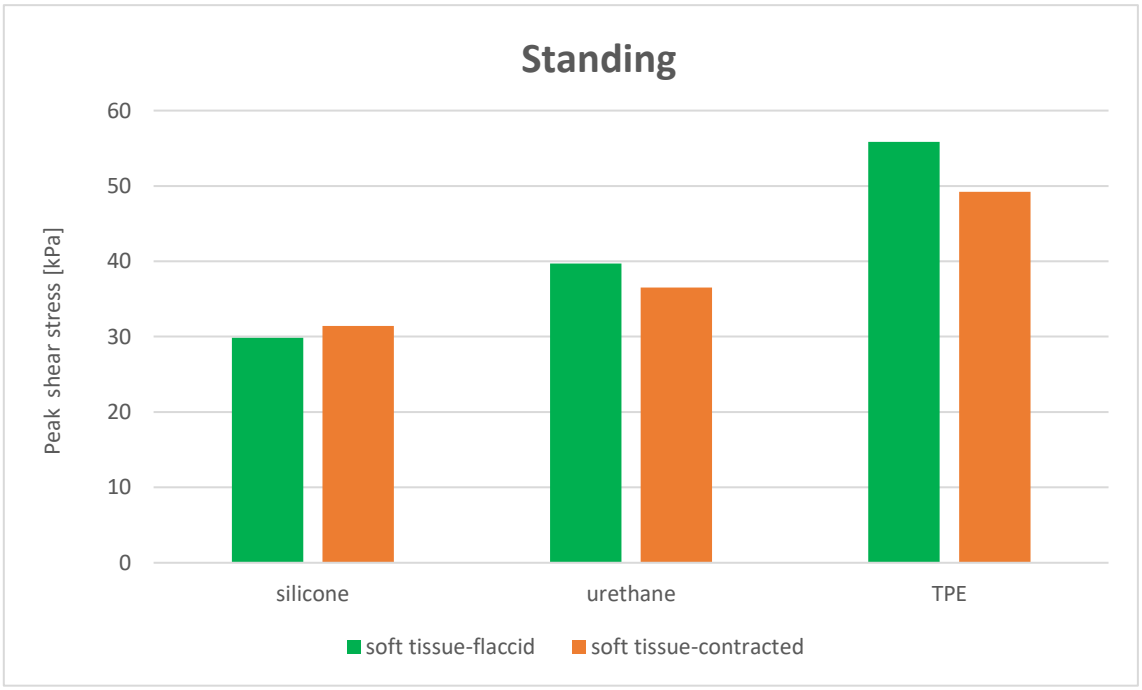

Figure 9.4 Comparison of CSHEAR in standing

Then, when the pressures are evaluated, Foot Flat exhibits a similar pattern. However, the values of urethane and TPE liners are comparable. Instead, shear stresses respond differently with regard to standing because the silicone shows the highest peak value, followed by TPE and urethane. Figures 9.5 and 9.6 depict the results. Using the

distribution of contact pressures and shear stresses as an alternative to peak values, the TPE liner produced better results.

The peak values can be compared to a work of Lee et al. [46] on a patient weighing 80 kg. A peak normal stress of roughly 250 kPa and a peak shear stress more than 100 kPa were detected during this period of the gait. These results are superior to those discovered in this paper, which might be explained by the fact that they applied higher loads, but also that they did not consider the liner. When compared to the work of Jia et al. [51], in which a patient of 80 kg was tested and the liner was present, the peak pressure is about 250 kPa, which is somewhat greater than the results of this work. CSHEAR findings with silicone and TPE liners, on the other hand, are comparable, since they got a value of 55 kPa. The discrepancies might be justified with the differences between the two models, regarding geometries, boundary conditions and contacts.

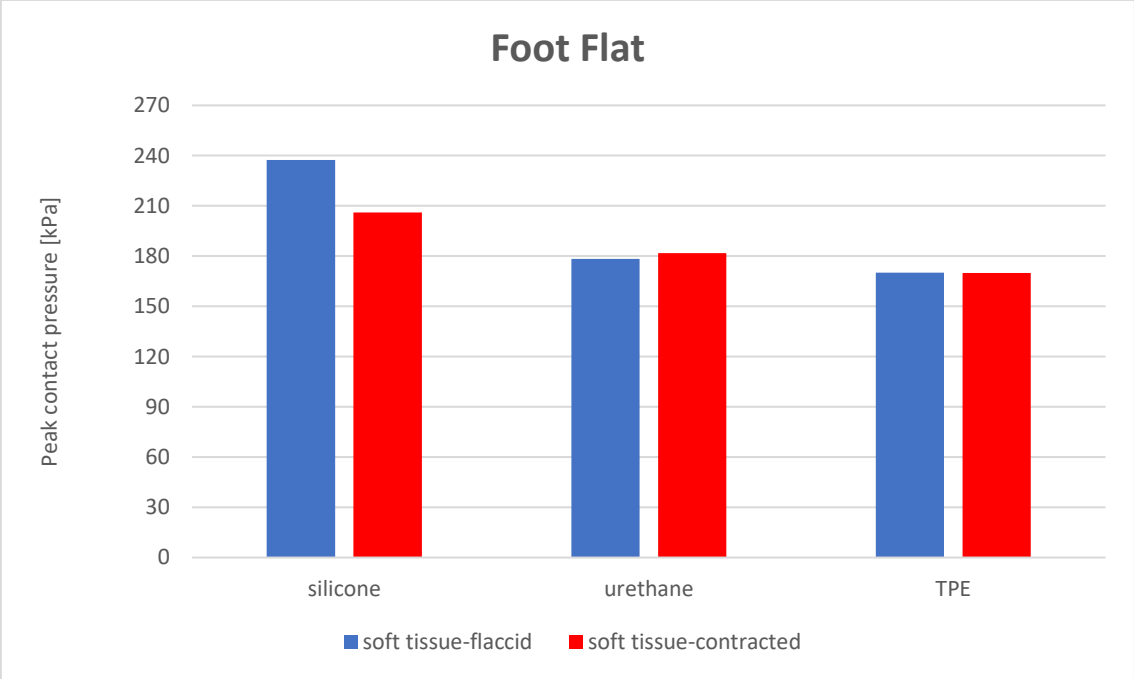

Figure 9.5 Comparison of CPRESS in Foot Flat

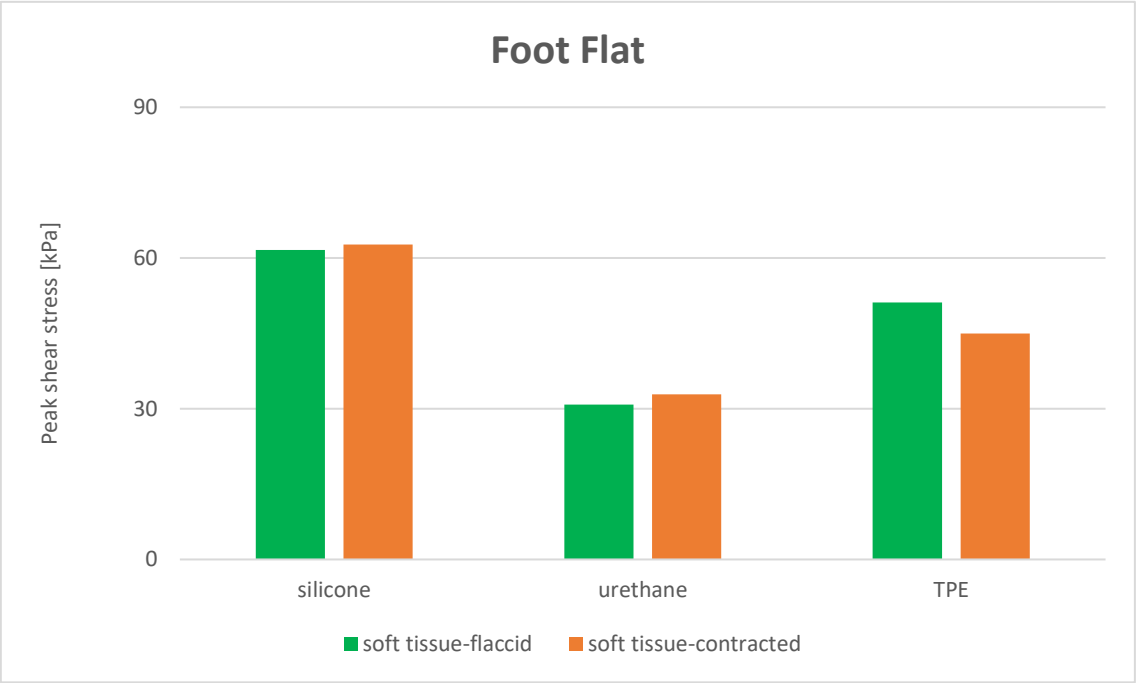

Figure 9.6 Comparison of CSHEAR in Foot Flat

Finally, midstance is analyzed. Again, the peak pressures decrease passing from silicone to urethane to TPE liners. However, peak normal stresses for both urethane and TPE are comparable. This trend is the same for the two types of soft tissue, but for the stiffer one, values are lower. Silicone also has a higher peak shear stress. Then it is followed by the TPE and then the urethane. In this case, flaccid soft tissue has lower outcomes except for the TPE liner. The results are shown in Figures 9.7 and 9.8. Then, considering the distribution of both contact pressures and shear stresses, no great differences are noticed. So, this means that except for the regions with the peak values silicone has a capacity to reduce stresses similar to urethane and TPE.

Compared to the study conducted by Lee et al. [46], peak normal stresses are similar, but the shear stresses of this work are smaller. This could be justified by the fact that loads applied in this phase are more comparable with respect to Foot Flat, but differences in the geometries and boundary conditions are still present. According to the study conducted by Jia et al. [51], peak normal pressure is around 250 kPa, which is higher compared to results of this work particularly in the presence of urethane or TPE liners. In terms of peak shear stress, they found a value between 50 and 60 kPa, which is similar to the silicone case or the TPE coupled with flaccid soft tissue but greater than when the urethane liner was used. The reasons for these distinctions might be found in the changes of the model, like geometries, boundary conditions and interactions.

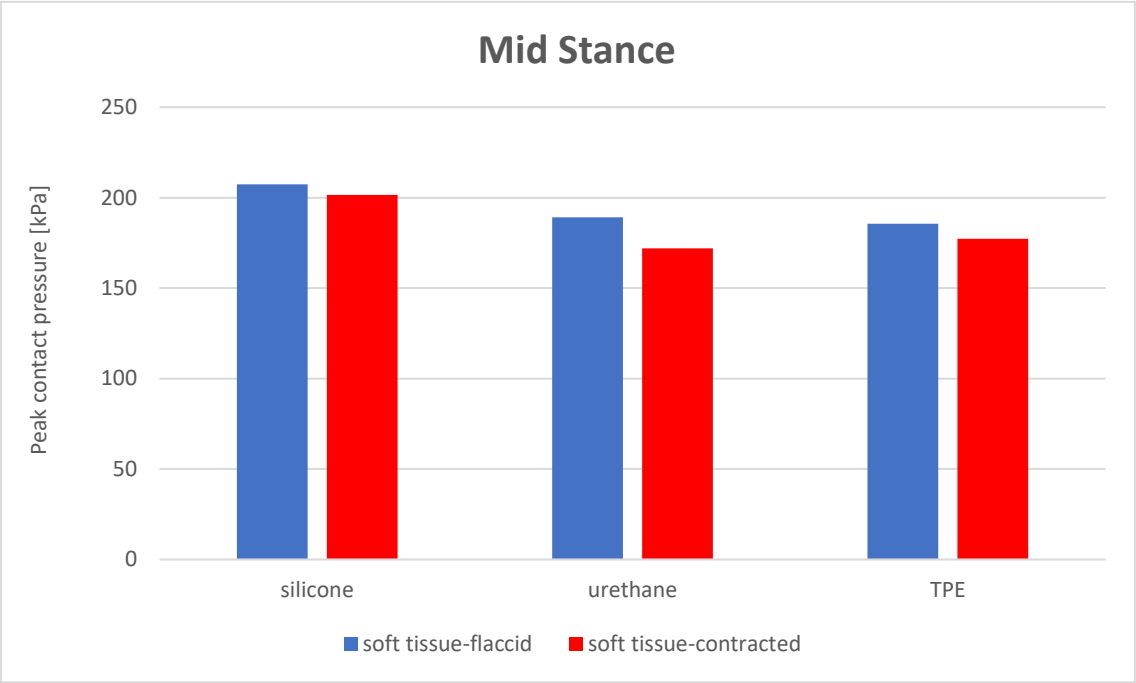

Figure 9.7 Comparison of CPRESS in Mid Stance

Figure 9.8 Comparison of CSHEAR in Mid Stance

As a consequence of these comparisons with the literature, the results of Foot Flat and Mid Stance are deemed fair. However, it is important to underline that changes in the finite element model bring to different results. So, the simulation must be as similar as possible to reality in order to obtain results closer to real stresses exerted on the

residual limb of the patient. This is a limitation of finite element model because simplifications are generally applied to reduce computational effort.

Then, based on these results, urethane and TPE appear to be superior to silicone, which has greater peak values. However, silicone exhibits a comparable distribution of contact pressures and shear stresses in standing and Mid Stance. The trends in liner materials are compared to Cagle's study [65]. He investigated the influence of liner materials in two load scenarios: one with simply an axial force and one with vertical, shear, and sagittal stresses as well as a sagittal moment. The soft sticky liner had the lowest peak pressure and peak shear stresses, according to his findings. Because it exhibits mechanical characteristics that are identical to those attributed to TPE, these results are verified. Instead, larger loads were discovered for the hard-slick liner, which is similar to urethane. However, in this study, urethane produces outcomes that are similar to TPE. The alterations in the finite element model can explain these variances.

Furthermore, when studying the distribution of the CPRESS in all the simulated phases, minor variations between the two types of soft tissue are observed, although they are not significant. Peak contact pressure study indicates that in most of the cases flaccid soft tissue has higher values, except in the donning. This is not true all over the stump since, for example, when peak pressures in the sub-patellar area are examined, generally the opposite pattern is observed, as shown in Tables 9.3, 9.4 and 9.5. As a result, for the contact pressure, a general assumption about the difference between the two types of soft tissue cannot be made, and each location of the stump must be analyzed. Despite this, variances in values are not particularly important. Instead, Table 9.2 shows that contracted soft tissue has higher contact pressures also in the sub-patellar region and the variation with the flaccid soft tissue is quite important. This could mean that a stiffer stump creates a higher resistance to the donning as supposed when peak values were analyzed. So, the coupling of the silicone liner with the contracted soft tissue does not seem a good choice. The changes in CSHEAR values are relatively tiny, as seen by a look at the peak findings. This might imply that the mechanical characteristics of soft tissue, unlike liner materials, have no impact on shear stresses across the stump. Another possible explanation is that the changes in parameters used to characterize the two types of soft tissue are too low, and so the differences are not significant.

	Silicone	**Urethane**	**TPE**
soft tissue-flaccid	73.8 kPa	68.3 kPa	58.31 kPa
soft tissue-contracted	89.18 kPa	83.6 kPa	72.54 kPa

Table 9.2 Peak CPRESS at sub-patellar region in donning

	Silicone	Urethane	TPE
soft tissue-flaccid	88 kPa	88.14 kPa	83.73 kPa
soft tissue-contracted	93.8 kPa	92.8 kPa	87.57 kPa

Table 9.3 Peak CPRESS at sub-patellar region in standing

	Silicone	Urethane	TPE
soft tissue-flaccid	180.6 kPa	159.36 kPa	151 kPa
soft tissue-contracted	182.5 kPa	165 kPa	144.37 kPa

Table 9.4 Peak CPRESS at sub-patellar region in Foot Flat

	Silicone	Urethane	TPE
soft tissue-flaccid	138.8 kPa	149 kPa	126.19 kPa
soft tissue-contracted	143.86 kPa	143.8 kPa	133.47 kPa

Table 9.5 Peak CPRESS at sub-patellar region in Mid Stance

Looking at the above tables, it is possible to notice that higher contact pressures are present in Foot Flat for all the liners. However, if the peak values are evaluated, urethane and TPE liners show comparable results in Foot Flat and Mid Stance. So, different regions of stump don't have the same behavior and must be evaluated separately. Moreover, in Foot Flat contact pressure variations between different liner materials are greater with respect to standing and Mid Stance as explained also for the peak values. So, silicone presents higher contact pressures in Foot Flat and comparable ones in standing and Mid Stance with respect to urethane and TPE liners. This could mean that it is more sensitive to higher loads and is not able to distribute them as well as urethane and TPE.

9.2. Analysis of internal stresses in the soft tissue

For what concerns internal stresses in the residual limb, no relevant differences are found changing the liner material, as it's possible to see in the images in the "Results" chapter. So, the liner has a greater role in the interface stresses than in reducing loads inside the soft tissue. On the contrary, moving from one kind of soft tissue to another, something changes, and this means that different soft tissue material properties have an influence on the internal stresses. The peak stresses are not considered in this

analysis because the maximum Von Mises value is concentrated on one element inside the soft tissue and the others are much lower. If it were used, the comparison would not be reasonable, and due to the fact that it is so different with respect to the other results, it could be an error of the analysis. So, the focus is the stress distribution inside the stump. Below standing and gait are discussed separately, and they referred to the graphs in "Results" chapter.

In the standing phase, significant variations are not present in values and the distribution of the stresses along the *path* is gradually shifted to the right for the flaccid soft tissue. So, the results are comparable. Taking *path* in different positions, outcomes do not change. This could mean that material properties of the soft tissue do not affect the results with lower loads.

Instead, during the walking phase a distinction between the two types of soft tissue is noticed. The distribution of stresses throughout the *path* remained unchanged, but the effects varied. Contracted soft tissue, in particular, has greater values than flaccid soft tissue. In Foot Flat and Mid Stance, the greatest difference is roughly 20 kPa and 10 kPa, respectively. This means that when the soft tissue becomes stiffer, the internal stresses increase. Thus, a proposal for future research may be made: mechanical properties should be as close to those of the patient as feasible in order to get more realistic results and more accurate assessment of deep tissue damage.

10. Conclusions and future developments

This work studied a transtibial amputee with a patient specific prosthesis by means of finite element analysis, in particular focusing on the influence that different liner materials and material properties of the stump have on stress distribution during different steps. First of all, the donning was simulated and so pre-stresses were added. Then, three different loading conditions were analyzed, corresponding to standing, Foot Flat and Mid Stance.

All the results obtained were below the pressure threshold for pain and tolerance got from the literature, so no pain due to excessive pressure was present. After this preliminary analysis, the comparison between the different materials was performed. Higher peak contact pressures were found with a silicone liner, followed by urethane and TPE liners. This last material showed the lower contact pressures when different areas of the stump were analyzed and so it might be considered better than the others. Instead, peak shear stresses were higher with TPE and urethane during donning and standing, whereas during Foot Flat and Mid Stance they were overcame by those obtained with silicone. Another difference noticed during the analysis was related to the silicone liner. In fact, it showed a greater decrease in contact pressures passing from Foot Flat to Mid Stance and standing, and it could mean that it was more sensitive to higher loads. Considering the two types of soft tissue, changes in both normal and shear stresses were not particularly important except for the donning where a stiffer soft tissue created a higher resistance to the displacement of the socket and so contact pressures increased. All values were analyzed with respect to other works in literature and they were comparable, even if some differences due to variations in the model were found. Then, a further analysis was performed and the internal stresses of the stump were evaluated. Changes in liner material did not have an influence in the results. Instead, if stiffer soft tissue was considered, higher stresses were obtained during Foot Flat and Mid Stance, even if the distribution inside the stump remained equal. This brought to the conclusion that different material properties of the residual limb affected the internal stresses and so, being able to have characteristics of the stump as similar as possible to the real ones should allow to get more accurate results.

This work can be a starting point, together with other studies in the literature, to help clinicians to make a better choice of the liner, that is an important component to reduce pressures on the residual limb, and so to improve the satisfaction of the patient, that is the final goal for each kind of prosthesis. However, it presents some limitations regarding the finite element analysis that brought to variations when results were compared with other woks. So, it can be improved and below some suggestions are discussed:

- Considering the geometry of the model, a strong simplification consisted in neglecting the separation of the internal volume of the stump into different components representing the muscles, fat tissue and other biological materials. The soft tissue part was considered as a homogeneous bulk in which skin layers, fat and muscles were joined. They had the same material properties and the behavior did not change. This assumption was made to reduce the complexity of the model, that was already high. So, other elements and interactions should be introduced to obtain a more accurate model even if this would increase a lot the computational cost. The analysis should be computed increasing the complexity gradually in order to check what changes are produced. Moreover, if the stump is discretized in a more realistic way, material properties become more accurate and this can allow to obtain a more correct distribution of the stresses inside the stump.
- Regarding the soft tissue, in this work two different status taken from the literature were evaluated. They were considered to see if the response during standing and gait changed with different liners and if a better match existed. However, they don't represent the characteristics of a real patient and the differences between them are not elevated. This choice was made to avoid abortion of the simulations in *Abaqus*. In fact, when the material properties were changed, some problems arose. In future works it would be interesting to measure the real material properties of the patient and used them as input in the finite element analysis. Moreover, changes in the residual limb, including volume, shape, tissue composition, sensitivity and scarring from surgical wounds could be taken into consideration. These factors may vary during the day due to temperature, activity and hydration, or over several months, as postoperative oedema subsides, muscles atrophy and soft tissues remodel to allow socket-skeleton load transfer. So, material properties of the residual limb change in time and the effects of these variations should be studied.
- For what concern the liner, this work analyzed silicone, urethane and TPE. The material properties used were only examples because on the market there are many liners each one with different features. Instead of focusing on a specific liner, future works can concentrate on finding the best combination of material properties for a specific patient. Then, it would be interesting to study more deeply the friction coefficient between liner internal surface and the skin. In particular, in this work it was kept constant in each simulation, but it changes in time due to the external temperature and humidity and the presence of moisture, grease or sweat. To better detect shear stresses on the stump this behavior should be analyzed.
- In this work results focused on stresses at the interface between soft tissue and liner, and stresses inside soft tissue volume. It would be interesting do a more in-depth study on pressure inside the soft tissue. This is an important issue

because it is related to deep tissue injures. There is a lack of material in literature and so future studies are needed to better understand this problem that causes discomfort to the patient. Moreover, it could be significant also focus on internal shear stresses and not only on Von Mises stresses to verify their role.

- Only the standing and two phases of the gait were simulated. The scenario with higher loads were the Foot Flat, but during the gait there are phases in which higher values are reached. So, this work can be continued with other settings to check if the results obtained continue to be valid.

Bibliography

[1] E. A. Al-Fakih, N. A. A. Osman, F. R. M. Adikan, *Techniques for Interface Stress Measurements within Prosthetic Sockets of Transtibial Amputees: A Review of the Past 50 Years of Research*, Sensors (Basel), 2016

[2] P. Varma, M. G. Stineman, T. R. Dillingham, W. J. Erdman, *Physical Medicine and Rehabilitation Clinics of North America Epidemiology of Limb Loss*, Phys Med Rehabil Clin N Am., 2014 Feb

[3] McLaughlin, M. J., *Lower Limb Amputation and Gait, Braddom's Rehabilitation Care: A Clinical Handbook*, Elsevier, pp. 57–65, 2018

[4] C. A. Kalbaugh, P. D. Strassle, N. J. Paul, K. L. McGinigle, M. R. Kibbe, W. A. Marston, *Trends in Surgical Indications for Major Lower Limb Amputation in the USA from 2000 to 2016*, Eur J Vasc Endovasc Surg, pp. 60, 88-96, 2020

[5] N. Unwin, *Epidemiology of lower extremity amputation in centres in Europe, North America and East Asia*, Br J Surg, 2000 Marc

[6] A. D. Deshpande, M. Harris-Hayes, M. Schootman, *Epidemiology of Diabetes and Diabetes-Related Complications*, Phys Ther. 2008 Nov

[7] C. S. Molina, J. Faulk, *Lower Extremity Amputation*, StatPearls Publishing; 2021 Jan

[8] URL http://my.clevelandclinic.org/health/disease/14737-neuropathy

[9] URL https://www.sciencedirect.com/topics/medicine-and-dentistry/traumatic-amputation

[10] A. Courvoisier, F. Sailhan, C. Thevenin-Lemoine, R. Vialle, J.-P. Damsin, *Congenital tibial deficiencies: Treatment using the Ilizarov's external fixator*, Orthopaedics & Traumatology: Surgery & Research, Vol. 95, Issue 6, pp. 431-436, October 2009

[11] H. Ansaripour, S. Chemello, *Finite element analysis of socket optimization in accordance with the deformation of external surface of the stump*, Politecnico di Milano, 2018

[12] URL https://www.physio-pedia.com/

[13] P. S. Mckechnie, A. John, *Anxiety and depression following traumatic limb amputation: a systematic review*, Injury, 2014 Dec

[14] J.L. Bramley, P.R. Worsley, D.L. Bader, C. Everitt, A. Darekar, L. King, A.S. Dickinson, *Changes in tissue composition and load response after transtibial amputation indicate biomechanical adaptation*, Annals of Biomedical Engineering, 2021

[15] E. Vaienti, G. Scita, F. Ceccarelli, F. Pogliacomi, *Understanding the human knee and its relationship to total knee replacement*, Acta Biomed., 2017

[16] V. Singh, *Textbook of Anatomy Abdomen and Lower Limb*, Elsevier India, Vol. II, 2014

[17] URL https://teachmeanatomy.info/lower-limb/

[18] G. Colombo, R. Morotti, C. Rizzi, *FE Analysis of Contact between Residual Limb and Socket during Simulation of Amputee Motion*, Computer-Aided Design and Applications, February 2014

[19] A. J. Cantrell; O. Imonugo; M. Varacallo, *Anatomy, Bony Pelvis and Lower Limb, Leg Bones*, StatPearls Publishing, 2021 Jan

[20] K. M. Norton, *A brief history of prosthetics*, inMotion, 2007

[21] F.Mattogno, L. Chiapparelli, R. Pellegrini, M. Borzi, G. Rosellini, E. Di Stanislao, *Protesi*, Manuale Dispositivi Ortopedici, 2014

[22] P. Abhilash, P. S. Anusha, M. Venkatesh Pavan, J. Purushothama, *A Project Report On "Automated Prosthetic Leg"*, AMC Engineering College, 2017

[23] A. Kumar, P. Kumar, *Endoskeletal prosthesis: a new era for amputee*, Med J Armed Forces India, 2001 Apr

[24] C. Morvan, V. Packirisamy, M. Rechsteiner, F. Friedel, *Prosthetic gait analysis for physioterapists*, ICRC, January 2014

[25] C. Gandolfi, G. Giudici, *Sviluppo di un invaso protesico per amputato transtibiale mediante CAD e analisi agli elementi finiti dell'interazione tra moncone e invasatura*, Politecnico di Milano, 2019

[26] L. Paternò, M. Ibrahimi, E. Gruppioni, A. Menciassi, L. Ricotti, *Sockets for limb prostheses: a review of existing technologies and open challenges*, IEEE Trans Biomed Eng., 2018 Sep

[27] M. R. Safari, M. R. Meier, *Systematic review of effects of current transtibial prosthetic socket designs—Part 1: Qualitative outcomes*, J Rehabil Res Dev., Vol. 52, 2015

[28] M. R. Safari and M. R. Meier, *Systematic review of effects of current transtibial prosthetic socket designs—Part 2: Quantitative outcomes*, J Rehabil Res Dev., 2015

[29] H. Gholizadeh, N.A. Abu Osman, A. Eshraghi, S. Ali, N.A. Razak, *Transtibial prosthesis suspension systems: Systematic review of literature*, Clin Biomech (Bristol, Avon), 2014 Jan

[30] E. A. Al-Fakih, N. A. A. Osman, F. R. M. Adikan, *Techniques for Interface Stress Measurements within Prosthetic Sockets of Transtibial Amputees: A Review of the Past 50 Years of Research*, Sensors (Basel), 2016 Jul

[31] E. Boutwell, R. Stine, A. Hansen, K. Tucker, S. Gard, *Effect of prosthetic gel liner thickness on gait biomechanics and pressure distribution within the transtibial socket*, JRRD, Vol. 49, Number 2, pp. 227–240, 2012

[32] J. C. Cagle, B. J. Hafner, N. Taflin, J. E. Sanders, *Characterization of Prosthetic Liner Products for People with Transtibial Amputation*, Journal of Prosthetics and Orthotics, Vol. 30, Issue 4, pp. 187-199, October 2018

[33] J. C. Cagle, P. G. Reinhall, B. J. Hafner, J. E. Sanders, *Development of Standardized Material Testing Protocols for Prosthetic Liners*, J Biomech Eng., 2017 Apr

[34] A. Cavaco, L. Durães, A. Ramalho, S. Pais, *A study on the influence of prosthetic interface material in transtibial amputees' gait*, Biomed Mater Eng., 2020

[35] R. Safari, *Lower limb prosthetic interfaces; Clinical and technological advancement and potential future direction*, Prosthetics and Orthotics International, pp. 1-25, 2020

[36] G. Colombo, G. Facoetti, S. Gabbiadini, C. Rizzi, *Socket modelling assistant for prosthesis design*, International Journal of Computer Aided Engineering and Technology, Vol. 5, pp. 216–241, January 2013

[37] E. S. Jaimes, G. C. P. Botía, P. H. R. G. Reis, J. C. C. Rubio, M. R. V. Lana, *Comparison of a transtibial socket design obtained by additive manufacturing and reverse engineering and a traditional model*, Journal of Physics: Conference Series, Vol. 1126, International Meeting on Applied Sciences and Engineering 3–7, September 2018

[38] E. C. Baars, E. Schrier, P. U. Dijkstra, J. H.B. Geertzen, *Prosthesis satisfaction in lower limb amputees*, Medicine (Baltimore), 2018 Sep

[39] G. Colombo, G. Facoetti, C. Rizzi, *A digital patient for computer-aided prosthesis design*, Interface focus, 2013

[40] C. W. Radcliffe, J. Foort, *The patellar-tendon-bearing below-knee prosthesis*, University of California, 1961

[41] M. C. Faustini, R. R. Neptune, R. H. Crawford, W. E. Rogers, G. Bosker, *An Experimental and Theoretical Framework for Manufacturing Prosthetic Sockets for Transtibial Amputees*, IEEE Transactions on Neural System and Rehabilitation Engineering, Vol. 14, No. 3, September 2006

[42] A. F. Mak, M. Zhang, D. A. Boone, *State-of-the-art research in lower-limb prosthetic biomechanics-socket interface: a review*, Journal of Rehabilitation Research and Development, Vol. 38, No. 2, pp. 161–174, March/April 2001

[43] G. K. Klute, B. C. Glaister, J. S. Berge, *Prosthetic liners for lower limb amputees: A review of the literature*, Prosthetics and Orthotics International, June 2010

[44] J.W. Steer, P.R. Worsley, M. Browne, A.S. Dickinson, *Key considerations for finite element modelling of the residuum-prosthetic socket interface*, Prosthetics and Orthotics International, November 11, 2020

[45] A.S. Dickinson, J.W. Steer, P.R. Worsley, *Finite element analysis of the amputated lower limb: A systematic review and recommendations*, Med Eng Phys., 2017 May

[46] W. Lee, M. Zhang, X. Jia, J. Cheung, *Finite element modeling of contact interface between trans-tibial residual limb and prosthetic socket*, Med Eng Phys., 2004 Oct

[47] C-L Wu, C-H Chang, A-T Hsu, C-C Lin, S-I Chen, G-L Chang, *A proposal for the pre-evaluation protocol of below-knee socket design - integration pain tolerance with finite element analysis*, Journal of the Chinese Institute of Engineers, 2003

[48] M. Zhang, C. Roberts, *Comparison of computational analysis with clinical measurement of stresses on below-knee residual limb in a prosthetic socket*, Medical Engineering & Physics, Vol. 22, Issue 9, pp. 607-612, November 2000

[49] J. C. Cagle, P. G. Reinhall, K. J. Allyn, J. McLean, P. Hinrichs, B. J. Hafner, J. E. Sanders, *A Finite Element Model to Assess Transtibial Prosthetic Sockets with Elastomeric Liners*, Med Biol Eng Comput., 2018 Jul

[50] Whiteside SR. Practice Analysis of Certified Practitioners. In: Whiteside SR, editor. *American Board for Certification in Orthotics.* Prosthetics, & Pedorthotics, Inc; 2015

[51] X. Jia, M. Zhang, W. C. C. Lee, *Load Transfer Mechanics Between Trans-Tibial Prosthetic Socket and Residual Limb—Dynamic Effects*, Journal of Biomechanics, Jan 2003

[52] S.G. Zachariah, E. Sanders, *Finite element estimates of interface stress in the trans-tibial prosthesis using gap elements are different from those using automated contact*, Journal of Biomechanics, Vol. 33, Issue 7, pp. 895-899, July 2000

[53] X.Jia, M.Zhang, X.Li, W. Lee, *A quasi-dynamic nonlinear finite element model to investigate prosthetic interface stresses during walking for trans-tibial amputees*, Clinical biomechanics 20, 2005

[54] C-C Lin, C-H Chang, C-L Wu, K-C Chung, I-C Liao, *Effect of liner stiffness for transtibial prosthesis: a finite element contact model*, Med Eng Phys, 2004 Jan

[55] J.E. Sanders and C.H. Daly, *Normal and shear stresses on a residual limb in a prosthetic socket during ambulation: Comparison of finite element results with experimental measurements*, Journal of Rehabilitation Research and Development, Vol 30, N.2, pp. 191 – 204, 1993

[56] T. Marinopoulos, L. Zani, S. Li, V. V. Silberschmidt, *Modelling indentation of human lower-limb soft tissue: simulation parameters and their effects*, Continuum Mechanics and Thermodynamics, 2020

[57] S. Portnoy, I. Siev-Ner, N. Shabshin, A. Gefen, *Effects of sitting postures on risks for deep tissue injury in the residuum of a transtibial prosthetic-user: a biomechanical case study*, Comput Methods Biomech Biomed Engin., 2011 Nov

[58] V. Restrepo, J. Villarraga, J. Velez, *Surface optimization of a socket for a transfemoral amputee that reduces the stresses varying the friction coefficient*, Blucher Mechanical Engineering Proceedings, Vol. 1, num. 1, May 2014

[59] F. M. Hendriks, D. Brokken, J. T. W. M. Van Eemeren, C. W. J. Oomens, F. P. T. Baaijens, J. B. A. M. Horsten, *A numerical-experimental method to characterize the non-linear mechanical behaviour of human skin*, Skin Research & Technology, 25 July 2003

[60] D. Lacroix, J. Patino, *Finite element analysis of donning procedure of a prosthetic transfemoral socket*, Annals of Biomedical Engineering, 2011

[61] M. Zhang, M. Lord, A. R. Turner-Smith, V. C. Roberts, *Development of a non-linear finite element modelling of the below-knee prosthetic socket interface*, Med Eng Phys., 1995

[62] R. B. Svensson, P. Hansen, T. Hassenkam, B. T. Haraldsson, P. Aagaard, V. Kovanen, M. Krogsgaard, M. Kjaer, S. P. Magnusson, *Mechanical properties of human patellar tendon at the hierarchical levels of tendon and fibril*, J Appl Physiol, 2012

[63] J. F. Ramírez, J. J. Pavón, A. Toro, *Experimental assessment of friction coefficient between polypropylene and human skin using instrumented sclerometer*, Journal of Engineering Tribology, March 19, 2014

[64] A. Gefen, *How do microclimate factors affect the risk for superficial pressure ulcers: A mathematical modeling study*, Journal of Tissue Viability, Vol. 20, Issue 3, pp. 81-88, August 2011

[65] J. Cagle, *A Computational Tool to Enhance Clinical Selection of Prosthetic Liners for People with Lower Limb Amputation*, University of Washington, 2016

[66] D. Systèmes, *Abaqus Analysis User's Guide*, Simulia

[67] S. Portnoy, G. Yarnitzky, Z. Yizhar, A. Kristal, U. Oppenheim, I. Siev-Ner, A. Gefen, *Real-time patient-specific finite element analysis of internal stresses in the soft tissues*

of a residual limb: a new tool for prosthetic fitting, Annals of Biomedical Engineering, Vol. 35, pp. 120–135, 2007

[68] G. Design, *Geomagic Design X User Guide*, 3D Systems, Inc. Geomagic Solutions, November 2013

[69] URL https://docs.fileformat.com/cad/stl/

[70] URL https://docs.fileformat.com/3d/step/

[71] URL https://www.meshmixer.com

[72] M. Shahzada, A. Kamranb, M. Z. Siddiquia, M. Farhana, *Mechanical Characterization and FE Modelling of a Hyperelastic Material*, Journal of Materials Research, 2015